


The glutathione *S*-transferase *Gstt1* drives survival and dissemination in metastases

Received: 21 December 2022

Accepted: 18 April 2024

Published online: 11 June 2024

 Check for updates

Christina M. Ferrer ^{1,2,3}✉, Hyo Min Cho^{1,2,10}, Ruben Boon ^{1,9,10},
Tiziano Bernasocchi ^{1,2}, Lai Ping Wong⁴, Murat Cetinbas⁴,
Elizabeth R. Haggerty¹, Irene Mitsiades ¹, Gregory R. Wojtkiewicz ⁵,
Daniel E. McLoughlin ^{1,6}, Reem Aboushousha ⁷, HEND Abdelhamid⁷,
Sita Kugel ⁸, Esther Rheinbay¹, Ruslan Sadreyev⁴, Dejan Juric^{1,6},
Yvonne M. W. Janssen-Heininger⁷ & Raul Mostoslavsky ^{1,2}✉

Identifying the adaptive mechanisms of metastatic cancer cells remains an elusive question in the treatment of metastatic disease, particularly in pancreatic cancer (pancreatic adenocarcinoma, PDA). A loss-of-function shRNA targeted screen in metastatic-derived cells identified *Gstt1*, a member of the glutathione *S*-transferase superfamily, as uniquely required for dissemination and metastasis, but dispensable for primary tumour growth. *Gstt1* is expressed in latent disseminated tumour cells (DTCs), is retained within a subpopulation of slow-cycling cells within existing metastases, and its inhibition leads to complete regression of macrometastatic tumours. This distinct *Gstt1*^{high} population is highly metastatic and retains slow-cycling phenotypes, epithelial–mesenchymal transition features and DTC characteristics compared to the *Gstt1*^{low} population. Mechanistic studies indicate that in this subset of cancer cells, *Gstt1* maintains metastases by binding and glutathione-modifying intracellular fibronectin, in turn promoting its secretion and deposition into the metastatic microenvironment. We identified *Gstt1* as a mediator of metastasis, highlighting the importance of heterogeneity and its influence on the metastatic tumour microenvironment.

Although successful survival and colonization by metastatic cells is a highly inefficient process¹, metastatic disease accounts for 90% of cancer-related deaths². To establish metastases, cancer cells from the primary tumour navigate numerous hurdles—traversing blood vessels, surviving in the circulation and proliferating to colonize foreign habitats³. Thus, distinct molecular programs are required to endow cancer cells with the ability to adapt to the metastatic niche and develop overt metastases. Until recently, much of the focus has been on identifying

early metastatic drivers within primary tumours. In pancreatic adenocarcinoma (PDA), several studies have shown that metastatic lesions lack additional driver mutations compared to primary tumours^{4,5}. Therefore, elucidating the circuitry distinguishing metastases from primary tumours is an urgent question for the field. Although various groups have identified specific epigenetic and stage-dependent adaptations between metastases and primary tumours^{6–9}, few pancreatic cancer studies have specifically addressed the importance of metastatic

¹The Massachusetts General Hospital Cancer Center, Harvard Medical School, Boston, MA, USA. ²The Broad Institute of Harvard and MIT, Cambridge, MA, USA. ³University of Maryland School of Medicine and the Greenebaum Comprehensive Cancer Center, Baltimore, MD, USA. ⁴Department of Molecular Biology, Massachusetts General Hospital, Boston, MA, USA. ⁵Center for Systems Biology, Massachusetts General Hospital, Boston, MA, USA. ⁶Termeer Center for Targeted Therapies, Massachusetts General Hospital, Boston, MA, USA. ⁷University of Vermont Lerner College of Medicine, Burlington, VT, USA. ⁸Fred Hutchinson Cancer Research Center, Seattle, WA, USA. ⁹Present address: Galapagos NV, 2800 Mechelen, Belgium. ¹⁰These authors contributed equally: Hyo Min Cho, Ruben Boon. ✉e-mail: cferrer@som.umaryland.edu; rmostoslavsky@mgh.harvard.edu

heterogeneity or the interplay between tumour cells and the metastatic tumour microenvironment^{8,10,11}.

Metastatic dissemination is an early event in cancer progression in various tumour types^{12–15}. This is particularly evident in PDA, where the majority of patients present with extra-pancreatic invasion and metastatic disease upon initial diagnosis¹⁶, and for which the five-year survival rate is only ~7.1% (refs. 15,16). Interventions aimed at targeting the mechanisms of primary tumour dissemination are therefore unlikely to be clinically successful strategies owing to the presence of synchronous or undetectable metastases¹⁷. Additionally, the biological heterogeneity observed among primary tumours, disseminated disease and overt metastases, as well as our limited understanding of these processes, present a clinical challenge and an urgent question in the field. Although some advancements have been made in understanding the mechanisms of metastatic dissemination^{15,18}, latency⁸ and outgrowth^{4,6–9}, these topics remain underexplored in PDA.

Utilizing orthotopic models of metastasis, we performed unbiased RNA sequencing (RNA-seq) on matched primary and metastatic solid tumours from established mouse models of PDA and breast cancer. Sequencing analysis was followed by a targeted functional short hairpin RNA (shRNA) screen to identify genes conferring a growth advantage under low-attachment conditions in metastasis-derived cells. In this study, we provide evidence that *Gstt1*, the gene encoding a glutathione *S*-transferase with no known roles in cancer metastasis, is uniquely expressed in and required for the formation of macrometastases while remaining dispensable for primary tumour growth. Within metastatic lesions, *Gstt1* displays a heterogeneous expression pattern, with *Gstt1*^{high} cells representing a highly metastatic, slow-cycling population with epithelial–mesenchymal transition (EMT) features. Importantly, this slow-cycling *Gstt1*^{high} subpopulation is not only retained in established lesions, but is also required for metastatic dissemination. Mechanistically, we find that *Gstt1* directly catalyses the glutathionylation of intracellular fibronectin, in turn enhancing the secretion of fibronectin from tumour cells and its deposition into the extracellular matrix (ECM), which appears to be critical for maintaining metastatic growth. Overall, we identify *Gstt1* as a metastatic driver, underscoring that tumour cell heterogeneity critically shapes the metastatic microenvironment.

Results

RNA-seq identifies an upregulated metastatic gene signature

Until recently, efforts to identify metastatic drivers primarily focused on characterizing the factors involved during the initiating events of metastasis^{2,19}. Here, we sought to identify the genes

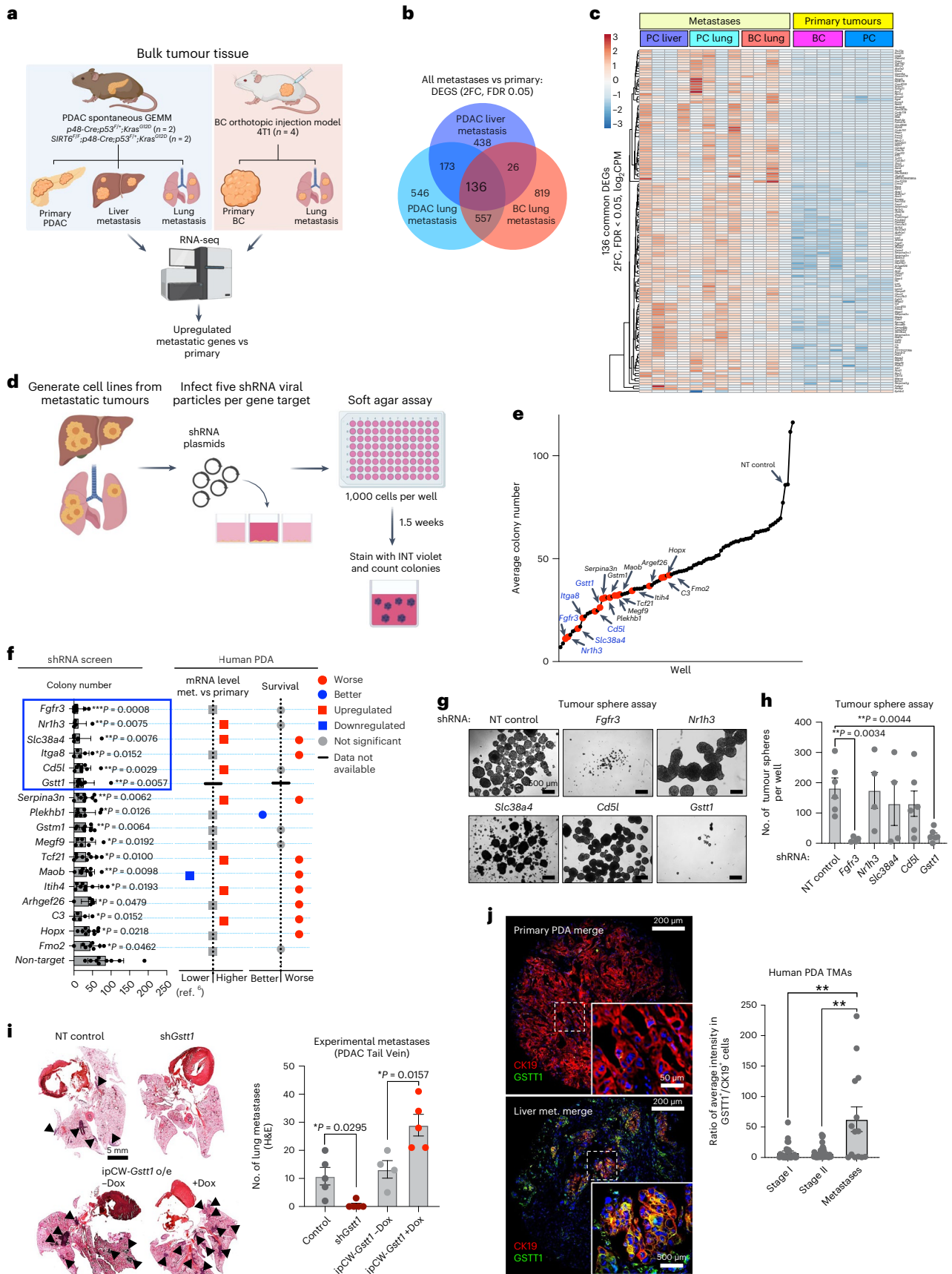
required for the late stages of the metastatic cascade (that is, metastatic outgrowth and maintenance) based on transcriptional differences between primary tumours and macrometastases. We first isolated tissue from matched primary and metastatic tumours from two genetic mouse models of pancreatic ductal adenocarcinoma (PDAC) (*Sirt6* wild-type (WT) *p48-Cre/p53F/+KrasL/+* and *Sirt6* knockout (KO) *p48-Cre/p53F/+KrasL/+*), which mimic the progression of human primary pancreatic cancer and generate spontaneous distant metastases, with the more aggressive *Sirt6* KO model readily developing lung metastases^{7,16,20,21} (Fig. 1a, left). To expand the transcriptional profile across carcinoma-derived metastases, we included the 4T1 breast cancer (BC) mouse model, which develops spontaneous metastases to the lung when orthotopically injected into the mammary fat pad of Balb/c mice²² (Fig. 1a, right). We performed RNA-seq on bulk tissue isolated from primary tumours and metastases to generate expression profiles corresponding to PDAC and BC primary tumours, as well as lung and liver metastases (Fig. 1a). Subsequent analysis identified a common differentially upregulated gene signature ($n = 136$) in liver and lung metastases compared to matched primary tumours across all tumour types (Fig. 1b,c and Supplementary Table 1).

Targeted screen to identify genes required for metastatic-cell growth

Previous screening methods have allowed for the identification of clonal metastatic drivers in the primary tumour^{11,22,23}, adaptations for cell survival in circulation^{24,25} or metastatic reactivation¹⁹, but few studies have focused on exploring mediators maintaining the growth of existing macrometastases^{2,7}. To functionally test whether our upregulated ‘metastatic signature’ was required for the growth and survival of established metastatic cells, we developed a targeted, 96-well shRNA screening method under anchorage-independent growth conditions (Fig. 1d). Using both models of metastasis, we generated a panel of cell lines from spontaneous metastatic tumours originating in the liver and lung. These cell lines were individually transduced with pooled shRNAs targeting each of the top 94 upregulated genes. Following puromycin selection for 48 h, viable clones were then subjected to a soft agar colony formation assay in a 96-well format. After two weeks, soft agar colonies were stained with *p*-iodonitrotetrazolium violet (INT-violet) and counted (Fig. 1d). We identified 17 genes that, when depleted, led to a statistically significant impairment of soft agar growth, indicating their requirement for anchorage-independent growth in metastatic cells (Fig. 1e,f). High mean expression of the top 17 gene hits (excluding *GSTT1*, discussed below) is associated with poor overall survival

Fig. 1 | A shRNA screen targeting metastatic genes identifies *Gstt1* as a regulator of metastasis. a, Diagram depicting the mouse models used for metastasis experiments. Left: the PDAC transgenic model. Right: orthotopic injection of the 4T1 mouse breast cancer cell line (BC) into the mammary fat pad. Bulk tissue primary tumours and matched metastases were subjected to RNA-seq analysis. Created with [Biorender.com](https://biorender.com). **b**, Venn diagram demonstrating common and unique differentially expressed genes between all metastatic and primary tumours ($n = 136$; $\log_2(\text{fold change (FC)})$; false discovery rate (FDR) < 0.05). **c**, Heatmap depicting the expression of 136 commonly differentially expressed genes in all metastases compared to primary tumours ($\log_2(\text{counts per million (CPM)})$). **d**, Schematic depicting a targeted soft-agar 96-well shRNA screen in metastatic cell lines generated from the mouse models indicated above ($n = 9$). Created with [Biorender.com](https://biorender.com). **e**, shRNA target genes ranked by average colony number per well (lowest to highest) compared to non-targeting (NT) control shRNA. Data represent the mean colony number from a minimum of $n = 4$ cell lines (maximum $n = 9$) per gene target. Red dots show the top 17 hits. The top six candidate genes are labelled in blue. **f**, Left: top 17 hits ranked by average colony number. Each data point represents an independent cell line. Mean and s.d. are shown. A two-sided *t*-test was used to compare each shRNA to non-targeting control (*P* values are shown). Middle: differential expression of the top 17 genes

in human PDA metastases compared to matched primary tumours. Right: TCGA datasets demonstrating the prognostic consequences of high gene expression on progression-free survival in PDA. **g**, Tumour sphere growth in metastatic cell lines stably expressing the top six shRNA gene targets. **h**, Quantification of the number of tumour spheres per well. The experiment was performed in triplicate ($n = 5$ pooled shRNAs per gene target) with at least $n = 4$ cell lines each. Data are represented as s.e.m. A two-sided *t*-test was used to determine statistical significance between groups (***P* = 0.0034, ****P* = 0.0044 as indicated). **i**, Metastatic cell lines expressing the indicated constructs were injected via the tail vein to generate lung metastases (1×10^4 cells). All mice were euthanized when the first group demonstrated clinical evidence of metastatic burden. Left: representative H&E images. Right: lung metastatic burden was evaluated using H&E and is represented as the total number of macrometastases per lung tissue. Data are presented as mean and s.e.m. A two-sided *t*-test was used to determine statistical significance between groups (**P* = 0.0295, **P* = 0.0157 as indicated). **j**, Left: cytokeratin 19 and GSTT1 immunofluorescence staining of primary tumour and metastatic PDA tissue microarray cores. Right: quantification of the staining in each core. Data are presented as mean and s.e.m. An analysis of variance (ANOVA) with a Brown–Forsythe post-hoc test for multiple comparisons was performed to determine statistical significance (***P* = 0.0070).



in patients with pancreatic cancer (Fig. 1f and Extended Data Fig. 1a), highlighting the importance of this gene signature in metastatic PDA.

To validate the differential expression of the top candidate genes and account for surrounding stromal contamination, we performed a parallel analysis on lineage-traced YFP/GFP⁺ primary and metastatic cells. Utilizing yellow fluorescent protein (YFP) and green fluorescent protein (GFP) expressing versions of our mouse models (*p48-Cre/p53 F/+KrasL/+ROSA26-LSL-YFP* (*Sirt6* WT and KO) and 4T1-GFP; Extended Data Fig. 1b), cells from primary tumours and matched metastases were isolated using fluorescence-activated cell sorting (FACS; Extended Data Fig. 1c), then RNA-seq was performed on the purified tumour-cell populations. Several of the 17 gene hits demonstrated differential expression or a trend toward differential expression (*Nr1h3*, *Gstm1*, *Itih4*, *Cd5l*, *Gstm1*, *C3* and *Hoxp3*; Extended Data Fig. 1d). Quantitative polymerase chain reaction (qPCR) analysis of the top six candidate genes (Fig. 1e,f, indicated in blue) demonstrated enrichment in *Fgfr3*, *Nr1h3*, *Slc38a4* and *Gstm1* in metastatic cell lines compared to matched primary-tumour lines (Extended Data Fig. 1e). Next, we performed functional validation of the top six candidates by examining the effect of individual shRNAs on soft agar growth. Inhibiting *Nr1h3*, *Slc38a4*, *Cd5l* and *Gstm1* verified our original screen results, with two individual targeting shRNAs demonstrating reduced metastatic cell growth in soft agar (Extended Data Fig. 1f–h). Together, these results suggest that a loss-of-function shRNA screen enables the identification of single genes implicated in the anchorage-independent survival of metastatic tumour cells.

To assess the relevance of candidate genes to human disease, we examined their expression in metastatic versus primary PDA⁶ using publicly available TCGA (The Cancer Genome Atlas) datasets. Five out of 17 genes identified in our screen (*Slc38a4*, *Serpina3n*, *Tcf21*, *Itih4* and *C3*) scored on both criteria: differential enrichment in metastases and worse prognosis (relapse-free survival) in human PDA (Fig. 1f)⁶. Interestingly, several of these genes have been well characterized as metastatic mediators in other tumour types^{2,26}, suggesting conserved mechanisms. Notably, however, *GSTM1* was largely absent from pancreatic cancer datasets (Fig. 1f) due to its absence from the reference genome, thus impeding analysis in the TCGA. In an independent assay testing for metastatic stemness under low-attachment conditions, we were surprised to find that both *Fgfr3* and *Gstm1* were required for the formation of tumour spheres (Fig. 1g,h). Members of the fibroblast growth factor receptor (FGFR) family have been previously implicated in cancer stemness; however, the requirement for *Gstm1* for tumour sphere growth was intriguing. Further validation of our screening strategy confirmed that *Gstm1* is uniquely required for the anchorage-independent growth of metastatic cells (Extended Data Fig. 1i–k) and dispensable under two-dimensional (2D) attachment conditions (Extended Data Fig. 1l), reinforcing the dependency for *Gstm1* specifically in the metastatic context.

The glutathione-conjugating enzyme *Gstm1* is required for metastasis

GSTM1 encodes the glutathione S-transferase (GST) theta 1 enzyme, a member of a superfamily of proteins that catalyse the conjugation of reduced glutathione (GSH) to a variety of electrophilic and hydrophobic compounds, including carcinogens, chemotherapeutic drugs and many oxidative metabolic by-products^{27,28}. GSTs play critical roles as cellular detoxifying enzymes, predisposing compounds to further modification and clearance in the liver. Notably, the *GSTM1* gene is haplotype-specific and absent from ~30% of the population^{27,29}, suggesting redundant functions in normal cells. Although various epidemiological investigations have reported *GSTM1*-null polymorphism as an independent risk factor for the development of certain cancers^{27–29}, functional studies directly linking *GSTM1* to tumour initiation, progression and metastatic disease remain inconclusive^{27–29}.

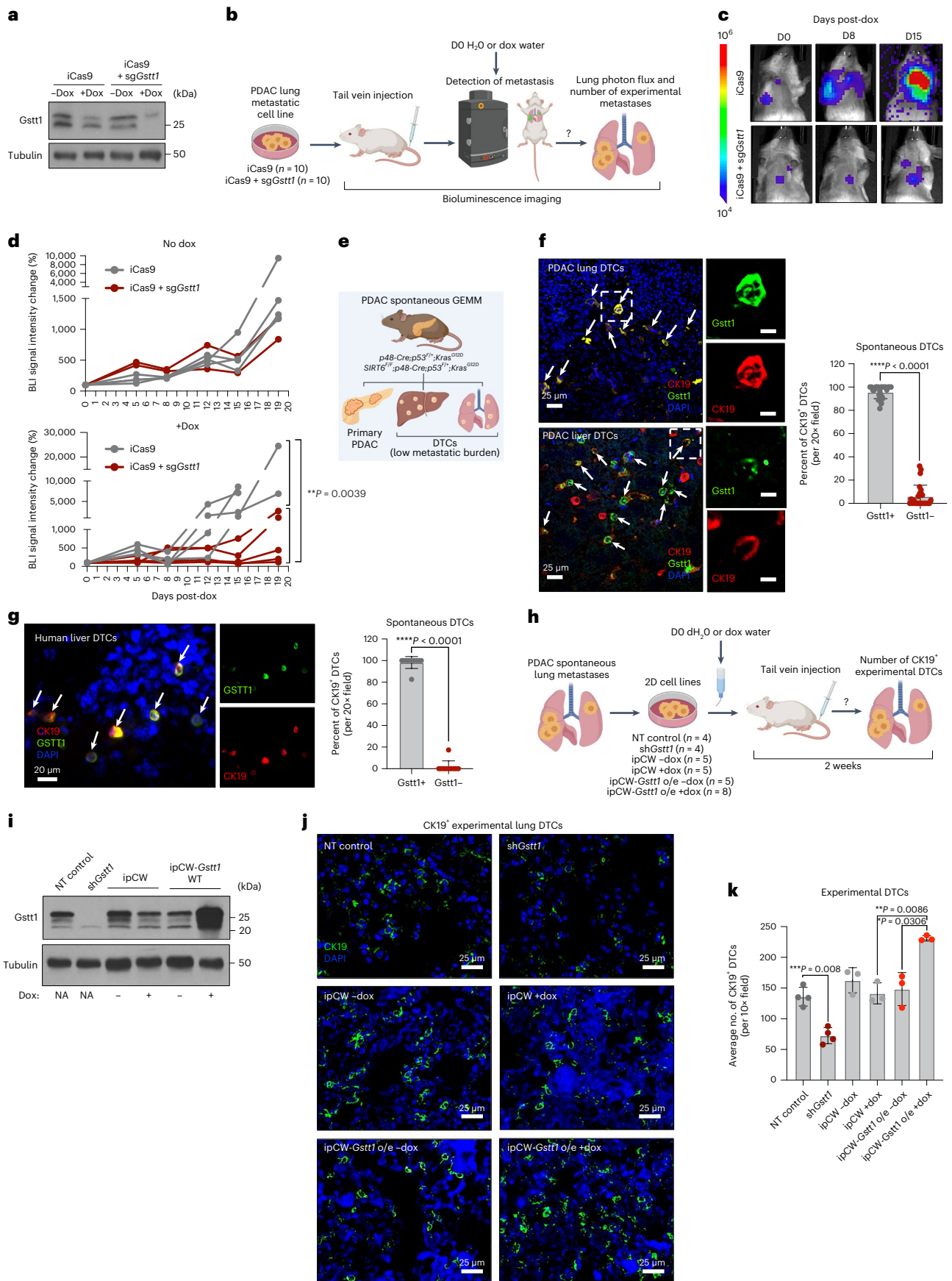
To validate the dependencies in both tumour models, we first sought to determine whether *Gstm1* is required for metastasis. Using our PDAC and BC metastasis models, lung-metastatic-derived cell lines stably expressing non-targeting control or a *Gstm1* shRNA (Extended Data Fig. 2a,g) were injected via tail-vein or retro-orbital injection, respectively, to generate experimental metastases (Extended Data Fig. 2b (top) and 2h). Notably, inhibition of *Gstm1* almost completely abolished the formation of metastatic lesions (Fig. 1i and Extended Data Fig. 2i). To investigate whether *Gstm1* could enhance the formation of metastases we used a doxycycline-inducible overexpression system (Extended Data Fig. 2a,b, bottom). Strikingly, overexpression of *Gstm1* increased the metastatic burden, indicating that *Gstm1* is both necessary and sufficient to drive metastases (Fig. 1i). Next, we asked whether the GST activity of *Gstm1* is required for the formation of metastases. The Arg amino acid at position 234 in rat and mouse *Gstm1* has been shown to demonstrate high catalytic efficiency³⁰. We introduced a Gly(G) in the place of this Arg(R) to generate an R234G mutant in the doxycycline-inducible *Gstm1*-overexpression construct (Extended Data Fig. 2c,d). Overexpression of wild-type *Gstm1* resulted in an approximately sixfold increase in metastatic burden compared to control, a phenotype that was completely abolished when expressing the R234G mutant (Extended Data Fig. 2e,f).

We next assessed the requirement of *Gstm1* for metastatic growth in a model of spontaneous metastasis. Primary-derived cell lines from our BC model stably expressing sh*Gstm1* (Fig. 2h) were injected orthotopically into the mammary fat pad, then the mice were monitored for both primary tumour size and the formation of end-stage metastases (Extended Data Fig. 2j). Remarkably, although the growth of primary tumours was unaffected (Extended Data Fig. 2k), *Gstm1* knockdown resulted in a significantly reduced number of spontaneous metastatic lesions (Extended Data Fig. 2l,m). Together, these data identified the glutathione S-transferase, *Gstm1* as a driver of metastatic disease.

Fig. 2 | *Gstm1* is required for metastatic maintenance and dissemination.

a, Western blot demonstrating Cas9 doxycycline (dox)-inducible KO of *Gstm1* in lung metastatic cells used for injections in **b**. **b**, SCID mice were injected via the tail vein with PDAC lung metastatic-derived cells expressing iCas9 control ($n = 10$) or iCas9 + sg*Gstm1* ($n = 10$) (1×10^4 cells). Upon evidence of metastatic burden (using bioluminescence imaging, BLI), mice were given either control or doxycycline in the drinking water. Imaging was continued until the mice displayed clinical evidence of metastatic burden, whereupon all groups were euthanized. Created with [Biorender.com](https://www.biorender.com). **c**, Representative bioluminescent images of lung metastatic burden pre-dox (day 0 (DO)) and post-dox (D8 and D15). **d**, Quantification of lung photon flux, represented as the percent change in BLI intensity relative to D0 dH₂O or dox treatment. Data represent individual mice imaged over time. A two-way ANOVA test was performed (** $P = 0.0039$). **e**, Diagram depicting mice displaying primary tumour burden and no evidence of macrometastases analysed for DTC content. Created with [Biorender.com](https://www.biorender.com). **f**, Left: immunofluorescence staining of *Gstm1* and cytokeratin 19 in PDAC-derived lung (top) and liver (bottom) DTCs from mice with low tumour burden. Insets:

magnified images of single DTCs. Scale bars (insets), 10 μ m. Right: quantification representing the average of 5–10 fields ($n = 4$ mice). Data are presented as mean and s.d. and a two-sided *t*-test was used to determine statistical significance between groups (**** $P < 0.0001$). **g**, Left: immunofluorescence staining of *GSTM1* and cytokeratin 19 in PDA-derived liver DTCs. Right: quantification representing the average of 10 fields ($\times 20$ magnification) for a single patient. Data are presented as mean and s.d. and a two-sided *t*-test was used to determine statistical significance between groups (**** $P < 0.0001$). **h**, Schematic describing the DTC experiment. All groups were euthanized two weeks post-injection, and lungs were collected and analysed via immunofluorescence for DTC burden. Created with [Biorender.com](https://www.biorender.com). **i**, Western blot depicting *Gstm1* levels for the cell lines injected in **j**. NA, not applicable. **j**, Cytokeratin 19 staining of experimental DTCs two weeks post-injection. **k**, Quantification of the CK19-positive experimental DTCs from **j**. Data are presented as the average of 5–10 fields from a minimum of $n = 3$ mice per group. Data are presented as mean and s.d. and a two-sided *t*-test was used to determine statistical significance between groups (*** $P = 0.008$, ** $P = 0.0086$, * $P = 0.0306$ as indicated).



GSTT1 is upregulated and required for metastatic growth in human PDA

Next, we performed immunofluorescence staining for *Gstt1* across primary and metastatic tissue in our mouse models of PDAC. This demonstrated that *Gstt1* is expressed in a subset of metastatic CK19⁺ tumour cells and is widely absent from primary tumours (Extended Data Fig. 2n,o). As previously noted, the dearth of available datasets for examining *GSTT1* presented a challenge for its characterization in human cancer. To overcome this, we analysed a panel of matched human primary and metastatic PDA lesions collected via rapid autopsy. Our analysis revealed upregulation of *GSTT1* protein across metastatic samples relative to primary tumours by both immunofluorescence of formalin-fixed paraffin-embedded (FFPE) sections (Extended Data Fig. 2p) and bulk tissue western blot (Extended Data Fig. 2q). To add to the robustness of the analysis, we obtained a pancreatic cancer tissue microarray (TMA) panel containing both primary PDA and metastatic cores. We observed a striking enrichment for *GSTT1* in CK19-positive metastatic cores compared to primary tumour-derived cores (Fig. 1j). To further validate the functional significance of *GSTT1* in human PDA, we silenced *GSTT1* in two metastatic-derived human pancreatic cancer cell lines, KP3 and CFPAC1 (Extended Data Fig. 2r). Inhibiting *GSTT1* resulted in a significant reduction in soft agar colony formation in these lines (Extended Data Fig. 2s). These observations provide strong support for our screening strategy in the mouse and identified *GSTT1* as being differentially upregulated in metastatic PDA, potentially contributing to survival outcomes in these patients.

Gstt1 is required for metastatic maintenance and ectopic spread

To assess the role of *Gstt1* in metastatic maintenance, we employed an inducible Cas9 (iCas9) system to target *Gstt1* in mice with established metastases. Lung metastatic PDAC-derived iCas9 control and sg*Gstt1*-expressing cells (Fig. 2a) were injected via tail vein and followed by weekly bioluminescence imaging (BLI) (Fig. 2b). Upon evidence of a metastatic signal, each group was treated with drinking water containing either doxycycline or control (water), followed by continuous BLI monitoring (Fig. 2b). BLI revealed a decrease in signal in the iCas9 + sg*Gstt1* mice as early as 12 days post-doxycycline compared to iCas9 control mice. iCas9 control mice continued to progress and eventually succumbed to metastatic disease by D15–D19 post-doxycycline, whereas sg*Gstt1*-expressing mice maintained a low metastatic signal (Fig. 2c,d), demonstrating that *Gstt1* is not only required for the formation of metastasis but is also critical in the maintenance of established tumours.

Similar metastasis-specific dependencies were observed in iCas9-expressing 4T1 cells where doxycycline was given before orthotopic cell injection, inhibiting *Gstt1* beginning at tumour cell implantation, followed by removal of the primary tumour and monitoring

of metastasis using BLI (Fig. 3a,b). Knockout of *Gstt1* from the time of implantation did not affect the growth of the orthotopic primary tumour (Extended Data Fig. 3c), but resulted in mice devoid of lung metastases, compared to iCas9 control animals (Extended Data Fig. 3d–f), pointing to roles for *Gstt1* in the metastatic process at stages after dissemination from the primary tumour.

To further test the specificity of *Gstt1* in mediating metastasis in vivo, we performed rescue experiments utilizing our *Gstt1* doxycycline-inducible overexpression system in primary tumour-derived cells from the 4T1 BC model. Mice were injected orthotopically with either control or sh*Gstt1*-expressing cells and treated with doxycycline in drinking water seven days before injection to induce *Gstt1* expression during tumour cell implantation, followed by BLI to monitor primary tumour growth. Following removal of the primary tumour, mice were imaged to monitor the formation of metastases (Extended Data Fig. 3g). Overexpression of *Gstt1* in control cells resulted in regression of primary tumours (Extended Data Fig. 3h–j), indicating that expression of *Gstt1* is detrimental to primary tumour growth, further highlighting the distinct roles for *Gstt1* in the primary tumour and during metastasis. However, re-expression in *Gstt1*-depleted cells (Extended Data Fig. 3h) did not affect the formation of primary tumours (Extended Data Fig. 3h–j). More importantly, reconstitution of *Gstt1* not only rescued the absence of lung metastases upon deletion of *Gstt1* (Extended Data Fig. 3k–m); overexpression also resulted in ectopic metastases throughout the mouse (Extended Data Fig. 3k,n,o), providing further evidence that *Gstt1* is dispensable, if not deleterious for primary tumour growth, and may play a crucial role in mediating tumour cell dissemination. Although we observed clear phenotypes for *Gstt1* in both pancreatic and breast cancer metastases, in the present study we will focus on pancreatic cancer for further characterization.

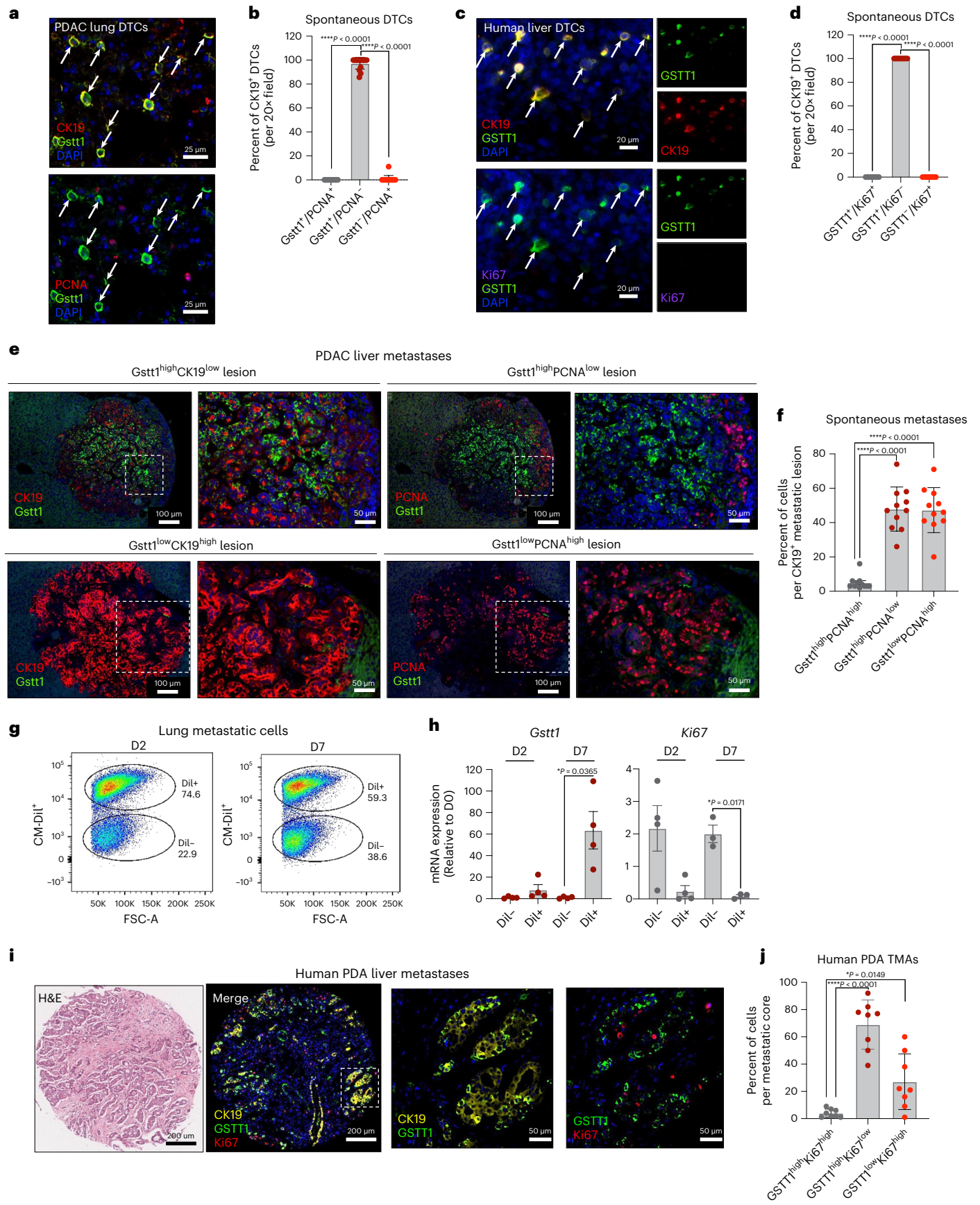
Gstt1 is required for tumour cell dissemination

Our results point to *Gstt1* as a potential mediator of tumour cell dissemination. Disseminated tumour cells (DTCs) are single cells or small cell clusters that have escaped the primary tumour and arrived at a distant organ^{3,8,17}. To assess whether *Gstt1* may be important for dissemination, we assessed *Gstt1* expression in DTCs from liver and lung tissues derived from PDAC genetically engineered mouse models (GEMMs) with primary tumours but no visible macrometastases (Fig. 2e). Strikingly, the majority of single DTCs and small clusters stained for both CK19 and *Gstt1* (Fig. 2f). Importantly, *GSTT1*-positive DTCs were also present in liver tissue from a rapid autopsy patient with primary PDA and no overt metastases (Fig. 2g).

To determine whether *Gstt1* is required for and sufficient to enhance tumour cell dissemination, we knocked down or overexpressed *Gstt1* in metastatic-derived PDAC cell lines and performed tail-vein injections to generate experimental lung DTCs. To stain for

Fig. 3 | *Gstt1* is expressed in latent DTCs and in a subpopulation of slow-cycling macrometastatic cells. **a**, Immunofluorescence staining of *Gstt1*, cytokeratin 19 and PCNA in spontaneous PDAC-derived DTCs in the lung of mice without overt metastases. **b**, Quantification of **a**, shown as the average of liver and lung metastases (5–10 fields from $n = 2$ mice, $\times 20$ magnification). Data are presented as mean and s.d. ANOVA with a Brown–Forsythe post-hoc test for multiple comparisons was performed to determine statistical significance ($****P < 0.0001$ as indicated). **c**, Immunofluorescence staining of *GSTT1*, Ki67 and cytokeratin 19 in human PDA-derived liver DTCs. **d**, Quantification of **c**, presented as the average of 10 fields ($\times 20$ magnification) for PDA patient no. 4. Data are presented as mean and s.d. ANOVA with a Brown–Forsythe post-hoc test for multiple comparisons was performed to determine statistical significance ($****P < 0.0001$ as shown). **e**, Immunofluorescence staining of *Gstt1* and cytokeratin 19 in two PDAC-derived macrometastatic lesions from the same tumour-bearing liver (left) and immunofluorescence staining of *Gstt1* and PCNA in the same lesions (right). **f**, Quantification of cell populations, presented

as the average of five fields per $n = 11$ independent liver and lung metastatic lesions ($\times 10$ magnification). Data are presented as mean and s.d. ANOVA with a Brown–Forsythe post-hoc test for multiple comparisons was performed to determine statistical significance ($****P < 0.0001$ as indicated). **g**, Flow sorting of lung metastatic cell populations two days and seven days post-incubation with the membrane dye CM-Dil (D0). **h**, Expression of *Gstt1* and *Ki67* in CM-Dil⁺ and CM-Dil⁻ sorted populations from **g** relative to D0 CM-Dil. Data points represent four independent sorting experiments in one cell line. Data are presented as mean and s.e.m. A two-sided *t*-test was used to determine statistical significance between groups ($*P = 0.0365$, $*P = 0.0171$ as indicated). **i**, H&E image (left) and immunofluorescence staining of cytokeratin 19, Ki67 and *GSTT1* in liver metastatic core from a human PDA tissue microarray (right). **j**, Quantification of the average number of cell populations per field in each TMA core, for independent abdominal and liver metastatic cores (stage IV, $n = 8$). Data are presented as mean and s.d. A two-sided *t*-test was used to determine statistical significance between groups ($*P = 0.0149$; $****P < 0.0001$ as indicated).



DTCs, we euthanized the mice at early timepoints (Fig. 2h,i). We found that depleting *Gstt1* resulted in significantly fewer disseminated single cells and clusters; conversely, overexpressing *Gstt1* enhanced the number of DTCs (Fig. 2j,k).

To determine the role of *Gstt1* in spontaneous tumour cell dissemination, we knocked down *Gstt1* in our primary tumour-derived PDAC cell lines and performed orthotopic injections into the pancreas. These mice develop a large primary tumour burden requiring euthanasia before the development of overt metastases; however, this model system allows for the detection of disseminated tumour cells (Extended Data Fig. 4a). As previously observed in our BC mouse model, *Gstt1* knockdown had no significant effect on primary tumour size (Extended Data Fig. 4b,c). Control-treated cells readily disseminated and we were able to detect both single and small groups of CK19⁺ DTCs (Extended Data Fig. 4d,f), which, unlike the primary tumour (Extended Data Fig. 4f, left), stained positive for *Gstt1* (Extended Data Fig. 4f, middle). Depleting *Gstt1* resulted in significantly fewer spontaneous DTCs (Extended Data Fig. 4d,e). Together, these results underline the requirement for *Gstt1* following escape from the primary tumour, allowing for the dissemination and survival of DTCs in the metastatic niche.

Gstt1^{high} cells represent a slow-cycling metastatic subpopulation

A growing body of evidence suggests that DTCs undergo a period of quiescence in the target organ, where a few cells may 'reawaken', leading to overt metastases^{17,19}. We stained for the proliferation marker proliferating cell nuclear antigen (PCNA) to assess the cycling status of *Gstt1*-positive DTCs. The majority of *Gstt1*-positive DTCs were PCNA-negative in our spontaneous GEMM (Fig. 3a,b), experimental (Extended Data Fig. 5a–c) and orthotopic models (Extended Data Fig. 4f, right). Similarly, GSTT1-positive human DTCs identified in liver tissue also stained negative for the proliferation marker, Ki67 (Fig. 3c,d).

Next, we analysed tissues with a high metastatic burden for *Gstt1* and proliferation markers. Immunofluorescence imaging of CK19-positive PDAC metastatic lesions demonstrated that *Gstt1* is heterogeneously expressed both within individual lesions and across metastatic lesions (Fig. 1j and Extended Data Fig. 2n). Interestingly, *Gstt1*^{high} cells were associated with a CK19^{low} phenotype, where a single organ contained both *Gstt1*^{high}/CK19^{low} and *Gstt1*^{low}/CK19^{high} metastases (Fig. 3e, left), a phenomenon previously observed in non-proliferating PDAC DTCs⁸. Furthermore, the majority of *Gstt1*^{high} cells were PCNA-negative (~95%), suggesting a slow-cycling state in *Gstt1*^{high} metastatic cells coexisting with *Gstt1*^{low}/PCNA^{high} subpopulations (Fig. 3e, right, and Fig. 3f). To further quantify the cycling profile of *Gstt1*, we labelled our PDAC-derived lung metastatic cell lines with

the membrane dye, CM-Dil³¹. In vitro cultures of labelled cells demonstrated a dilution of the membrane dye over time, resulting in two distinct populations (Fig. 3g and Extended Data Fig. 5d). CM-Dil⁺ and CM-Dil⁻ populations were then isolated by FACS and analysed for the expression of *Gstt1* and *Ki67*. qPCR demonstrated that CM-Dil⁺ cells (day 7 post-labelling) have higher *Gstt1* expression and lower *Ki67* expression than CM-Dil⁻ cells (Fig. 3h). Together, these results indicate that *Gstt1* marks a slow-cycling metastatic population.

To assess whether this heterogeneity is conserved in human metastases, we analysed PDA-derived metastatic TMA cores for CK19, GSTT1 and Ki67. Immunofluorescence staining demonstrated intratumoral heterogeneity, where, similar to the pattern we observed in mouse metastatic tumours, GSTT1^{high} cells are found to be largely non-proliferative (~80%; Fig. 3i,j), validating the presence of a slow-cycling, GSTT1^{high} cell population in human metastases.

Slow-cycling *Gstt1*^{high} cells are enriched for EMT signatures

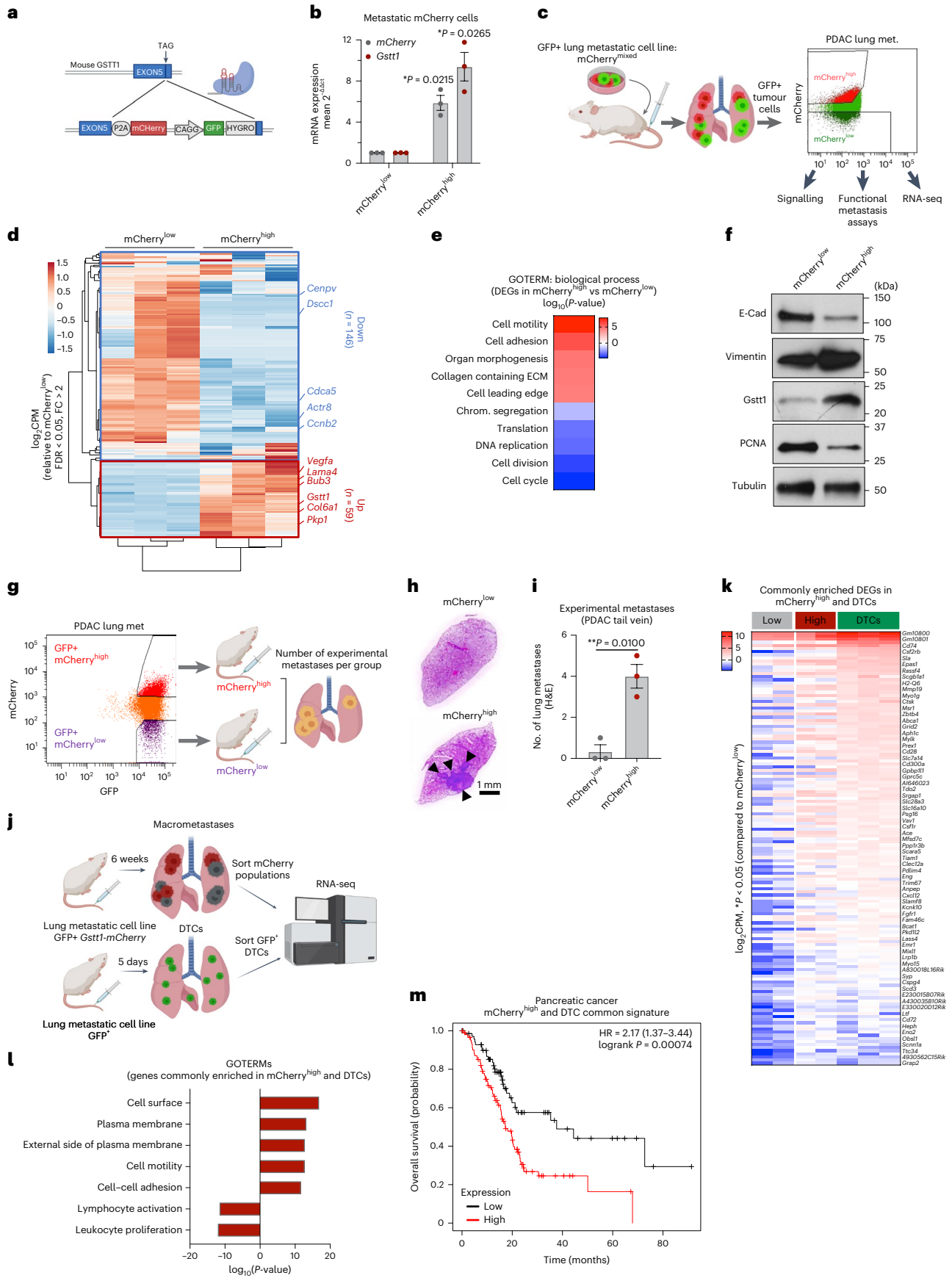
To dissect the functional and molecular features of the *Gstt1*^{high} metastatic subpopulation, we tagged the endogenous mouse *Gstt1* locus with an *mCherry* reporter (Fig. 4a). As proof of principle, in vitro sorting of *mCherry* populations in tagged PDAC-derived lung metastatic cells demonstrated enriched *mCherry* and *Gstt1* expression in the *mCherry*^{high} population (Fig. 4b). To analyse gene expression in *Gstt1*^{high} and *Gstt1*^{low} subpopulations as they exist in vivo, we first injected green fluorescent protein (GFP)-positive, *Gstt1*-*mCherry*-expressing PDAC-derived lung metastatic cells via the tail vein to generate lung metastases. Upon clinical evidence of macrometastases, the lungs were dissociated and GFP⁺ cells (tumour cell marker) were sorted into *mCherry*^{low} (bottom 20%) and *mCherry*^{high} (top 20%) populations for bulk RNA-seq and functional metastasis experiments (Fig. 4c and Extended Data Fig. 6a). Unsupervised principal component analysis (PCA) identified differentially expressed transcriptional signatures in *mCherry*^{high} and *mCherry*^{low} populations consistent with enriched *Gstt1* expression in *mCherry*^{high} tumour cells (Extended Data Fig. 6b, Fig. 4b and Supplementary Table 2). *mCherry*^{high} downregulated signatures included genes involved in cell-cycle and cell-division pathways (*Cenpv*, *Dsccl*, *Cdca5*, *Actr8* and *Ccnb2*), further supporting the slow-cycling nature of *Gstt1*^{high} cells (Fig. 4d,e). Additionally, *mCherry*^{high} cells were enriched in pathways involved in cell motility and cell adhesion (*Vegfa*, *Lama4*, *Col6a1* and *Pkpl1*; Fig. 4d,e), suggesting higher dissemination and metastatic potential.

In addition to cell-cycle pathways, gene set enrichment analysis (GSEA) of the *mCherry*^{high} population identified an EMT, transforming growth factor- β (TGF- β) and an angiogenesis gene expression

Fig. 4 | *Gstt1*^{high} cells represent a slow-cycling, aggressive metastatic subpopulation and retain features of latent DTCs. a, Diagram depicting Cas9 targeting of *mCherry* into the endogenous mouse *Gstt1* locus. b, qRT-PCR expression levels of *mCherry* and *Gstt1* in lung metastatic cells stably expressing the *Gstt1*-*mCherry* construct from three independent sorting experiments. Data are presented as mean and s.e.m. A two-sided *t*-test was used to determine statistical significance between groups (**P* = 0.0215, ***P* = 0.0265, as indicated). c, PDAC-derived lung metastatic cells generated to express GFP⁺ and tagged *Gstt1*-*mCherry* were injected via the tail vein into SCID mice. GFP⁺ tumour cells were isolated from surrounding lung stroma using FACS. The top (20%) *mCherry*^{high} and bottom (20%) *mCherry*^{low} tumour cell populations were sorted and collected for signalling experiments, functional metastasis assays, and bulk RNA-seq. Created with Biorender.com. d, Heatmap and hierarchical clustering depicting differentially expressed genes (DEGs) enriched in the *mCherry*^{high} population (log₂(CPM), relative to average *mCherry*^{low}, >2FC; FDR 0.05). Data represent *n* = 3 independent sorting experiments from *n* = 3 mice per group. e, GO_TERM (Biological Process) pathways enriched (red) and downregulated (blue) in *mCherry*^{high} metastatic cells (ranked by log₁₀(*P* value); unpaired, two-sided *t*-test using Bonferroni correction). f, Western blot analysis of the indicated proteins in sorted *mCherry*^{high} and *mCherry*^{low} populations. g, *mCherry*^{high} and

mCherry^{low} populations were sorted and injected via the tail vein into SCID mice to generate experimental metastases to the lung. Created with Biorender.com. h, Representative image of H&E-stained lungs from each experimental group. i, Quantification of metastatic burden in the H&E-stained slides, *n* = 3 mice per group. Data are represented as mean and s.e.m. A two-sided *t*-test was used to determine statistical significance between groups (***P* = 0.010, as indicated). j, Schematic depicting isolation of GFP⁺ DTCs for a gene expression comparison to *mCherry*^{low} and *mCherry*^{high} macrometastatic populations. Created with Biorender.com. k, Heatmap depicting commonly enriched genes in DTCs and *mCherry*^{high} populations (*n* = 139 DEGs) compared to *mCherry*^{low} populations (log₂(CPM), >2FC). A negative binomial test was used to calculate *P* values (**P* < 0.05 values are listed in Supplementary Table 4). l, GOTERM gene signatures of commonly enriched and downregulated DTCs and in *mCherry*^{high} macrometastatic cells (ranked by log₁₀(*P* value) using an unpaired, two-sided *t*-test with post-hoc Bonferroni correction. m, Top upregulated genes common to DTCs and *mCherry*^{high} cells (FDR 0.05; >2FC, *n* = 40) were analysed for impact on overall survival in pancreatic cancer (KMplot). Data represent overall survival in an *N* = 177 patient dataset based on mean expression of selected genes. A Mantel-Haenszel log-rank test was used to determine significance. **P* = 0.00074.

mCherry^{low} populations were sorted and injected via the tail vein into SCID mice to generate experimental metastases to the lung. Created with Biorender.com. h, Representative image of H&E-stained lungs from each experimental group. i, Quantification of metastatic burden in the H&E-stained slides, *n* = 3 mice per group. Data are represented as mean and s.e.m. A two-sided *t*-test was used to determine statistical significance between groups (***P* = 0.010, as indicated). j, Schematic depicting isolation of GFP⁺ DTCs for a gene expression comparison to *mCherry*^{low} and *mCherry*^{high} macrometastatic populations. Created with Biorender.com. k, Heatmap depicting commonly enriched genes in DTCs and *mCherry*^{high} populations (*n* = 139 DEGs) compared to *mCherry*^{low} populations (log₂(CPM), >2FC). A negative binomial test was used to calculate *P* values (**P* < 0.05 values are listed in Supplementary Table 4). l, GOTERM gene signatures of commonly enriched and downregulated DTCs and in *mCherry*^{high} macrometastatic cells (ranked by log₁₀(*P* value) using an unpaired, two-sided *t*-test with post-hoc Bonferroni correction. m, Top upregulated genes common to DTCs and *mCherry*^{high} cells (FDR 0.05; >2FC, *n* = 40) were analysed for impact on overall survival in pancreatic cancer (KMplot). Data represent overall survival in an *N* = 177 patient dataset based on mean expression of selected genes. A Mantel-Haenszel log-rank test was used to determine significance. **P* = 0.00074.



signature, previously identified as critical features of latent PDA metastases⁸ (Extended Data Fig. 6c). This was confirmed in our mCherry populations via western blot, with an enrichment in vimentin (EMT marker) and a downregulation of E-cadherin in *Gstt1*^{high}/*CK19*^{low}/*PCNA*^{low} cells (Fig. 4f). Consistent with functional results and with *Gstt1* as a regulator of a slowly proliferating metastatic subpopulation, genome-wide transcriptional profiling on *Gstt1*-depleted metastatic cells demonstrated an enrichment in cell cycle, cell division and mitotic microtubule formation pathways (Extended Data Fig. 7a and Supplementary Table 3). Complementary to the results observed in *Gstt1*^{low} tumour cells, knocking down *Gstt1* resulted in an increase in cell-cycle genes involved in G2M transition (*Wee1*, *Cenpe*, *Ccnf* and *Kntc1*; Extended Data Fig. 7b), as well as an increase of cells in the G2M phase of the cell cycle (Extended Data Fig. 7c), together pointing to *Gstt1* as a functional regulator of metastatic cell proliferation.

Previous reports in head and neck cancer have demonstrated that slow-cycling populations function as metastasis-initiating cells^{31–33}. To directly assess the functional significance of the *Gstt1*^{high} population on metastatic phenotypes, we sorted the mCherry populations and performed soft agar assays in vitro. mCherry^{high}*Gstt1*^{high} cells were significantly more efficient at forming colonies in soft agar (Extended Data Fig. 6d,e, left), and importantly, overexpression of wild-type *Gstt1*, but not the R234G mutant in *Gstt1*^{low} cells, was sufficient to increase colony numbers to those observed in *Gstt1*^{high} cells (Extended Data Fig. 6d,e, right), corroborating our previous results demonstrating that the glutathione-transferase activity of *Gstt1* is required for the formation of experimental metastases (Extended Data Fig. 2f,g). To functionally test whether the slow-growing *Gstt1*^{high} population is more efficient at promoting metastasis, we injected equal numbers of sorted mCherry^{high} and mCherry^{low} cells via the tail vein to generate experimental lung metastases (Fig. 4g). mCherry^{high} (*Gstt1*^{high}) cells formed significantly more experimental metastases, suggesting that *Gstt1*^{high} cells have higher metastasis-initiating potential (Fig. 4h,i). To test the metastasis-initiating potential of each population, we performed limiting dilution injections of each cell population (10¹, 10² and 10³ cells per mouse) via tail vein. Notably, as few as ten cells could form experimental metastases in 75% of mice injected with mCherry^{high} cells, whereas the mCherry^{low} cells were much less efficient (Extended Data Fig. 6g,h). Together, these results indicate that *Gstt1*^{high} cells represent a highly metastatic, slow-cycling population within established metastases with enhanced EMT features.

Gstt1^{high} metastases retain latent DTC gene signatures

Because we observed the presence of *Gstt1* in both single disseminated cells (Fig. 2f,g) and in a subpopulation within macrometastases (Fig. 3e,i), we asked whether the *Gstt1*^{high} population in existing

metastases retains DTC characteristics. To test this, we compared the gene expression profiles from mCherry macrometastatic populations (Fig. 4d) to that of DTCs (Fig. 4j). DTCs were generated from experimental metastases five days after tail-vein injection, and were isolated based on GFP expression (Fig. 4j). Expression analysis comparing mCherry^{high} and DTC populations to mCherry^{low} cells demonstrated 139 commonly differentially expressed transcripts with pathways enriched in cell adhesion and migration (Fig. 4k,l and Supplementary Table 4). Strikingly, this shared transcriptional signature is associated with poor overall survival in patients with pancreatic cancer (Fig. 4m), supporting our findings that *Gstt1*^{high} cells display enhanced metastasis-initiating capabilities.

To determine whether *Gstt1*^{high} metastatic cells retain dissemination signatures, we applied our transcriptional profiles to a gene expression dataset found to be important for early breast cancer dissemination¹². We found that mCherry^{high}/*Gstt1*^{high} cells retained several early dissemination markers (*Myo9a*, *Dclre1c*, *Ahnak*, *Ddx46* and *Rpb1*), to similar levels seen in DTCs (Extended Data Fig. 7d), which, together with cell adhesion and migration gene signatures, could explain the enhanced metastasis-initiating potential observed in mCherry^{high}/*Gstt1*^{high} cells. Indeed, high expression of this five-gene dissemination signature was associated with poor overall survival in patients with PDA (Extended Data Fig. 7e), underscoring the impact of early dissemination on patient survival. This was associated with a decreased proliferation signature in mCherry^{high} cells, with transcript levels of *Ki67*, *Wee1* and *Pcna* comparable to those of latent DTCs (Extended Data Fig. 7f). Altogether, these results demonstrate that the *Gstt1*^{high} subpopulation within established metastases is a slow-cycling subpopulation that retains latent disseminated cell features and enhanced metastasis-initiating potential.

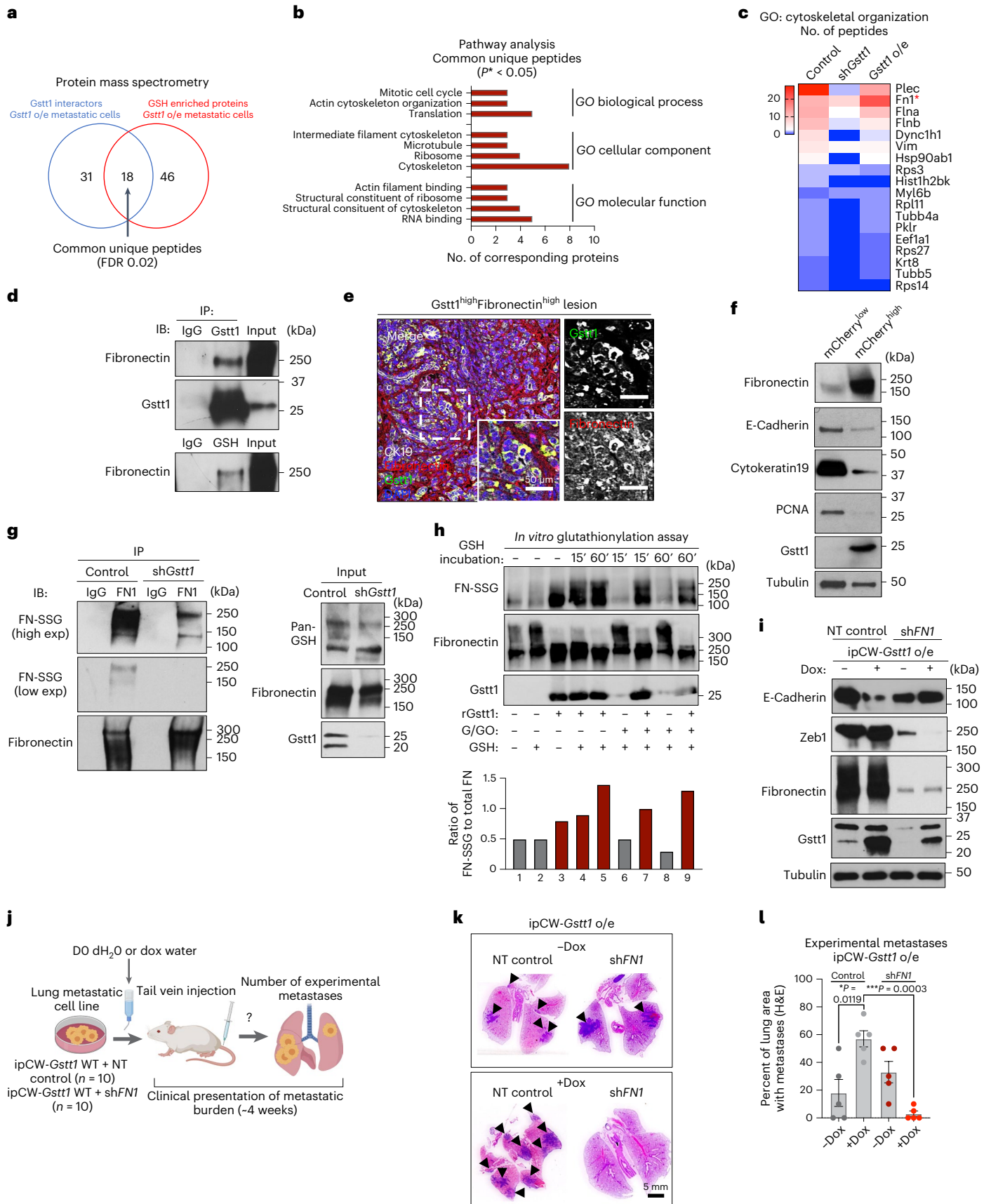
GSTT1 glutathione-modifies fibronectin to promote metastasis

Although GSTT1 is known for detoxifying xenobiotic compounds^{27,29,34}, its role in metastatic lesions remains unknown. To define specific functions for GSTT1 in metastatic tumours, we investigated potential interactors and protein substrates of this glutathione transferase. Extracts from PDAC-derived liver and lung metastatic cell lines were immunoprecipitated using an anti-*Gstt1* or pan-glutathione antibody (anti-GSH) followed by mass spectrometry (MS) analysis (Extended Data Fig. 8a and Supplementary Table 5). We identified 18 commonly enriched peptides between both *Gstt1* and GSH pull-downs (Fig. 5a). Strikingly, the top commonly enriched peptides encode for proteins involved in cytoskeletal and cell junction pathways (Fig. 5b). These structural proteins include plectin, fibronectin, filamin A, filamin B and vimentin, with fibronectin demonstrating the highest enrichment in *Gstt1*-overexpressing cells (Fig. 5c). Endogenous fibronectin (Fig. 5d)

Fig. 5 | *Gstt1* interacts with and glutathione-modifies fibronectin to enhance metastasis.

a, Lung and liver metastatic cell lines stably expressing wild-type ipCW-*Gstt1* were subjected to immunoprecipitation using a *Gstt1* and pan-glutathione (GSH) antibody. Pull-downs were analysed for peptide interactors using unbiased MS, which identified 18 unique peptides commonly enriched in conditions (performed in $n = 2$ independent cell lines; FDR 0.02). **b**, Eighteen commonly enriched peptides mainly fell into gene pathways encoding cytoskeletal, cell junction and structural molecule activity proteins (GO_TERMs, unpaired, two-sided t -test using Bonferroni correction). **c**, Heatmap depicting the number of unique peptides per treatment group as identified by MS. Data represent results from two independent cell lines. **d**, *Gstt1* and GSH pull-downs in liver metastatic cells were blotted for validation of the interaction with fibronectin. Data represent a minimum of three independent experiments. **e**, Confocal imaging of immunofluorescence staining of *Gstt1*, fibronectin and cytokeratin 19 in a PDAC mouse liver metastatic tumour region. A minimum of five metastatic lesions across three independent mice were analysed for co-staining. Scale bar insets: 50 μ m. **f**, Western blot analysis of the indicated proteins in FACS-sorted mCherry^{high} and mCherry^{low} populations. Data are

representative of $n = 3$ independent sorting experiments. **g**, Left: fibronectin pull-downs in whole-cell lysate from liver metastatic cells were immunoblotted using both fibronectin and pan-GSH antibody. Right: input controls. Data are representative of a minimum of three independent experiments. **h**, Top: in vitro glutathionylation assay followed by western blot utilizing purified fibronectin and recombinant human *Gstt1*. Bottom: quantification of the ratio of FN-SSG to total fibronectin, showing results from a single in vitro assay. Each lane represents an independent FN-SSG reaction. **i**, Western blot in liver metastatic cells stably expressing control or ipCW-*Gstt1* and a non-targeting control or sh*FN1*. Data represent a minimum of three independent experiments. **j**, Schematic describing experimental metastasis using cell lines from **i**. All groups were euthanized when the first group demonstrated clinical signs of metastasis, and the lungs were analysed via H&E for metastatic burden. Created with [Biorender.com](https://www.biorender.com). **k**, Representative H&E images of lung metastatic burden from the experiment in **j**. **l**, Lung metastatic burden was evaluated using H&E and represented as total lung tissue area versus the metastatic tissue area. Data are presented as mean and s.e.m. A two-sided t -test was used to determine statistical significance between groups ($*P = 0.0119$, $***P = 0.003$, as indicated).



and plectin (Extended Data Fig. 8b) were validated in both Gsst1 and GSH pull-downs from mouse metastatic lysates. Furthermore, although no difference in *FNI* mRNA expression was observed between mCherry^{high} and mCherry^{low} populations (Extended Data Fig. 8c), downstream integrin cell-surface genes were enriched in mCherry^{high} cells (Extended Data Fig. 8d), highlighting the importance of fibronectin signalling in Gsst1^{high} metastatic cells.

Fibronectin is a glycoprotein abundantly present in the extracellular matrix (ECM) of primary and metastatic tumours. It is commonly secreted by pancreatic stellate cells³⁵ and aligned by cancer associated fibroblasts (CAFs)³⁶, a mechanism important for establishing a permissive DTC niche^{37,38}. A few studies have demonstrated that tumour cells can assemble and deposit fibronectin into the tumour microenvironment³⁹, as a mechanism to facilitate metastasis. To analyse fibronectin localization in our metastatic tumours, we performed confocal imaging of liver sections containing multiple metastases and, as expected, identified extracellular fibronectin fibrils localized in the periphery of metastatic lesions (Fig. 5e and Extended Data Fig. 8e). Surprisingly, we also detected co-localization of intracellular fibronectin exclusively within Gsst1^{high} tumour cells (Fig. 5e and Extended Data Fig. 8e). This enrichment of intracellular fibronectin was confirmed in sorted mCherry^{high} cells (Fig. 5f). Of note, in primary tumours, intracellular fibronectin was present in both Gsst1-devoid tumour cells and in the tumour periphery⁴⁰ (Extended Data Fig. 8f), suggesting a Gsst1-independent role for fibronectin in primary tumour biology.

We next assessed whether Gsst1 directly glutathione-modifies fibronectin. Indeed, we detected glutathione modification on fibronectin in metastatic-cell lysates (hereon referred to as FN-SGS), and this modification was significantly reduced following inhibition of *Gsst1* (Fig. 5g). To definitively test whether GSTT1 could S-glutathionylate fibronectin, we performed an in vitro glutathionylation assay (Fig. 5h). The reduced form of commercial fibronectin was incubated with human recombinant GSTT1 (rGSTT1) in the presence or absence of 5 mM glutathione (GSH), 280 μM glucose (G) or 10 mU ml⁻¹ glucose oxidase (G/GO) for either 15 or 60 min. The G/GO system was used to generate low fluxes of hydrogen peroxide (H₂O₂) to prevent overoxidation of cysteines that are no longer available for glutathionylation. Following incubation, samples were subjected to western blotting under non-reducing conditions to assess the FN-SGS levels. In the absence of GSTT1, addition of glutathione (GSH) to fibronectin did not increase FN-SGS. Surprisingly, the addition of GSTT1 to fibronectin was sufficient to elicit FN-SGS, even in the absence of exogenous GSH or G/GO, suggesting that GSTT1 was pre-bound to glutathione and that exposure to aerobic conditions during the reaction may have been sufficient to allow cysteine sulfenic acid formation on the

fibronectin. Incubation of GSTT1 with fibronectin and glutathione (GSH) for 60 min resulted in modest additional increases in FN-SGS. Importantly, G/GO plus GSH (conditions that are sufficient to induce protein S-glutathionylation (PSSG) over time) in the absence of GSTT1 did not induce FN-SGS within this timeframe. In contrast, addition of GSTT1 to the GSH/G/GO reaction mix led to strong increases in FN-SGS, providing conclusive evidence for the glutathione-conjugating activity of GSTT1 on a fibronectin substrate (Fig. 5h). Although additional studies are required to address the modification site and structural requirements for GSTT1 to catalyse FN-SGS, these observations clearly demonstrate that GSH-bound GSTT1 in an aerobic environment is sufficient to induce FN-SGS.

To further assess whether Gsst1 enzymatic activity is required for FN-SGS, we performed immunoprecipitation of fibronectin in the presence of wild-type *Gsst1* and the *Gsst1* catalytically dead mutant, *Gsst1*-R234G. In the context of wild-type *Gsst1* overexpression, we were able to detect FN-SGS, and the modification was absent in the context of the *Gsst1* catalytically dead mutant (Extended Data Fig. 8g). This result was verified by immunofluorescence staining for fibronectin and glutathione. In *Gsst1* wild-type overexpressing cells, ~25% of fibronectin-positive cells are also positive for glutathione. This co-staining, as well as the fibronectin protein itself, were significantly reduced in *Gsst1*-R234G mutant cells (Extended Data Fig. 8h–j). Together, these results identify fibronectin as a putative Gsst1 substrate in metastatic cells.

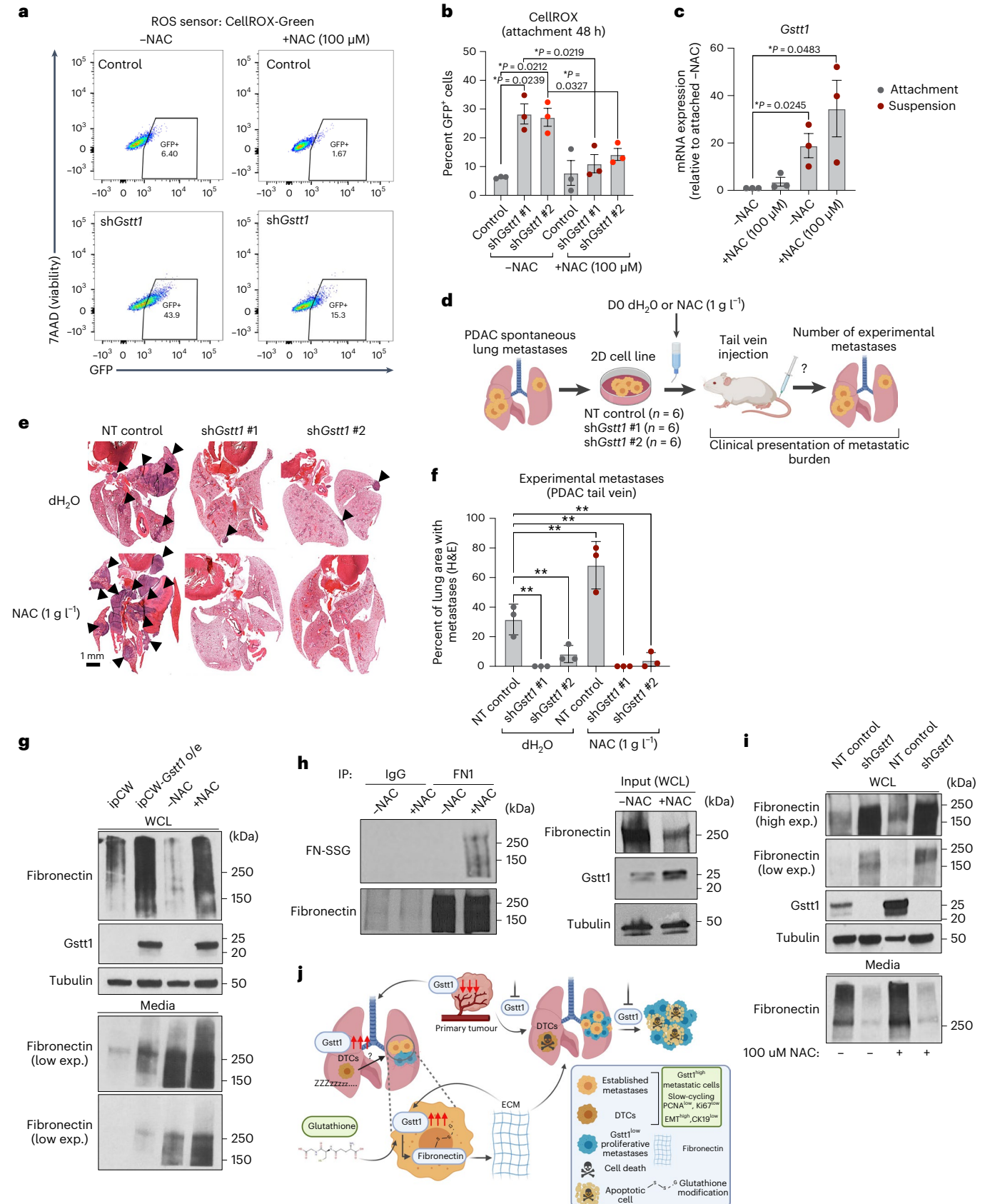
ECM proteins such as fibronectin are integral to the maintenance of a supportive metastatic niche^{37–39,41,42}. However, these studies have focused solely on the role of extracellular deposition of fibronectin fibrils. The presence of intracellular fibronectin staining largely restricted to Gsst1-positive metastatic cells (Fig. 5e,f and Extended Data Fig. 8e) suggests a biological role for fibronectin in the aggressive metastatic traits observed in this cell population. To begin to identify the functional role of intracellular fibronectin in Gsst1-induced metastasis, we knocked down fibronectin (*FNI*) in both Gsst1^{high} (*Gsst1* overexpressing and mCherry^{high} sorted cells) and Gsst1^{low} metastatic cell lines. *FNI* depletion demonstrated that mCherry^{high}/Gsst1^{high} cells are dependent on fibronectin for soft agar growth (Extended Data Fig. 9a,b), as well as EMT status (Fig. 5i and Extended Data Fig. 9c). Of note, *FNI* knock-down resulted in a concomitant reduction in Gsst1 levels (Fig. 5i and Extended Data Fig. 9c), suggesting a feedback mechanism in which Gsst1 regulates fibronectin secretion, in turn influencing Gsst1 levels in metastatic cells. To directly assess whether glutathionylation of fibronectin by Gsst1 regulates its secretion, we measured fibronectin deposition upon overexpression or knockdown of *Gsst1* using an enzyme-linked immunosorbent assay (ELISA) as well as western

Fig. 6 | Glutathione availability dictates Gsst1 expression to enhance fibronectin deposition and promote metastasis. **a**, Metastatic cells were grown for 48 h under 2D attachment conditions with or without 100 μM NAC. Representative CellROX flow plot images are shown. **b**, Quantification of percent GFP⁺ cells using CellROX-Green analysed by flow cytometry. Data are presented as mean and s.e.m. A two-sided *t*-test was used to determine statistical significance between groups (**P* = 0.0239, **P* = 0.0212, **P* = 0.0219, **P* = 0.0327, as indicated). Data are representative of a minimum of three independent experiments. **c**, Gsst1^{low} mouse PDAC-derived metastatic cells were treated with either dH₂O control or 100 μM NAC under 2D attachment or low-attachment ‘suspension’ conditions for 48 h. The results are from a qRT-PCR analysis for *Gsst1*. Data are presented as mean and s.e.m. A two-sided *t*-test was used to determine statistical significance between groups (**P* = 0.0245, **P* = 0.0483, as indicated). Data are representative of a minimum of three independent experiments. **d**, SCID mice were injected via tail vein (1 × 10⁴ cells) to generate experimental metastases. Groups were randomly segregated and given either control dH₂O or NAC (1 g l⁻¹) in drinking water. All groups were euthanized when the first group demonstrated clinical signs of metastasis. Lungs were collected and analysed via H&E for metastatic burden. Created with [BioRender.com](#).

e, Representative H&E images of lung metastatic burden from **d**. **f**, Lung metastatic burden was evaluated using H&E and represented as total lung tissue area versus metastatic tissue area. Data are presented as mean and s.d. Statistical significance of all groups compared to NT control (–NAC) was determined using ANOVA with Brown–Forsythe post-hoc test for multiple comparisons (***P* = 0.0015, applicable to all conditions compared to NT control). **g**, Gsst1^{low} mouse PDAC-derived metastatic cells were treated with either dH₂O control or 100 μM NAC under 2D attachment conditions for 48 h or induced with doxycycline to express ipCW control or the ipCW-*Gsst1* construct. Cell lysates and conditioned media were subjected to western blotting for the indicated antibodies. **h**, Mouse PDAC-derived metastatic cells were treated with either dH₂O control or 100 μM NAC for 48 h under attachment conditions. Cell lysates were subjected to immunoprecipitation (IP) of fibronectin. IPs were then analysed for FN-SGS using pan-glutathione antibody (GSH), fibronectin and Gsst1. **i**, Cell lysates from mouse PDAC-derived metastatic cells expressing either NT control vector or *Gsst1* shRNA were treated with either dH₂O control or 100 μM NAC for 48 h. Cell lysates and matching conditioned media were subjected to western blotting for the indicated antibodies. **j**, Model. Created with [BioRender.com](#).

blotting from cell-conditioned media. *Gstt1* knockdown significantly reduced the extracellular deposition of fibronectin, whereas *Gstt1* overexpression led to an increase that was dependent on intracellular *FNI* expression (Extended Data Fig. 9d,e).

To directly assess whether *Gstt1* acts through fibronectin to promote metastasis, we injected control or *Gstt1*-overexpressing cells in the context of *FNI* knockdown via tail vein to generate experimental lung metastases (Fig. 5j). Notably, *FNI* knockdown alone did not reduce



the number of macrometastases in *Gstt1*^{low}-expressing metastatic cells, suggesting that tumour-cell derived fibronectin is not universally required for metastasis in PDAC. However, *FNI* knockdown completely rescued the increased metastases we observed in *Gstt1*-overexpressing cells, highlighting tumour-cell-derived fibronectin as an important mediator of metastasis in *Gstt1*^{high} cells (Fig. 5k,l).

Glutathione availability enhances *Gstt1* expression and fibronectin deposition to promote metastasis

Recent studies have identified oxidative stress as a major bottleneck to colonization and metastasis^{43,44}. Glutathione is not only the major cellular antioxidant used to counter cellular reactive oxygen species (ROS), but also serves as a glutathione substrate for GSTs⁴⁵. To directly assess the link between *Gstt1* and oxidative stress in pancreatic metastasis, we performed oxidative stress measurements in *Gstt1*-depleted metastatic cells under both two-dimensional (2D) attachment and suspension conditions using CellROX. At 48 h after plating, *Gstt1* inhibition resulted in an increase in cellular ROS under both attachment and suspension conditions, which were reduced to baseline levels with the addition of the glutathione precursor and ROS scavenger *N*-acetyl cysteine (NAC; Fig. 6a,b and Extended Data Fig. 10a). Interestingly, analysis of *Gstt1* mRNA expression under attachment and suspension conditions demonstrated that *Gstt1*^{low} metastatic cells grown under low-attachment conditions had increased *Gstt1* expression compared to cells grown in two dimensions (Fig. 6c and Extended Data Fig. 10b). Furthermore, 48-h treatment with NAC alone enhanced *Gstt1* mRNA expression under attachment conditions and contributed to a more significant increase in *Gstt1* protein levels in suspension (Fig. 6c and Extended Data Fig. 10b,c). Together, these results suggest that *Gstt1* is induced and employed as a mechanism to combat cellular oxidative stress in metastatic cells.

We next sought to investigate whether elevated intracellular ROS plays a role in the increased metastatic phenotype observed in *Gstt1*-depleted cells. To address this question, we injected pancreatic metastasis-derived cells expressing control or two individual shRNAs targeting *Gstt1* via tail vein into NOD.Cg-Prkdcscid/J (SCID) mice to generate lung metastases. On the day of injection, mice were randomly segregated into groups, with one set of mice given the glutathione-precursor NAC in drinking water (1 g l⁻¹)^{43,44} (Fig. 6d). Similar to the reported results for other tumour types^{43,44,46}, NAC treatment enhanced the number of metastases in control cells (Fig. 6e,f). However, NAC treatment failed to rescue metastasis in *Gstt1*-depleted cells, suggesting that although oxidative stress is attenuated (Fig. 6a,b), in the absence of the enzyme, the addition of the substrate (that is, glutathione) is not sufficient to rescue metastasis (Fig. 6e,f).

These results led us to further investigate the role of glutathione in *Gstt1*-dependent fibronectin deposition in metastatic cells. Analysing the total levels of fibronectin in both cell lysates and conditioned media demonstrated that NAC addition resulted in increased fibronectin deposition into the extracellular space, mimicking effects seen in cells generated to overexpress *Gstt1* (Fig. 6g) and suggesting that glutathione availability upstream of *Gstt1* is important for fibronectin deposition as part of the metastatic process. Next, to directly assess whether the increased *Gstt1* expression observed in response to NAC influences FN-SSG, we immunoprecipitated fibronectin in metastatic cells treated with or without 100 μM NAC for 48 h, followed by western blotting using a pan-glutathione antibody. Our results demonstrate that NAC treatment not only induces *Gstt1* expression, but also leads to intracellular FN-SSG in metastatic cells (Fig. 6h), similar to effects seen after glutathione addition in vitro (Fig. 5h). To determine whether *Gstt1* is required for glutathione-dependent fibronectin deposition, we analysed the total levels of fibronectin in cell lysates and conditioned media from control and *Gstt1*-depleted cells in the presence or absence of NAC. Our results indicate that fibronectin deposition into the media in response to NAC requires *Gstt1* (Fig. 6i), and, as our

feedback mechanism suggests, the failure of NAC to rescue metastasis in *Gstt1*-depleted cells is probably due to the inability of these cells to produce FN-SSG and deposit fibronectin into the extracellular metastatic tumour microenvironment. Altogether, our data support a mechanism whereby expression of *Gstt1* in metastatic cells in the presence of available glutathione modifies fibronectin to promote an ECM that supports metastatic cell survival, and it is this modification of fibronectin by *Gstt1*, rather than protection against oxidative stress, that defines *Gstt1* as a critical modulator of metastatic disease (Fig. 6j).

Discussion

Utilizing mouse models of spontaneous metastasis, we have developed a targeted, loss-of-function screen to identify the non-genetic factors that are important for metastatic cell growth. Although our study focuses primarily on PDAC, these genes were found to be important for both pancreatic and breast cancer-derived metastases, suggesting a requirement for metastatic success across cancer types. Validation in human metastatic PDA studies and their effect on patient survival highlight their specific requirement for metastatic growth. We identify *Gstt1* as being enriched in metastatic lesions, acting as a modulator of a subpopulation of slow-cycling metastatic cells. In vivo studies demonstrate a specific requirement for *Gstt1* for metastatic growth and dissemination, though it is dispensable, if not deleterious, for primary tumour growth. We observed that a large majority of DTCs express *Gstt1* and that the characteristics of slow-cycling disseminated cells are retained within the *Gstt1*^{high} subpopulation of established macrometastatic lesions. This subset of CK19^{low}*Gstt1*^{high} cells appears to be slow cycling, EMT-enriched and highly metastatic. Mechanistically, we find that *Gstt1* interacts with and glutathione-modifies intracellular fibronectin, influencing fibronectin deposition into the metastatic tumour microenvironment in a mechanism that is critical to driving metastasis. Previous work has postulated that most of the fibronectin contribution in the metastatic niche comes from pancreatic stellate cells³⁵ and CAFs^{38,41}. Our work challenges this notion, indicating that the tumour cells within the metastatic niche appear to play a critical role in the secretion and deposition of fibronectin into the ECM. Consistent with our results, at least one previous study found fibronectin in both tumour cells^{39,47} and the stroma of the primary tumour niche⁴⁷, implicating fibronectin in metastatic spread.

One of the critical steps of cancer metastasis requires the ability of cells to survive and disseminate in circulation following detachment from an ECM⁴⁸. This detachment-associated cell death is often a result of the induction of oxidative stress^{48,49}. We observe that both low-attachment conditions and treatment with a glutathione-precursor, NAC, result in the induction of *Gstt1* expression (Fig. 6c and Extended Data Fig. 10b,c). This could explain our observation that *Gstt1* is dispensable for growth under 2D conditions (Extended Data Fig. 2l), but required for anchorage-independent growth, dissemination and metastasis. This phenomenon could also explain the importance of GSTT1 specifically in the metastatic context, as observed by other groups in response to NAC treatment^{43,44,46}. Under low-attachment conditions and the high oxidative environment encountered in circulation, GSTT1 may be required for metastatic success, but dispensable, if not deleterious, for primary tumour growth. The GST family has been implicated in the detoxification of metabolic by-products such as ROS, thereby protecting the cell from oxidative damage⁵⁰. GSTT1, however, has not been previously implicated in the detoxification of ROS. Our results demonstrate that a reduction in *Gstt1* levels induces oxidative stress in metastatic cells, and the addition of exogenous glutathione in the form of NAC is sufficient to quench this induction (Fig. 6a,b and Extended Data Fig. 10a). However, NAC treatment is unable to rescue the reduction in metastasis observed in response to *Gstt1* or *FNI* knockdown, indicating that GSTT1 has functions beyond quelling oxidative stress that promote successful dissemination and metastasis. Our results indicate that GSTT1 induction during

the metastatic process is mainly functioning to glutathione-modify protein substrates such as fibronectin to allow for reattachment and outgrowth in the metastatic niche, providing a mechanism linking cellular redox status to the metastatic tumour microenvironment. Future studies will shed light on the mechanisms regulating the precise ECM structural roles that glutathionylated fibronectin provides to support dissemination success and survival.

A recent single-cell lineage study in a mouse model of PDAC revealed an EMT continuum in disseminated metastases, with hybrid EMT states correlating with the most aggressive clones⁵¹. Notably, the majority of metastatic clones resided in a single transcriptional cluster. Due to the highly aggressive and rapidly metastasizing nature of their PDAC model system, their study infers that the H1 hybrid-EMT cluster may represent a latent subpopulation of metastatic cells. Interestingly, the majority of our 136 ‘metastatic signature’ genes identified within these clusters ($n = 18$) fell into the H1 category (Supplementary Table 1), with *Gstt1* expression highly enriched in metastatic clones within that cluster. Additionally, the top differentially expressed genes we found to be commonly enriched in the mCherry^{high}/*Gstt1*^{high} population and downregulated in *Gstt1* knockdown cells (*Elf3*, *Spns2*, *C77370*, *17000SIOSRik*, *Nexnif*; Supplementary Tables 2 and 3) also fall into the H1 EMT cluster, some of which are important for metastatic colonization²⁴. Our data points to three possible mechanisms for clonal selection of slow-cycling *Gstt1*^{high} cells during the metastatic process. In the first, a rare pre-existing *Gstt1*⁺ cell population in the primary tumour preferentially disseminates, and a portion of DTCs are maintained as non-proliferating *Gstt1*⁺ and others are converted into *Gstt1*^{low}/proliferating cells. The second scenario dictates an upregulation of *Gstt1* expression in DTCs during extravasation, survival and dissemination—a process that requires survival under low-attachment conditions, followed by a downregulation of expression to stimulate outgrowth. In the third scenario, *Gstt1*^{high} cells remain as such, promoting metastatic growth through a paracrine influence on neighbouring cells. Future studies will investigate the origin and dynamic selection process of *Gstt1* heterogeneity in more detail.

In summary, *Gstt1* has emerged from a loss-of-function shRNA screen as a mediator of metastatic disease. We have found that *Gstt1* is preferentially upregulated in both mouse and human metastases and functions as a specific driver of metastases, without influencing the growth of primary lesions. Effective treatments for eliminating metastases are limited due to clonal heterogeneity in primary tumours and across metastatic tumours as well as the slow-cycling nature and lack of detection methods for disseminated cells. The identification of this subpopulation required for the maintenance of established metastases provides insight into metastatic heterogeneity and a strong rationale for the targeting of *Gstt1* to treat metastatic disease.

Online content

Any methods, additional references, Nature Portfolio reporting summaries, source data, extended data, supplementary information, acknowledgements, peer review information; details of author contributions and competing interests; and statements of data and code availability are available at <https://doi.org/10.1038/s41556-024-01426-7>.

References

- Weiss, L. Metastatic inefficiency. *Adv. Cancer Res.* **54**, 159–211 (1990).
- Anderson, R. L. et al. A framework for the development of effective anti-metastatic agents. *Nat. Rev. Clin. Oncol.* **16**, 185–204 (2019).
- Lambert, A. W., Pattabiraman, D. R. & Weinberg, R. A. Emerging biological principles of metastasis. *Cell* **168**, 670–691 (2017).
- Maddipati, R. & Stanger, B. Z. Pancreatic cancer metastases harbor evidence of polyclonality. *Cancer Discov.* **5**, 1086–1097 (2015).
- Makohon-Moore, A. P. et al. Limited heterogeneity of known driver gene mutations among the metastases of individual patients with pancreatic cancer. *Nat. Genet.* **49**, 358–366 (2017).
- McDonald, O. G. et al. Epigenomic reprogramming during pancreatic cancer progression links anabolic glucose metabolism to distant metastasis. *Nat. Genet.* **49**, 367–376 (2017).
- Roe, J. S. et al. Enhancer reprogramming promotes pancreatic cancer metastasis. *Cell* **170**, 875–888 (2017).
- Pommier, A. et al. Unresolved endoplasmic reticulum stress engenders immune-resistant, latent pancreatic cancer metastases. *Science* **360**, eaao4908 (2018).
- Mostoslavsky, R. & Bardeesy, N. Reprogramming enhancers to drive metastasis. *Cell* **170**, 823–825 (2017).
- Chiou, S. H. et al. BLIMP1 induces transient metastatic heterogeneity in pancreatic cancer. *Cancer Discov.* **7**, 1184–1199 (2017).
- Maddipati, R. et al. Myc levels regulate metastatic heterogeneity in pancreatic adenocarcinoma. *Cancer Discov.* **12**, 542–561 (2022).
- Hosseini, H. et al. Early dissemination seeds metastasis in breast cancer. *Nature* **540**, 552–558 (2016).
- Klein, C. A. Parallel progression of primary tumours and metastases. *Nat. Rev. Cancer* **9**, 302–312 (2009).
- Hüsemann, Y. et al. Systemic spread is an early step in breast cancer. *Cancer Cell* **13**, 58–68 (2008).
- Rhim, A. D. et al. EMT and dissemination precede pancreatic tumor formation. *Cell* **148**, 349–361 (2012).
- Ryan, D. P., Hong, T. S. & Bardeesy, N. Pancreatic adenocarcinoma. *N. Engl. J. Med.* **371**, 2140–2141 (2014).
- Giancotti, F. G. Mechanisms governing metastatic dormancy and reactivation. *Cell* **155**, 750–764 (2013).
- Ting, D. T. et al. Single-cell RNA sequencing identifies extracellular matrix gene expression by pancreatic circulating tumor cells. *Cell Rep.* **8**, 1905–1918 (2014).
- Gao, H. et al. Forward genetic screens in mice uncover mediators and suppressors of metastatic reactivation. *Proc. Natl Acad. Sci. USA* **111**, 16532–16537 (2014).
- Kugel, S. et al. SIRT6 suppresses pancreatic cancer through control of Lin28b. *Cell* **165**, 1401–1415 (2016).
- Siegel, R. L., Miller, K. D., Fuchs, H. E. & Jemal, A. Cancer statistics, 2022. *CA Cancer J. Clin.* **72**, 7–33 (2022).
- Aslakson, C. J. & Miller, F. R. Selective events in the metastatic process defined by analysis of the sequential dissemination of subpopulations of a mouse mammary tumor. *Cancer Res.* **52**, 1399–1405 (1992).
- Gobeil, S., Zhu, X., Doillon, C. J. & Green, M. R. A genome-wide shRNA screen identifies GAS1 as a novel melanoma metastasis suppressor gene. *Genes Dev.* **22**, 2932–2940 (2008).
- van der Weyden, L. et al. Genome-wide in vivo screen identifies novel host regulators of metastatic colonization. *Nature* **541**, 233–236 (2017).
- Xia, F. et al. Genome-wide in vivo screen of circulating tumor cells identifies. *Sci. Adv.* **8**, eabo7792 (2022).
- Celià-Terrassa, T. & Kang, Y. Distinctive properties of metastasis-initiating cells. *Genes Dev.* **30**, 892–908 (2016).
- Townsend, D. M. & Tew, K. D. The role of glutathione-S-transferase in anti-cancer drug resistance. *Oncogene* **22**, 7369–7375 (2003).
- Townsend, D. & Tew, K. Cancer drugs, genetic variation and the glutathione-S-transferase gene family. *Am. J. Pharmacogenomics* **3**, 157–172 (2003).
- Allocati, N., Masulli, M., Di Ilio, C. & Federici, L. Glutathione transferases: substrates, inhibitors and pro-drugs in cancer and neurodegenerative diseases. *Oncogenesis* **7**, 8 (2018).
- Tars, K. et al. Structural basis of the suppressed catalytic activity of wild-type human glutathione transferase T1-1 compared to its W234R mutant. *J. Mol. Biol.* **355**, 96–105 (2006).

31. Pascual, G. et al. Targeting metastasis-initiating cells through the fatty acid receptor CD36. *Nature* **541**, 41–45 (2017).
 32. Ganesh, K. et al. L1CAM defines the regenerative origin of metastasis-initiating cells in colorectal cancer. *Nat. Cancer* **1**, 28–45 (2020).
 33. Perego, M. et al. A slow-cycling subpopulation of melanoma cells with highly invasive properties. *Oncogene* **37**, 302–312 (2018).
 34. Tew, K. D. & Townsend, D. M. Glutathione-S-transferases as determinants of cell survival and death. *Antioxid. Redox Signal.* **17**, 1728–1737 (2012).
 35. Amrutkar, M., Aasrum, M., Verbeke, C. S. & Gladhaug, I. P. Secretion of fibronectin by human pancreatic stellate cells promotes chemoresistance to gemcitabine in pancreatic cancer cells. *BMC Cancer* **19**, 596 (2019).
 36. Erdogan, B. et al. Cancer-associated fibroblasts promote directional cancer cell migration by aligning fibronectin. *J. Cell Biol.* **216**, 3799–3816 (2017).
 37. Efthymiou, G. et al. Shaping up the tumor microenvironment with cellular fibronectin. *Front. Oncol.* **10**, 641 (2020).
 38. Kaplan, R. N. et al. VEGFR1-positive haematopoietic bone marrow progenitors initiate the pre-metastatic niche. *Nature* **438**, 820–827 (2005).
 39. Barney, L. E. et al. Tumor cell-organized fibronectin maintenance of a dormant breast cancer population. *Sci. Adv.* **6**, eaaz4157 (2020).
 40. Hu, D. et al. Stromal fibronectin expression in patients with resected pancreatic ductal adenocarcinoma. *World J. Surg. Oncol.* **17**, 29 (2019).
 41. Sahai, E. et al. A framework for advancing our understanding of cancer-associated fibroblasts. *Nat. Rev. Cancer* **20**, 174–186 (2020).
 42. Fane, M. E. et al. Stromal changes in the aged lung induce an emergence from melanoma dormancy. *Nature* **606**, 396–405 (2022).
 43. Le Gal, K. et al. Antioxidants can increase melanoma metastasis in mice. *Sci. Transl. Med.* **7**, 308re308 (2015).
 44. Piskounova, E. et al. Oxidative stress inhibits distant metastasis by human melanoma cells. *Nature* **527**, 186–191 (2015).
 45. Arfsten, D. P., Johnson, E. W., Wilfong, E. R., Jung, A. E. & Bobb, A. J. Distribution of radio-labeled *N*-acetyl-L-cysteine in Sprague-Dawley rats and its effect on glutathione metabolism following single and repeat dosing by oral gavage. *Cutan Ocul Toxicol* **26**, 113–134 (2007).
 46. Ubellacker, J. M. et al. Lymph protects metastasizing melanoma cells from ferroptosis. *Nature* **585**, 113–118 (2020).
 47. Naba, A., Clauser, K. R., Lamar, J. M., Carr, S. A. & Hynes, R. O. Extracellular matrix signatures of human mammary carcinoma identify novel metastasis promoters. *eLife* **3**, e01308 (2014).
 48. Simpson, C. D., Anyiwe, K. & Schimmer, A. D. Anoikis resistance and tumor metastasis. *Cancer Lett.* **272**, 177–185 (2008).
 49. Labuschagne, C. F., Cheung, E. C., Blagih, J., Domart, M. C. & Vousden, K. H. Cell clustering promotes a metabolic switch that supports metastatic colonization. *Cell Metab.* **30**, 720–734 (2019).
 50. Hayes, J. D., Flanagan, J. U. & Jowsey, I. R. Glutathione transferases. *Annu. Rev. Pharmacol. Toxicol.* **45**, 51–88 (2005).
 51. Simeonov, K. P. et al. Single-cell lineage tracing of metastatic cancer reveals selection of hybrid EMT states. *Cancer Cell* **39**, 1150–1162 (2021).
- Publisher's note** Springer Nature remains neutral with regard to jurisdictional claims in published maps and institutional affiliations.
- Springer Nature or its licensor (e.g. a society or other partner) holds exclusive rights to this article under a publishing agreement with the author(s) or other rightsholder(s); author self-archiving of the accepted manuscript version of this article is solely governed by the terms of such publishing agreement and applicable law.
- © The Author(s), under exclusive licence to Springer Nature Limited 2024

Methods

This study was conducted in strict accordance with all relevant ethical guidelines and regulations. All clinical data and tumour specimens were collected and analysed in accordance with the institutional review board-approved protocol (DFHCC 13-416), to which patients provided written informed consent, and all studies were conducted in accordance with the Declaration of Helsinki. Participants were not compensated for participation in DFHCC 13-416. All animal experiments were conducted under protocol no. 2019N000111, approved by the Subcommittee on Research Animal Care at Massachusetts General Hospital. The maximal tumour size allowed under this protocol was 1,500 mm³. No tumours in our experiments exceeded this size.

RNA isolation from mouse tumours and RNA sequencing

For bulk tissue RNA-seq, flash-frozen tissues were homogenized using a benchtop homogenizer (Precellys 24, Bertin Instruments), and RNA isolation was conducted using the RNeasy Mini Kit (Qiagen, 74104). For sorted cells, YFP/GFP or Cas9-*Gstt1-mCherry*-expressing tissues were minced, enzymatically digested, serially filtered and sorted using a FACS Aria II device (BD Biosciences) and BD FACSDiva software (v.8.0.2). The obtained data were analysed using FlowJo v.10. Cells were collected into RNA isolation buffer followed by RNA isolation using the RNeasy Micro Total RNA Isolation kit (Thermo, AM1931). For RNA isolation from cell lines, cells derived from *p48-Cre/p53F/+KrasL/+ (Sirt6 WT and KO)* liver and lung metastases (see above) and grown in 2D culture were stably transduced with pLKO.1 vectors (control and sh*Gstt1* #1, sh*Gstt1* #2). RNA isolation was conducted using the RNeasy Mini Kit (Qiagen, 74104). Complementary DNA (cDNA) was synthesized and RNA-seq libraries were constructed using the TruSeq RNA Sample Prep kit from Illumina (bulk tissue, cell lines) or the SMART-Seq v4 Ultra-Low Input RNA kit to produce cDNA (Clontech, 634888) (for all sorted cell populations). Pooled libraries were quantified using the Kapa Biosystems Library Quantification kit (KK4828). Each lane of sequencing was pooled in 6-plex (six samples per lane) with unique barcodes. Pooled libraries were sequenced on the Illumina HiSeq 2000 instrument, producing ~30 million paired-end 50-bp reads per sample.

RNA sequencing analysis

STAR aligner was used to map sequencing reads to the mouse reference transcriptome (mm9 assembly)^{52,53}. Read counts over transcripts were calculated using HTSeq (v.0.6.0) based on a current Ensembl annotation file for NCBI37/mm9 assembly. Differential expression analysis was performed using EdgeR⁵⁴, and genes were classified as differentially expressed based on cutoffs of at least two folds change and FDR < 0.01 or FDR < 0.05 where indicated. Analysis of enriched functional categories among detected genes was performed using GSEA⁵⁵ and DAVID^{56,57}.

Cell lines

Mouse cell lines from primary tumours as well as lung and liver metastases were isolated from the *p48-Cre/p53F/+KrasL/+ (Sirt6 WT and KO)* and 4T1 orthotopic mouse model. The 4T1 parental cell line was purchased from ATCC (CRL#2539). Freshly isolated tumours and tissues were minced with sterile razor blades, digested with trypsin for 30 min at 37 °C, and then resuspended in RPMI 1640 medium and supplemented with 10% fetal bovine serum and 1% penicillin (100 U ml⁻¹)/streptomycin (100 Ug ml⁻¹) (Invitrogen Gibco) and seeded on plates coated with rat-tail collagen (BD Biosciences). Cells were passaged by trypsinization. All studies were performed on cells cultured for fewer than ten passages. Cells were cultured in RPMI 1640 supplemented with 10% fetal bovine serum and 1% penicillin (100 U ml⁻¹)/streptomycin (100 Ug ml⁻¹) (Invitrogen Gibco). A total of 12 independent cell lines from liver and lung metastases were used for subsequent in vitro and in vivo experiments.

Metastasis-derived human pancreatic cancer cell lines (KP3, KP4 and CFPAC1) were obtained from the Center for Molecular Therapeutics

at the Massachusetts General Cancer Center. The CFPAC1 cell line is available through ATCC (CRL#1918). Cells were cultured in RPMI 1640 medium supplemented with 10% fetal bovine serum and 1% penicillin (100 U ml⁻¹)/streptomycin (100 Ug ml⁻¹) (Invitrogen Gibco).

Targeted shRNA library preparation and lentiviral preparation

A library of 470 shRNAs targeting the top 94 genes (mouse) identified to be differentially expressed between primary tumours and metastases was assembled in the lentiviral vector pLKO.1 and obtained from the Molecular Profiling Laboratory at Massachusetts General Hospital Cancer Center. shRNA sequences for each gene target are available in Supplementary Table 6. For each gene target, five individual shRNA plasmids were obtained in 96-well format. Transfection-grade DNA was obtained for each individual shRNA plasmid by utilizing the Qiagen Plasmid Plus 96 Miniprep Kit (Qiagen, 16181). Individual lentiviruses were prepared according to the 96-well-format lentivirus shRNA Broad Institute Genetic Perturbation Platform (<https://www.broadinstitute.org/genetic-perturbation-platform>), followed by pooling five shRNA viral particles per gene target.

Anchorage-independent shRNA screen

Cells from liver (PDAC-derived, $n = 3$) and lung (PDAC-derived, $n = 3$; BC-derived, $n = 3$) metastases were plated into 96-well plates (1×10^3 cells per well). Utilizing individual shRNAs for each gene target, metastases-derived cell lines were infected with five pooled shRNA lentiviral particles in a 96-well format to establish stably expressing cells. Stable cell lines were generated by selection using puromycin ($5 \mu\text{g ml}^{-1}$) for 48 h.

After selection, metastatic cells were subjected to a soft agar colony formation assay in a 96-well format (a minimum of $n = 4$ and maximum of $n = 9$ total cell lines per gene target). After two weeks, soft agar colonies were stained using 0.05% INT-violet overnight (Sigma, I10406), counted and photographed using a Leica DMI 4000b white-light microscope. Wells were then ranked by colony number from lowest to highest. Significant differences in soft agar growth were compared to two pLKO.1 non-targeting shRNA-containing wells.

Human datasets

To analyse expression of the top 17 screen hits in human primary versus metastatic PDA, we utilized the Human Metastatic Cancer Database (HMCD) study derived from ref. 6. This dataset compares PDA primary tumour-derived cells from liver and lung metastases (EXP00257) and is available via GEO accession no. GSE63124. Expression data are represented as 'higher' in metastases versus primary tumours and 'lower' in metastases versus primary tumours or unchanged.

To determine whether expression of the top 17 screen hits correlates with relapse-free survival in pancreatic cancer, we utilized KMPlot⁵⁸. This dataset includes $n = 177$ patients of all stages. Gene effect on survival is represented as 'worse' survival in patients with high overall expression and 'better' survival in patients with higher overall expression (log-rank P value).

Lentivirus vectors and stable cell lines

Lentivirus generation and infection were performed as previously described²⁰. Stable cell lines for shRNA knockdowns were generated by infection with the lentiviral vector pLKO.1-puro carrying the shRNA sequence for scrambled (Addgene) mouse *Gstt1* (sh#1CACAACCTCACAGTTCACAATT; sh#2CGCCATTT-ATATCTCGCCAA; sh#3CCTGTGGCATAAGGTGATGTT; sh#4CCATTTA-TATCTTCGCCAAGA; sh#5CCCTCATCATAAAGCAGAAGCT), human *Gstt1* (sh#1 GCTTGCTTAAGACTTGCCCAA; sh#2CTTTGCCAAGAAG-AACGACAT) or mouse *FNI* (sh#5GCCAGTTTCCATCAATTATAA).

To generate lentiviral vectors for doxycycline-inducible overexpression of wild-type and mutant (R234G) mouse *Gstt1*, we replaced

the CAS9 sequence in the ipCW-CAS9 vector (Addgene 50661) with the 3X FLAG-tagged coding sequence (CDS) of TV1 of murine *Gstt1* through Gibson cloning. The *Gstt1* mutant was generated by mutating the position-234 amino acid (R, arginine) to a glycine (G) using Gibson cloning and with the wild-type ipCW-FLAG-*Gstt1* as template^{30,59,60}. Stable cell lines were generated by puromycin selection. Cell lines were treated with doxycycline ($1 \mu\text{g ml}^{-1}$) for a minimum of three days to achieve overexpression.

Stable doxycycline-inducible Cas9 cell lines were generated by infection with the PCW-Cas9 vector, followed by puromycin selection and infection with Lenti-sgRNA (Addgene 104993) containing a guide targeting exon 3 of murine *Gstt1* (GAACCTTACTTGTGTGCC). Cells were selected with blasticidin-containing medium 48 h after infection. Cell lines were treated with doxycycline ($1 \mu\text{g ml}^{-1}$) for a minimum of three days to achieve gene knockout.

Tumour sphere assay

Metastatic-derived cell lines were plated as a single-cell suspension as described in ref. 20. Tumour spheres were counted and photographed at day 10 using a Leica DMI4000b white-light microscope.

Real-time PCR analysis

Total RNA was isolated as described above in the section 'RNA isolation from mouse tumours and RNA sequencing'. For cDNA synthesis, $1 \mu\text{g}$ of total RNA was reverse-transcribed using the QuantiTect reverse transcription kit (Qiagen). Real-time PCR was run in duplicate using SYBR green master mix (Roche) and real-time monitoring of PCR amplification was performed using the LightCycler 480 detection system (Roche). Data were expressed as relative mRNA levels normalized to the β -actin expression level in each sample. Primer sequences for mouse *Gstt1* (forward GTTCTGGAGCTGTACCTGGATC; reverse AGGAACCTTACTTGTGTGCC), *mCherry* (forward CATCCCGACTACTTGAAGC; reverse CCCATGGTCTTCTTTCAT) and mouse β -actin (forward ACTATTGGCAACGACGGTTC; reverse AAGGAAGGCTGGAAAAGAGCC), and primer sequences for mouse *Fgfr3*, *Nr1h3*, *Slc38a4*, *Itga8*, *Cd5l* and *Ki67* are available upon request.

Immunoblotting

Cell and tissue lysates were prepared in RIPA lysis buffer (150 mM NaCl, 1% NP40, 0.5% deoxycholate, 50 mM Tris-HCl at pH 8, 0.1% sodium dodecyl sulfate (SDS), 10% glycerol, 5 mM ethylenediamine tetraacetic acid (EDTA), 20 mM NaF and 1 mM Na_2VO_4) supplemented with a protease inhibitor cocktail. Lysates were sonicated and cleared by centrifugation at $16,000g$ for 20 min at 4°C and analysed by SDS-polyacrylamide gel electrophoresis (PAGE) and autoradiography. Proteins were analysed by immunoblotting using the following primary antibodies: anti-Gstt1 (Abcam, ab175418), β -actin (Sigma-Aldrich, A5316), tubulin (Sigma-Aldrich, T6199), E-cadherin (BD, 610181), vimentin (BD, 550513), PCNA (PC10) (Santa Cruz, sc-56), fibronectin (Abcam, ab199056) and GSH (D8) (Santa Cruz, 52399). All primary antibodies were used at a 1:1,000 dilution.

Histology and immunostaining

Tissues. Tissue samples were fixed overnight in 10% buffered formalin, then embedded in paraffin and sectioned at a thickness of $5 \mu\text{m}$. Haematoxylin and eosin (H&E) staining was performed using standard methods, and entire slides were scanned using the Aperio CS2 scanner.

For tissue immunofluorescence, deparaffinization, rehydration and antigen retrieval were performed on unstained slides with Trilogy solution (Cell Marque). Sections were blocked with 5% goat serum (Cell Signaling), 1% bovine serum albumin (BSA, Sigma) and 0.2% gelatin (Sigma) in phosphate buffered saline (PBS) with 0.1% Triton-X for 1 h at room temperature, then incubated overnight with primary antibodies at 4°C . The following primary antibodies and their dilutions were used: anti-GSTT1 (Abcam, ab175418, 1:200 for mouse and human tissues),

anti-TromaIII (DSHB, 1:500, for mouse tissues), anti-cytokeratin (Dako, M351529-2, 1:500, for human tissues), cytokeratin 19-555 (Abcam, 203444, 1:500, for human tissues), anti-PCNA (PC10) (Santa Cruz, sc-56, 1:200, for mouse tissues), anti-Ki67 (Abcam, 1:200, for human tissues) and anti-fibronectin (Santa Cruz, 271098, 1:200, for mouse and human tissues). Slides were kept in dark containers. Samples were washed three times for 10 min each in PBST and incubated with secondary antibodies for 2 h at room temperature. The following secondary antibodies and their dilutions were used: anti-rabbit, anti-mouse and anti-rat conjugated to Alexa Fluor 488 (Molecular Probe; 1:500), Alexa Fluor 555 (Molecular Probe; 1:500) and Alexa Fluor 647 (Molecular Probe; 1:500). Stained slides were mounted using Prolong Gold Antifade mounting reagent (Vector lab, H-1200) containing 4',6-diamidino-2-phenylindole (DAPI) for nuclei staining. Images were obtained using a Nikon Eclipse Ni-U fluorescence microscope. Confocal images were obtained using either the Leica SP8 confocal microscope or Nikon Ti2-Eclipse AXR confocal system. Quantification of positive and negative cells was performed using ImageJ.

The human PDA tissue microarray was obtained from USA Biomax (PA-2081c) as an FFPE slide with a total of 192 cores, including $n = 68$ primary PDA (stages I and II) and $n = 14$ (stages III and IV/metastatic) cores followed by scanning on a Vectra Polaris microscope and analysis by the MGH Cancer Center Translational Imaging Core. The average intensity per channel was measured and the data represented as the ratio of double-positive cells per core (CK19^+ and Gstt1^+). Numbers of GSTT1^+ and Ki67^+ cells per CK19^+ lesion were quantified using ImageJ.

Tumour specimens derived from primary tumours and metastatic lesions from cadavers of rapid autopsy patients analysed in this study were collected as stated above and de-identified by the clinical staff. Freshly isolated specimens from pancreatic cancer primary and metastatic sites were divided into two parts and (1) stored in formalin for making FFPE tissue blocks (for H&E and immunofluorescence) or (2) used for bulk tissue homogenization for protein lysates. De-identified tumour specimen information for each participant is detailed in Supplementary Table 7.

Glutathione and fibronectin immunofluorescence in metastatic cells.

PDAC liver metastatic-derived cell lines stably expressing wild-type ipCW-FLAG-*Gstt1*, R234G mutant or ipCW empty vector were induced with doxycycline ($1 \mu\text{g ml}^{-1}$) as described above. Cells were fixed for 30 min in 4% buffered formalin, permeabilized and blocked with 5% goat serum (Cell Signaling), 1% BSA (Sigma) in PBS with 0.1% Triton-X for 1 h at room temperature, and then incubated overnight with primary antibodies at 4°C . The following primary antibodies and their dilutions were used: anti-fibronectin (Abcam, ab199056, 1:100) and anti-GSH (D8) (Santa Cruz, 52399, 1:100). The following secondary antibodies and their dilutions were used: anti-rabbit and anti-mouse conjugated to Alexa Fluor 488 (Molecular Probe; 1:500) and Alexa Fluor 555 (Molecular Probe; 1:500). DAPI was used for nuclei staining. Confocal images were obtained using the Nikon Ti2-Eclipse AXR confocal system. Quantification of GSH/fibronectin-positive cells was performed using ImageJ.

Label-retaining membrane dye experiments

PDAC-derived lung metastatic cell lines were labelled with CellTracker Membrane Dye CM-Dil (Invitrogen) as described previously⁶¹. CM-Dil^+ and CM-Dil^- populations were isolated using FACS at the indicated timepoints. A representative flow sorting schematic is shown in Fig. 3g. Cell populations were collected and analysed for *Gstt1* and *Ki67* mRNA expression using qRT-PCR and presented as expression relative to day 0 (fully labelled cells).

Generation of *Gstt1-mCherry* cell line, FACS and RNA sequencing
Endogenous tagging of murine *Gstt1*. To create *Gstt1-mCherry* tagged cell lines, we generated an integration donor made of two 750-bp

homology arms flanking the stop codon of murine *GSTT1*, followed by a selection cassette containing GFP and hygromycin. A CRISPR guide targeting the 150-bp region around the stop codon (GTGCATG-GTACCAGCGAGTGG) was cloned into the PX330 vector (Addgene 110403). 1×10^6 lung metastatic-derived PDAC cells were then nucleoporated using a Nucleofector 2b device (Addgene AAB-1001) using the Amaxa Cell Line Nucleofector Kit R (VCA-1001, Lonza) and plated into a 10-cm tissue culture dish. Cells were treated 500 μ g of hygromycin to select for positive clones. After selection, resistant clones were expanded, and screened for correct integration by PCR by using primer pairs #1 (forward CAAACCAGGTCTCCATCTGCGTGTCTTG; reverse GAACTCCTTGATGATGGCAATCCTGGTCCG) and #2 (forward TTCAA-GAATGCATGCGTCAATTTACGCAGACTATCTTTCTAGGG; reverse TCTCCCCGTCCCCACTCCCACTACAG).

Flow sorting of mCherry populations. A lung metastatic-derived cell line generated to express *mCherry* from the endogenous *Gstt1* locus was cultured under 2D conditions, trypsinized, and filtered through 40- μ m mesh filters. DAPI (3 nm) was added to the cell suspension to negatively select live cells. *mCherry*^{high} and *mCherry*^{low} populations were gated on live populations as well as GFP⁺. For all in vitro and in vivo assays, the top 15–20% and bottom 15–20% were chosen as *mCherry*^{high} and *mCherry*^{low} populations, respectively, utilizing appropriate single-colour and negative controls. Cells were analysed and sorted using a FACSAria II device (BD Biosciences) and BD FACSDiva software (v.8.0.2). The obtained data were analysed by FlowJo v.10. An example gating strategy is described in Fig. 4c. Cells were then plated under soft agar conditions for tail-vein injections (2×10^4 cells) per population per mouse, for western blot analysis and for RNA-seq as already described.

Cell-cycle analysis

Non-synchronized mouse liver PDAC-derived cell lines expressing either non-targeting control, *shGstt1* #1 or *shGstt1* #2 were plated in 2D growth conditions and grown for three days. On day 3, cells were trypsinized, washed with $1 \times$ PBS and fixed using ice-cold 95% ethanol in a dropwise manner under low-speed vortexing. On the day of flow cytometry analysis, ethanol-fixed cells were stained with staining solution containing: 0.1% Triton X-100, $1 \mu\text{g ml}^{-1}$ RNase, 2% propidium iodide in $1 \times$ PBS for 20 min using end-over-end rotation. Single-cell suspensions were analysed for cell-cycle phase (propidium iodide) using the BD Canto II system. Analysis of cell populations was carried out using FlowJo v.10.

Immunoprecipitation and mass spectrometry

PDAC liver metastatic-derived cell lines as described in the above section 'Cell Lines' were cultured under 2D conditions as described above. Cell lysates were prepared in RIPA lysis buffer, supplemented with protease inhibitors as described above. Lysates were sonicated and cleared by centrifugation at 16,000g for 20 min at 4 °C and subsequently subjected to immunoprecipitation using magnetic Dynabeads Protein-G (Invitrogen, 10007D). Before immunoprecipitation, magnetic beads were conjugated with specific primary antibodies (*Gstt1*, Abcam, ab199337; fibronectin, Abcam, ab199056; GSH (D8), Santa Cruz, 52399; normal rabbit immunoglobulin G, Cell Signaling, 2729S). Samples were incubated at 4 °C with constant rotation overnight in immunoprecipitation buffer (RIPA, 0.25 mM phenylmethylsulfonyl fluoride (PMSF) supplemented with protease inhibitor cocktail tablets (Sigma-Aldrich, 4693116001) followed by washing with immunoprecipitation buffer. The immunoprecipitations were run on a 4–20% SDS-PAGE gel for 5 min before fixing the gel with Coomassie (ProtoBlue Safe, Scientific Labs). Coomassie-stained *Gstt1* and GSH immunoprecipitations were submitted to the Taplin Biological Mass Spectrometry Facility at Harvard Medical School for peptide identification. Analysis of enriched functional categories among overlapping peptides was performed using DAVID^{56,57}.

In vitro glutathionylation assay using purified human GSTT1 and fibronectin

Commercial fibronectin was purchased from Innovative Research (#IMSFBN1MG). Due to the presence of a previous FN-SSG modification detected in the commercial fibronectin, 5 μ g of fibronectin was reduced by incubating it with 20 mM dithiothreitol for 1 h at room temperature. Excess dithiothreitol was removed in a 10-kDa spin column with multiple washes. The resulting reduced fibronectin was incubated with 18 μ g of recombinant human GSTT1 (rGSTT1; My BioSource, cat. no. MBS636253) in the presence or absence of 5 mM GSH, 280 μ M glucose (G) and 10 mU ml⁻¹ glucose oxidase (GOx) at room temperature for the indicated timepoints. The G/GOx system was employed to generate low fluxes of H₂O₂ (ref. 62) to prevent overoxidation of cysteines. Samples were run on a 10% SDS-PAGE gel under non-reducing conditions and subjected to western blotting for GSH, fibronectin and GSTT1, with the antibodies described in the previous section.

Fibronectin-deposition ELISA and western blot

PDAC liver metastatic-derived cell lines as described in the above section 'Cell Lines' stably expressing either control, the ipCW-*Gstt1* construct and *shGstt1* were cultured under 2D conditions as described above. After seven days, 1 ml of conditioned medium was collected from all cell conditions and filtered through 0.45- μ m filters. An ELISA was performed on conditioned medium according to the manufacturer's instructions (Abcam, ab108849) and normalized to the protein concentration for each sample. Normalized protein from the conditioned medium was subjected to western blotting for fibronectin (anti-fibronectin, Abcam, ab199056, 1:1,000).

Measurement of oxidative stress

On day 0, cells were plated in triplicate either in low-attachment or cell-culture-treated six-well plates. Cells in each condition were then treated with either 100 μ M NAC or water for 48 h. After 48 h in culture, the cells were incubated with CellROX Green (Invitrogen) for 30 min at 37 °C. The GFP fluorescence on live cells (DAPI-negative) was measured using a BD Canto cell analyser (BD Biosciences). The data were analysed using FlowJo v.10.

Mouse models and in vivo assays

Detailed experimental schematics are supplied throughout the manuscript figures (images produced using BioRender).

Mouse models. The PDAC genetically engineered models (*p48-Cre/p53F/+KrasL/+ (Sirt6 WT and KO), +/- ROSA26-LSL-YFP*) have been described previously⁷²⁰ and were maintained on a mixed 129SV/C57BL/6 background. Metastatic tissues were considered 'high burden' or 'low burden' based on the presence of macrometastases or the absence of overt metastatic tumours, respectively. The 4T1 BC metastasis model has been described previously²². 4T1 BC cells were stably transduced with retrovirus-containing pMSCV-luc-PGK-Neo-IRES-eGFP to generate GFP-expressing cells. To generate lung metastases, 6–8-week-old female BALB/c mice were injected with 1×10^5 4T1 BC cells into the fourth inguinal mammary fat pad. After four weeks, mice were euthanized, and primary and metastatic tumours collected for experiments.

Primary tumour growth and generation of spontaneous metastases using orthotopic models. Breast (BC) model.

The 4T1 cell line or cell line derived from 4T1 primary tumours (see above) was stably transduced with various vectors (pLKO.1, ipCW-Cas9 expressing control or *Gstt1* constructs) and collected by trypsinization, washed twice in PBS, resuspended at 1×10^4 in 90 μ l of PBS and 10% Matrigel (Corning) and injected into the fourth inguinal mammary fat pad of 6–8-week-old female BALB/c mice (Jackson Laboratory) to establish mammary tumours. Primary tumour growth was monitored weekly by taking measurements of tumour length (*L*) and width (*W*). For inducible experiments,

doxycycline (200 µg ml⁻¹) was administered in the drinking water of all experimental mice and was replaced every week. Tumour volume was calculated using the formula $LW^2/2$. Mice were euthanized when tumours reached a volume of 600 mm³. For tumour resection experiments, the primary tumour (~350 mm³) was surgically removed under isoflurane anaesthesia⁶³. Surgical procedures were performed in the aseptic hood of the pathogen-free facility, and mice were housed singly to aid in wound healing. Mice were continuously measured for lung metastases using BLI once a week until the mice presented with evidence of clinical metastasis (hunched posture, lethargy and weight loss) in accordance with animal welfare guidelines. Primary and metastatic tumours were collected for further analysis.

Pancreatic PDAC model. Cell lines derived from primary tumours from *p48-Cre/p53F/+KrasL/+ (Sirt6* WT and KO) mice were stably transduced with pLKO.1 vectors (control and individual shRNA targeting *Gstt1*), collected by trypsinization, washed twice in PBS, and resuspended at 1×10^4 in 10 µl PBS. Mice were anaesthetized using isoflurane, and the cells were surgically injected into the head of the pancreas of male 6–8-week-old NOD.CB17-Prkdcscid/J mice (Jackson Laboratory). Surgical procedures were performed in the aseptic hood of the pathogen-free facility and mice were housed singly to aid in wound healing. Mice were monitored weekly for evidence of poor body condition (ascites, weight loss and hunched posture) and euthanized at the endpoint according to animal welfare guidelines. The excised primary tumour volume was taken at the endpoint and calculated using the formula $pLW^2/2$.

Experimental metastases. Retro-orbital. For the validation of shRNA target genes, cell lines derived from 4T1 metastatic lung tumours or *p48-Cre/p53F/+KrasL/+ (Sirt6* WT and KO) metastatic lung tumours (see above) were stably transduced with pLKO.1 vectors (control and pooled shRNAs targeting *Gstt1*), collected by trypsinization, washed twice in PBS, resuspended at 1×10^4 in 100 µl PBS and injected into the venous sinus of 6–8-week-old female BALB/c mice (4T1) (Jackson Laboratory) or male 6–8-week-old NOD.CB17-Prkdcscid/J (Jackson Laboratory) mice (PDAC model) to establish lung metastases. Mice were euthanized for all experiments at the endpoint evidenced by overall poor body condition in accordance with animal welfare guidelines. Metastatic lesions were confirmed by histological analysis by a pathologist (R. Bronson) at the DF/HCC Research Pathology Core.

Tail vein. Cell lines derived from *p48-Cre/p53F/+KrasL/+ (Sirt6* WT and KO) metastatic liver or lung tumours (see above) were stably transduced with the indicated vectors (pLKO.1, ipCW-Cas9, PX330-iCas9, expressing control or *Gstt1* constructs), collected by trypsinization, washed twice in PBS, resuspended at 1×10^4 in 100 µl of PBS and injected into the tail vein of male 6–8-week-old NOD.CB17-Prkdcscid/J mice (Jackson Laboratory) to home cells to the lung. To generate experimental DTCs, mice were euthanized after five days or two weeks, where indicated. For metastatic regression experiments, on day 14 post-injection, all mice were subject to BLI once a week, as described in the next section. Once lung metastatic tumours were detected, doxycycline (200 µg ml⁻¹) was administered in the drinking water of all experimental mice and replaced every week. Mice were continuously measured for lung metastases using BLI once a week until reaching the endpoint in accordance with animal welfare guidelines. For the NAC rescue experiment, mice were randomly segregated into groups and given either regular drinking water or NAC (1 g l⁻¹; Sigma) in their drinking water as described in ref. 64. When the first group showed evidence of clinical metastasis, all groups were euthanized in accordance with animal welfare guidelines.

For limiting dilution experiments, 10^1 , 10^2 and 10^3 cells were injected per population per mouse into a minimum of four mice per group. Each dilution group was followed until the first group presented with evidence of clinical metastasis. Upon evidence of metastatic burden, all

mice in each cell dilution group were euthanized in accordance with animal welfare guidelines.

All mouse primary tumours, liver and lung tissues were collected, H&E-stained, analysed and quantified in a blinded fashion by a pathologist (R. Bronson) at the DF/HCC Research Pathology Core.

BLI imaging. The cell lines used for imaging were generated to express pMSCV-luc-PGK-Neo-IRES-eGFP. Beginning at day 7 post-injection, mice were subjected to BLI once a week. Under isoflurane anaesthesia, 300 µl of D-luciferin (15 mg ml⁻¹) was injected intraperitoneally, and the mice were imaged every 5 min after injection with a 0.5-s to 60-s exposure time on an Ami X imaging system (Spectral Instruments Imaging) until the total flux and maximal radiance peaked. Total flux (photons s⁻¹) and maximal radiance (photons s⁻¹ cm⁻² sr⁻¹) were measured by a Spectral Ami X system (Spectral Instruments Imaging). A region of interest was drawn around the mammary fat pad and lung region for each mouse, as well as a background region of interest, which was subtracted from the total flux and maximum radiance for each mouse.

Statistical analysis and reproducibility

A Student's two-sided *t*-test was performed for two-group comparisons. Unequal variances were adjusted according to Welch's correction. Multiple comparisons were performed using an ANOVA with post-hoc Holm–Sidak's, Bonferroni or Geisser–Greenhouse adjusted *P* values. A log-rank test was used to determine significance for Kaplan–Meier analyses. We wished to obtain 80% power at a two-sided alpha level of 0.05 to detect an effect size of 1.3, using a two-sample *t*-test, requiring a minimum of at least five mice per group. Mice were excluded from data points when injections failed, or where mice reached euthanasia status or died before completion of the experiment, as indicated in the figure legends. Data distributions were assumed to be normal, but this was not formally tested. GraphPad Prism 8 was used for plotting graphs and statistical analysis. Statistical significance (*P* values) is displayed in the figures and figure legends. For animal experiments, mice injected with the same conditions were randomly assigned to treatment groups (for example, doxycycline, NAC). All shown western blots were repeated a minimum of two times. Representative immunofluorescence images demonstrate a minimum of *n* = 5 areas from each section. All H&E (that is, metastatic burden) analyses and quantifications were performed by the pathologist in a blinded manner. Assessment of metastatic burden via BLI was performed blindly by the Center for Systems Biology Imaging Core at Massachusetts General Hospital. Mice were assigned cage numbers blindly, and the imaging technician was unaware of the nature of the study. Assessment of immunofluorescence staining and quantification in TMA slides was performed using automated software.

Reporting summary

Further information on research design is available in the Nature Portfolio Reporting Summary linked to this Article.

Data availability

All RNA-seq data that support the findings of this study have been deposited in the Gene Expression Omnibus (GEO) under accession code [GSE232199](https://www.ncbi.nlm.nih.gov/geo/query/acc.cgi?acc=GSE232199). There is no restriction on data availability. Previously published data that were re-analysed here can be accessed through the Human Metastatic Cancer Database (HMCDDB) and are available under accession code [GSE63124](https://www.ncbi.nlm.nih.gov/geo/query/acc.cgi?acc=GSE63124). Mass spectrometry data have been deposited in ProteomeXchange with the primary accession code [PXD051110](https://www.ebi.ac.uk/pride/) (<https://www.ebi.ac.uk/pride/>). Human PDA survival data were derived from KMPlot (<https://kmplot.com/analysis/>). The dataset derived from this resource that supports the findings of this study is available at <https://doi.org/10.1038/s41598-021-84787-5>. All other data supporting the findings of this study are available from the corresponding author on reasonable request. Source data are provided with this paper.

Code availability

In-house codes were previously used in the published works. Appropriate references to the original works are provided.

References

- Anders, S., Pyl, P. T. & Huber, W. HTSeq—a Python framework to work with high-throughput sequencing data. *Bioinformatics* **31**, 166–169 (2015).
- Dobin, A. et al. STAR: ultrafast universal RNA-seq aligner. *Bioinformatics* **29**, 15–21 (2013).
- Robinson, M. D., McCarthy, D. J. & Smyth, G. K. edgeR: a Bioconductor package for differential expression analysis of digital gene expression data. *Bioinformatics* **26**, 139–140 (2010).
- Subramanian, A. et al. Gene set enrichment analysis: a knowledge-based approach for interpreting genome-wide expression profiles. *Proc. Natl Acad. Sci. USA* **102**, 15545–15550 (2005).
- Sherman, B. T. et al. DAVID: a web server for functional enrichment analysis and functional annotation of gene lists (2021 update). *Nucleic Acids Res.* **50**, W216–W221 (2022).
- Huang, da W., Sherman, B. T. & Lempicki, R. A. Systematic and integrative analysis of large gene lists using DAVID bioinformatics resources. *Nat. Protoc.* **4**, 44–57 (2009).
- Lánczky, A. & Györfy, B. Web-based survival analysis tool tailored for medical research (KMplot): development and implementation. *J. Med. Internet Res.* **23**, e27633 (2021).
- Shokeer, A., Larsson, A. K. & Mannervik, B. Residue 234 in glutathione transferase T1-1 plays a pivotal role in the catalytic activity and the selectivity against alternative substrates. *Biochem. J.* **388**, 387–392 (2005).
- Shokeer, A. & Mannervik, B. Residue 234 is a master switch of the alternative-substrate activity profile of human and rodent theta class glutathione transferase T1-1. *Biochim. Biophys. Acta* **1800**, 466–473 (2010).
- Lawson, M. A. et al. Osteoclasts control reactivation of dormant myeloma cells by remodelling the endosteal niche. *Nat. Commun.* **6**, 8983 (2015).
- Bauer, J. A., Zámocká, M., Majtán, J. & Bauerová-Hlinková, V. Glucose oxidase, an enzyme ‘Ferrari’: its structure, function, production and properties in the light of various industrial and biotechnological applications. *Biomolecules* **12**, 472 (2022).
- Danna, E. A. et al. Surgical removal of primary tumor reverses tumor-induced immunosuppression despite the presence of metastatic disease. *Cancer Res.* **64**, 2205–2211 (2004).
- Choi, J. E. et al. A unique subset of glycolytic tumour-propagating cells drives squamous cell carcinoma. *Nat. Metab.* **3**, 182–195 (2021).

Acknowledgements

We thank all the members of the Mostoslavsky laboratory for critical discussions throughout the years and editing of the

manuscript, especially T. L. Clarke. We would also like to thank N. Bardeesy for experimental discussions and critical evaluation of the manuscript, and S. Martin and J. Ju for technical confocal expertise and experimental discussions. R.M. is the Laurel Schwartz Endowed Chair in Oncology. This work is supported by NIH grants (R01CA235412 and R01GM128448) and a Krantz Breakthrough Award to R.M., and an ACS Postdoctoral Fellowship and NIH grant (K99/R00CA252600-01) as well as the Maryland Department of Health’s Cigarette Restitution Fund Program and the National Cancer Institute–Cancer Center Support Grant (CCSG) (P30CA134274) to C.M.F. We also thank the members of the HSCI-CRM Flow Cytometry Facility at Massachusetts General Hospital, R. Bronson at the Rodent Histopathology Core at Harvard Medical School, the NextGen Sequencing Core at Massachusetts General Hospital, Center for Innovative Biomedical Resources at the University of Maryland School of Medicine and Greenebaum Comprehensive Cancer Center, the Massachusetts General Hospital Translational Imaging Core for their technical expertise.

Author contributions

C.M.F. conducted experiments, wrote the manuscript, and designed and interpreted most experiments. R.B., H.M.C., T.B. and E.R.H. conducted and assisted with experiments. L.P.W., M.C. and R.S. provided all the computational analysis for transcriptomic experiments. G.R.W. performed mouse BLI. D.E.M. and D.J. provided access to rapid autopsy samples and clinical expertise. S.K. generated the genetically engineered pancreatic mouse models. E.R. and I.M. evaluated pancreatic cancer datasets for bioinformatic analysis of gene expression and survival. Y.M.J.-H., R.A. and H.A. performed and interpreted in vitro FN-SSG experiments. R.M. designed experiments, interpreted the data, and wrote and edited the manuscript.

Competing interests

The authors declare no competing interests.

Additional information

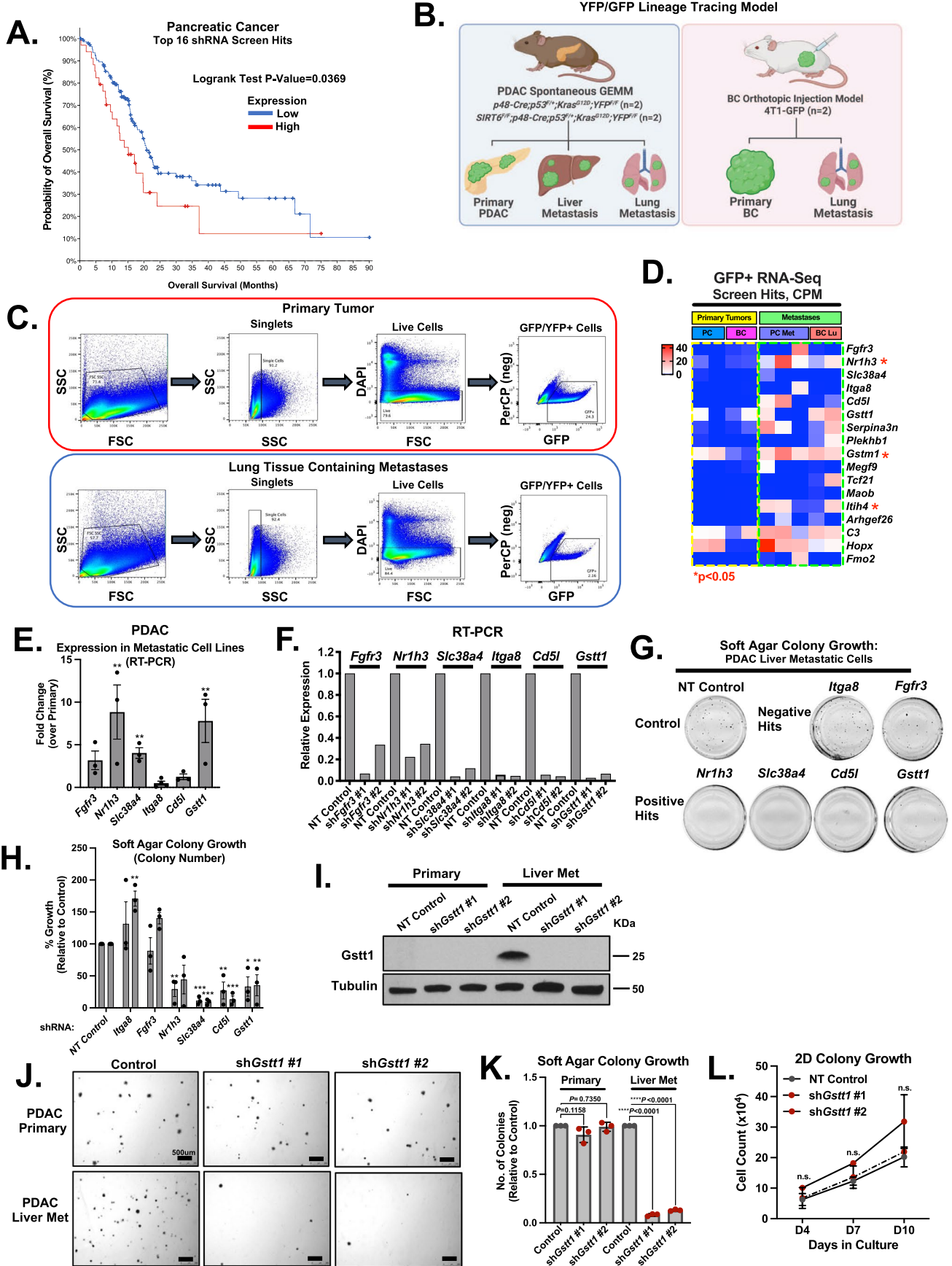
Extended data is available for this paper at <https://doi.org/10.1038/s41556-024-01426-7>.

Supplementary information The online version contains supplementary material available at <https://doi.org/10.1038/s41556-024-01426-7>.

Correspondence and requests for materials should be addressed to Christina M. Ferrer or Raul Mostoslavsky.

Peer review information *Nature Cell Biology* thanks the anonymous reviewers for their contribution to the peer review of this work.

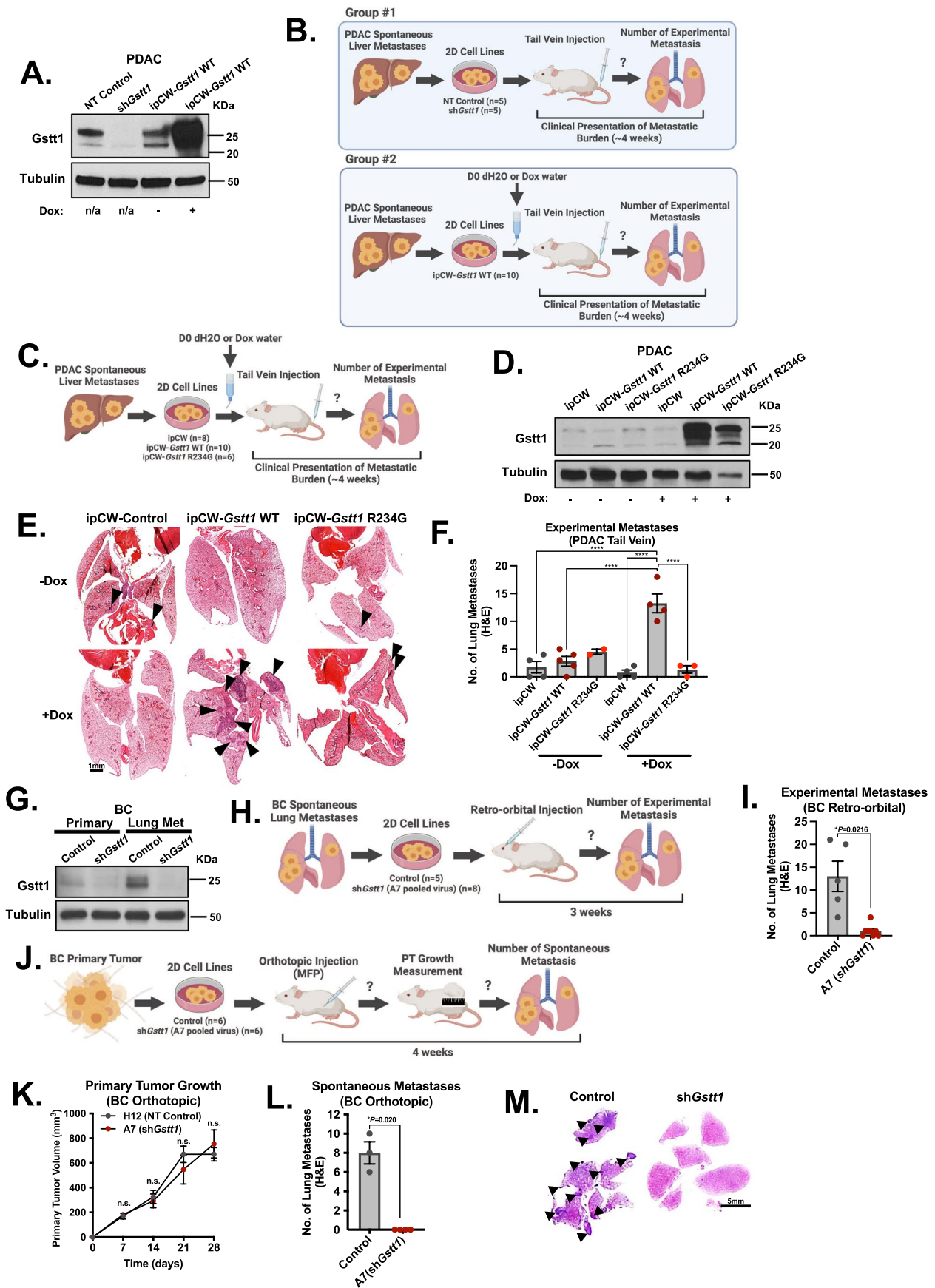
Reprints and permissions information is available at www.nature.com/reprints.



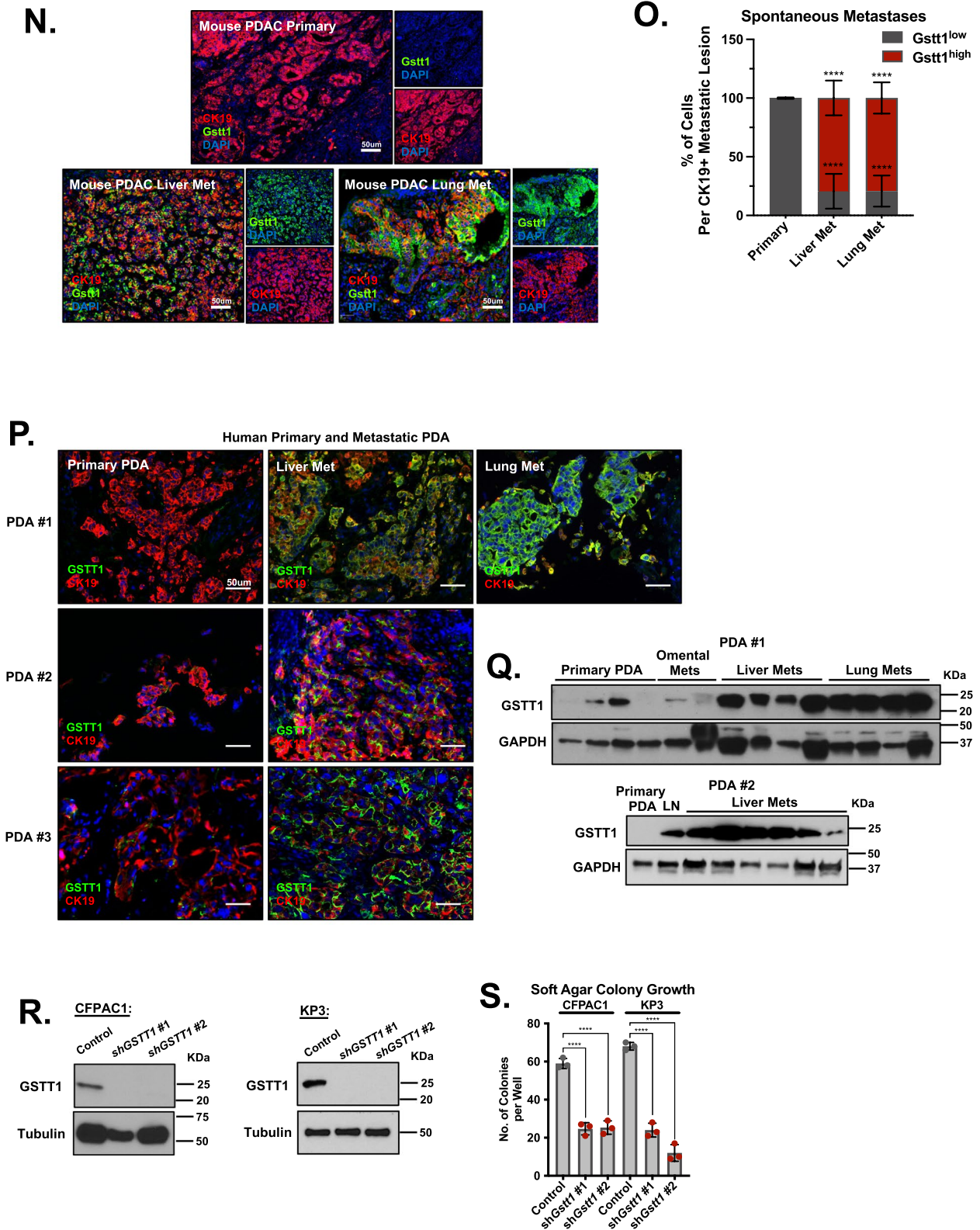
Extended Data Fig. 1 | See next page for caption.

Extended Data Fig. 1 | Functional validation of shRNA screen hits including *Gstt1* in metastatic cells. (A) Top 17 shRNA screen hits (minus *GSTT1*, $n = 16$) were analyzed for impact on overall survival in pancreatic cancer (KMPlot) based on mean expression of selected genes ($N = 177$ samples). A long-rank test was used to determine significance ($*P = 0.0369$). (B) Schematic depicting PDAC mouse models used for obtaining YFP/GFP+ primary and metastatic cells. Created with Biorender.com. (C) Representative fluorescence-activated cell sorting (FACS) strategy to obtain YFP/GFP+ metastatic cells. (D) Expression of Top 17 hits in primary matched GFP+ sorted cells represented as CPM values. Genes significantly differentially expressed between metastases ($n = 5$) and primary tumors ($n = 4$) from both mouse models displayed with red asterisk. Two-sided t -test was used to determine statistical significance between primary tumors and metastases (*Nr1h3*, $*P = 0.0220$, *Gstm1*, $*P = 0.0496$, *Itih4*, $*P = 0.050$). (E) qRT-PCR expression analysis of top 6 gene targets in primary ($n = 3$) and matched metastatic ($n = 3$) PDAC cell lines. Data represented as metastatic cell line mRNA expression relative to primary tumor-derived cells, s.e.m. Two-way ANOVA was used to determine statistical significance between groups ($**P = 0.0065$). (F) qRT-PCR for individual shRNA gene knockdowns. Data represents gene expression in a single cell line with $n = 2$ technical replicates. (G) Individual metastatic cell

lines ($n = 3$) were generated to express each shRNA once and subjected to soft agar assay in (G) for $n = 3$ replicates. Brightfield images of soft agar colonies from liver metastatic cell lines using individual shRNAs validating top 6 screen hits. (H) Soft agar growth using two independent shRNAs per each gene target. Gene knockdown validation was performed once with three technical replicates for each gene. Data are represented as percent growth relative to NT Control, s.e.m. Two-sided t -test was used to determine statistical significance between groups ($*P = 0.0264$, $**P = 0.0031$, $**P = 0.0083$, $**P = 0.0033$, $**P = 0.0093$, $*P = 0.0199$, $*P = 0.0480$). (I) Western blot depicting PDAC-derived primary and metastatic cell lines stably expressing control or two independent *Gstt1* shRNAs. (J) Soft agar assay growth in matched primary and metastatic cell lines. Representative brightfield image (2.5X). (K) Quantification of soft agar growth. Data are represented as number of colonies per well relative to control. The experiment was performed in triplicate with three technical replicates each. Data are represented as mean s.d. Two-sided t -test was used to determine statistical significance between groups ($****P < 0.0001$). (L) 2D growth curve in metastatic cell lines. The experiment was performed in triplicate with three technical replicates each. Data are represented as mean s.e.m. Two-sided t -test was used to determine statistical significance between groups.



Extended Data Fig. 2a | See next page for caption.

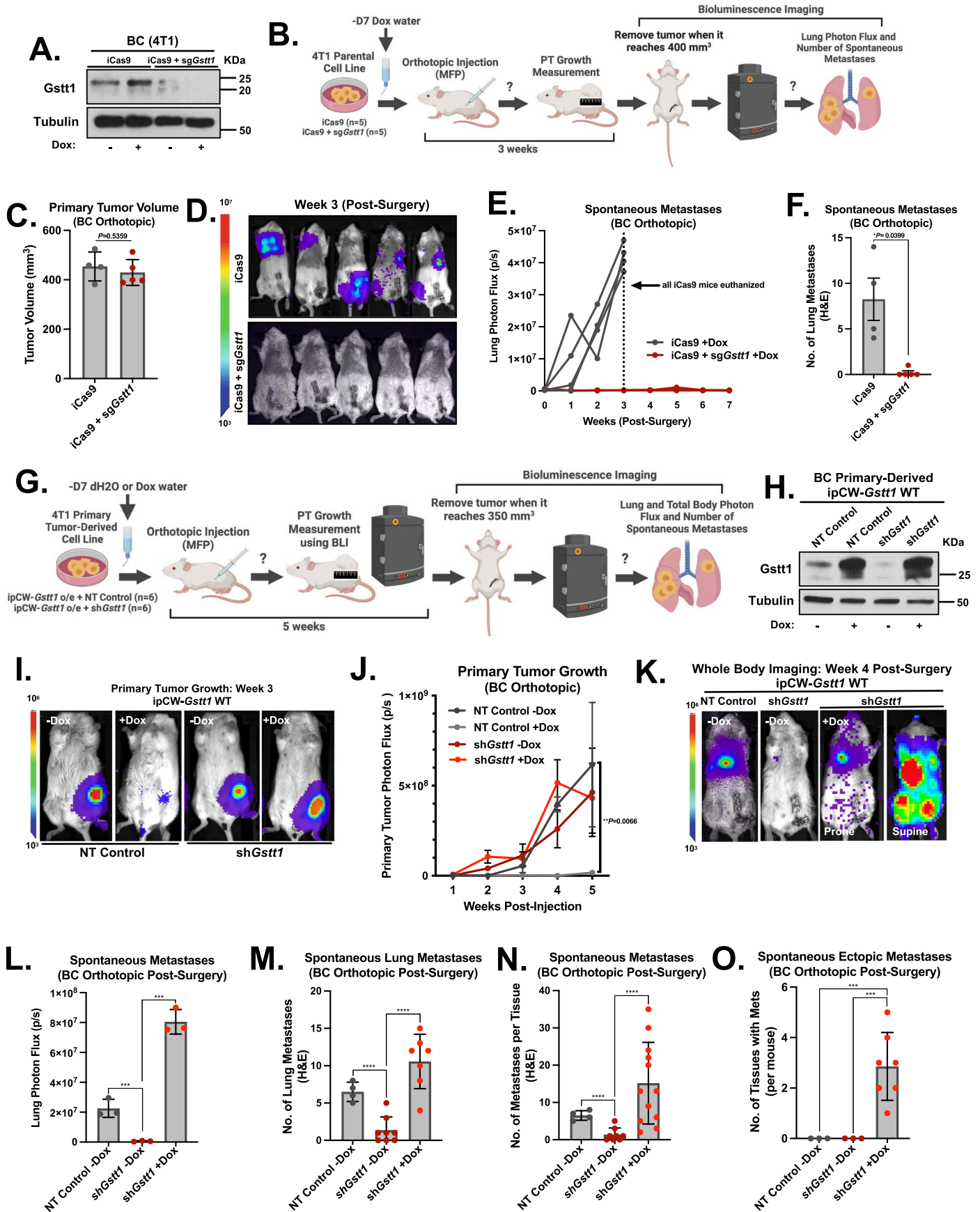


Extended Data Fig. 2b | See next page for caption.

Extended Data Fig. 2 | Gstt1 expression and catalytic activity is required for spontaneous and experimental metastases in BC and PDAC mouse models.

(A) Liver metastatic (PDAC) cell lines stably expressing indicated constructs were analyzed by western blot for *Gstt1* expression 3 days post-doxycycline (relates to cells injected in Fig. 1I). (B) Diagram depicting experimental schematic for data in Fig. 1I. Created with Biorender.com. (C) Schematic depicting experimental metastasis experiment. Mice were sacrificed when the first group demonstrated clinical evidence of metastatic burden and lungs were harvested and analyzed via H&E. Created with Biorender.com. (D) Cells injected in Fig S2C were analyzed by western blot for *Gstt1* expression. (E) Representative H&E Images from lungs from each condition, taken at endpoint. (F) Lung metastatic burden was evaluated using H&E and represented as total number of macrometastases per lung tissue. Data are represented as mean s.e.m. ANOVA with Brown-Forsythe post-hoc test for multiple comparisons was performed to determine statistical significance of all groups compared to ipCW-*Gstt1* WT +Dox group (**** $P < 0.0001$). (G) Western blot depicting BC-derived primary and lung metastatic cell lines stably expressing pooled *Gstt1* shRNAs. (H) Metastatic-derived lung cell line from the 4T1BC mouse model stably expressing control or pooled sh*Gstt1* were injected retro-orbitally to generate experimental lung metastases ($n = 5$ or $n = 8$ mice per group). Mice were sacrificed when the first group demonstrated clinical evidence of metastatic burden. Created with Biorender.com. (I) *In vivo* validation of *Gstt1* knockdown demonstrates reduced metastatic burden in BC experimental metastasis model. Data represented as mean s.e.m. Two-sided *t*-test was used to determine statistical significance between groups ($*P = 0.0216$). (J) Primary-derived cell lines from the 4T1BC mouse model stably expressing pooled sh*Gstt1* were injected orthotopically into the mammary fat pad, and mice were monitored for primary tumor size and the formation of end-stage metastases. Primary tumors were measured

over time, metastases were quantified at endpoint. Created with Biorender.com. (K) Primary tumor growth curves of orthotopically injected 4T1 cells into the mammary fat pad ($n = 3$ mice per group). Data are represented as mean s.e.m. for each timepoint. Two-way ANOVA with a post-hoc Holm-Sidak's multiple comparisons test. *P*-values taken at each timepoint. (L) Quantification of spontaneous metastases derived from 4T1 orthotopic injections in the mammary fat pad ($n = 3$ mice per group). Data are represented as mean s.e.m. Two-sided *t*-test was used to determine statistical significance between groups ($*P = 0.020$). (M) Representative H&E images from spontaneous lung metastases in (L). (N) Immunofluorescence staining of *Gstt1* and Cytokeratin 19 in mouse PDAC primary tumor, liver and lung metastases. (O) Quantification of immunofluorescence staining of *Gstt1* populations in all CK19+ primary and metastatic lesions. Data represented as percent of CK19+ cells per metastatic lesion. Quantification represents the average of 6 fields from a minimum of 5 individual metastatic lesions from $n = 3$ independent mice. Data are represented as mean s.d. Two-sided *t*-test was used to determine statistical significance between groups (**** $P < 0.0001$). (P) Representative immunofluorescence images of *GSTT1* and Cytokeratin 19 in PDA-derived primary matched liver metastases from 3 independent rapid autopsy patients. (Q) Western blot analysis of *GSTT1* levels in multiple primary and matched metastatic tissues derived from two rapid autopsy patients with pancreatic cancer. (R) Western blot analysis of *GSTT1* levels in two metastatic derived human cell lines expressing control and two individual short hairpins targeting *GSTT1*. (S) Quantification of soft agar colony growth in liver metastasis-derived pancreatic cancer cell lines expressing either control or short hairpins targeting *GSTT1*. Data represent average of three technical replicates from three independent experiments. Data are represented as mean s.e.m. Two-sided *t*-test was used to determine statistical significance between control and each individual shRNA for each cell line (**** $P < 0.0001$).

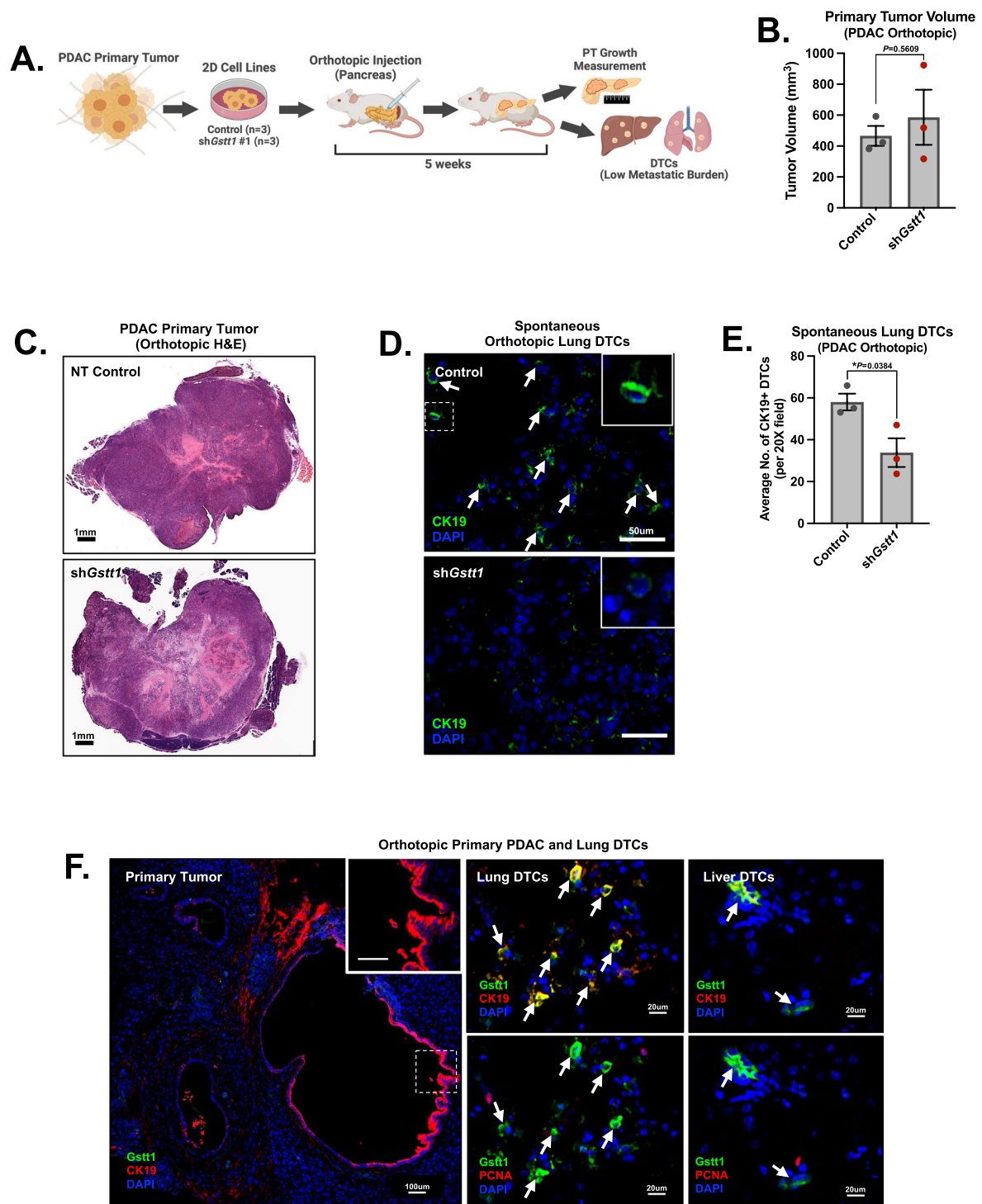


Extended Data Fig. 3 | See next page for caption.

Extended Data Fig. 3 | *Gstt1* is dispensable for primary tumor growth and regulates metastatic dissemination after primary tumor resection. (A)

Western blot depicting *Gstt1* and Tubulin protein levels in 4T1 cells expressing indicated constructs. (B) Schematic depicting effect of *Gstt1* on spontaneous metastases in an orthotopic resected BC model. Created with [Biorender.com](https://biorender.com). (C) Tumor size of surgically removed primary tumors. 1 iCas9 mouse was excluded from analysis due to delayed primary tumor growth. Data are represented as mean s.d. Two-sided *t*-test was used to determine statistical significance between groups (n.s.). (D) Representative bioluminescent image of metastatic burden 3 weeks post-surgery. iCas9 mouse #3 (middle) imaged prior to PT removal. (E) Measurement of lung photon flux (p/s) over time post-surgical removal of the primary tumor. Each set of data points represents an individual mouse. (F) H&E quantification of spontaneous lung metastases post-surgery, harvested at endpoint. Data are represented as mean s.e.m. Two-sided *t*-test was used to determine statistical significance between groups (**P* = 0.0399). (G) Schematic depicting effect of *Gstt1* re-expression on spontaneous metastases in an orthotopic resected BC model. Created with [Biorender.com](https://biorender.com). (H) Western blot depicting *Gstt1* and Tubulin protein levels in primary-derived 4T1 cells expressing indicated constructs. (I) Representative bioluminescent image of primary tumors 3 weeks after tumor cell injection. (J) Bioluminescence imaging of weekly primary tumor growth prior to surgical removal. Values are represented as mean

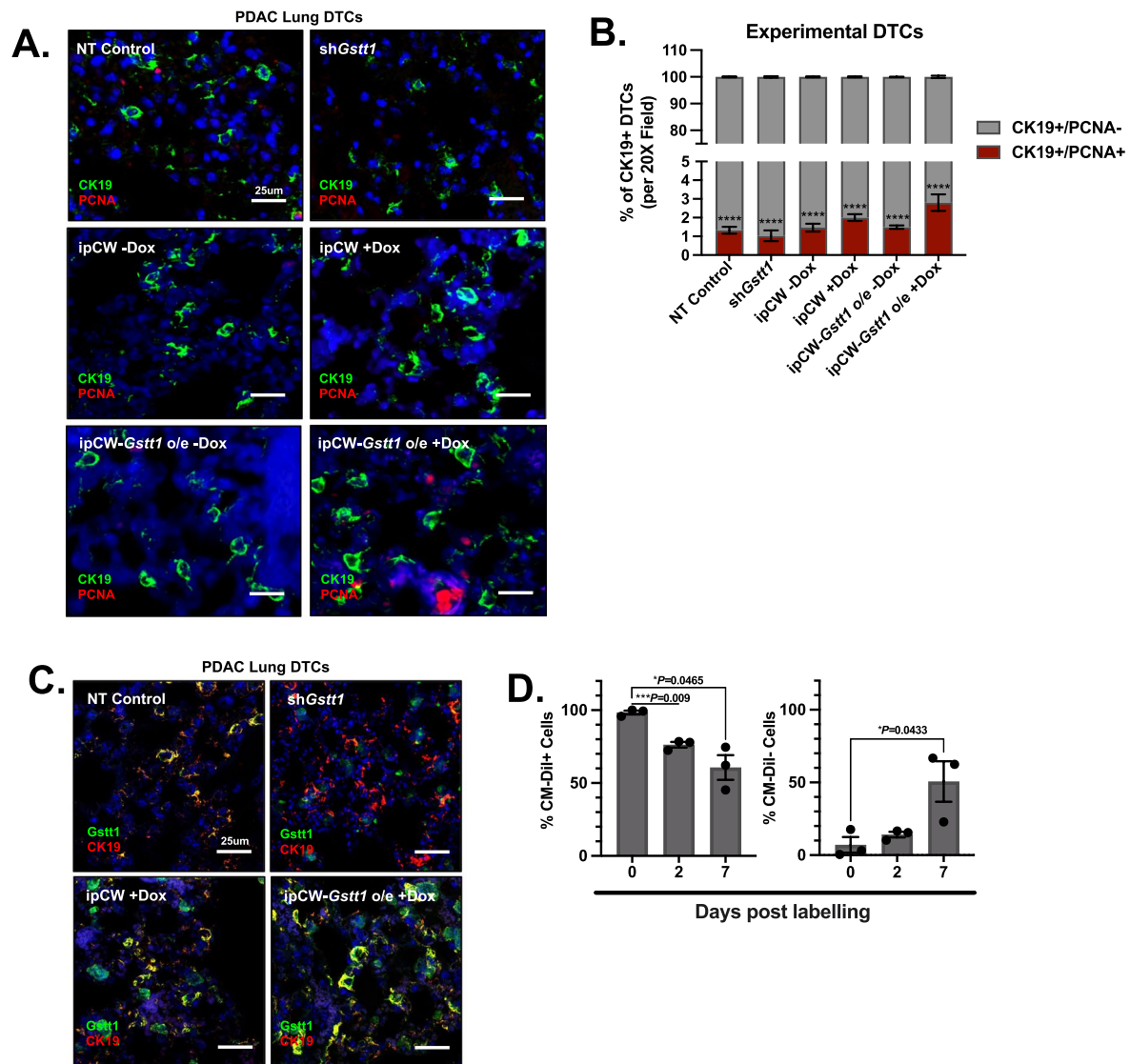
s.d. Two-way ANOVA with a post-hoc Geisser-Greenhouse multiple comparisons test was used to determine statistical significance between groups. *P*-values taken at final endpoint (***P* = 0.0040). (K) Representative bioluminescent image of end-point metastatic burden 4 weeks post-surgery. (L) Measurement of lung photon flux (p/s) over time, taken at endpoint. Data are represented as mean s.d. ANOVA with Brown-Forsythe post-hoc test for multiple comparisons was performed to determine statistical significance between groups (***P* = 0.003). (M) Experiment in (G) was repeated without BLI for post-mortem metastatic tissue analysis. H&E quantification of spontaneous lung metastases post-surgery, taken at endpoint. Data points derived from a combination of both experiments (NT Control -Dox, n = 4 mice; sh*Gstt1* -Dox, n = 8 mice; sh*Gstt1* +Dox, n = 7 mice). Data are represented as mean s.d. ANOVA with Brown-Forsythe post-hoc test for multiple comparisons was performed to determine statistical significance between groups (*****P* < 0.0001). (N) H&E quantification of the number of spontaneous macrometastases discovered outside the lung per tissue. Data are represented as mean s.d. ANOVA with Brown-Forsythe post-hoc test for multiple comparisons was performed to determine statistical significance between groups (*****P* < 0.0001). (O) H&E quantification of number of tissues outside the lung presenting with macrometastatic tumors. Data are represented as mean s.d. ANOVA with Brown-Forsythe post-hoc test for multiple comparisons was performed to determine statistical significance between groups (****P* = 0.0007).



Extended Data Fig. 4 | *Gstt1* is dispensable for primary tumor growth and required for dissemination of latent DTCs in an orthotopic model of PDAC.

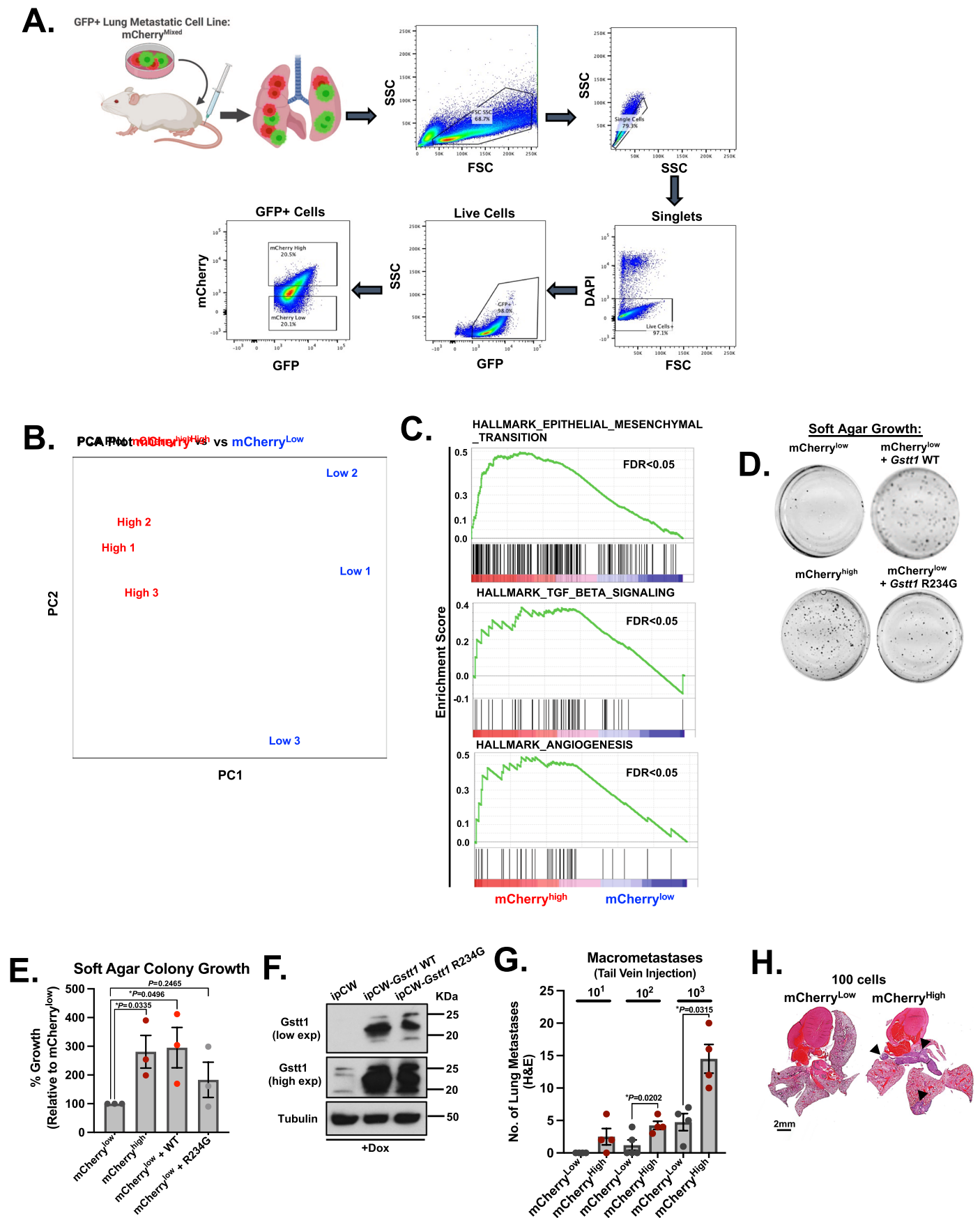
(A) PDAC-derived primary tumor cells expressing either Control or sh*Gstt1* were orthotopically injected into the pancreas (1×10^4 cells, $n = 3$ mice per group). Mice were euthanized when primary tumor burden resulted in poor body condition (abdominal ascites, hunched posture, lethargy, ~5 weeks), primary tumor size was measured, and liver and lung tissues analyzed for DTC content. Created with [Biorender.com](https://biorender.com). (B) Measurement of primary tumor volume, post-euthanasia. Data are represented as mean s.e.m. A two-sided *t*-test was used to determine statistical significance between groups ($P = 0.5609$, not-significant).

(C) Representative image of H&E stained orthotopic primary tumors from each group. (D) Immunofluorescence staining of orthotopically-derived disseminated tumor cells (DTCs) using Cytokeratin 19. Inset panel demonstrates a magnified image of CK19-positive DTCs. (E) Quantification of single DTCs ~5 weeks post-orthotopic injection, representing the average of 10 fields (20X field) from a minimum of $n = 3$ mice per group. Data are represented as mean s.d. two-sided *t*-test was used to determine statistical significance between groups ($*P = 0.0384$). (F) Immunofluorescence staining of Cytokeratin 19, *Gstt1* and PCNA in spontaneous primary tumors and DTCs from orthotopic derived lung and liver tissues.



Extended Data Fig. 5 | *Gstt1* is required for and enhances dissemination of *Gstt1*^{Hgh}/*PCNA*^{Low} latent DTCs. (A) Immunofluorescence staining of experimental disseminated tumor cells (DTCs) using 2-weeks post-injection. DTCs were identified using Cytokeratin-19 as a tumor cell marker and co-stained with PCNA. (B) Quantification of the percent of PCNA+ and PCNA- CK19+ DTCs from (A). Quantification represents the average of 10 fields from a minimum of $n = 3$ mice per group (20X field). Data are represented as mean s.d. 2-way ANOVA was used to determine statistical significance between groups (all PCNA- vs PCNA+ groups, **** $P < 0.0001$). (C) Experimental disseminated

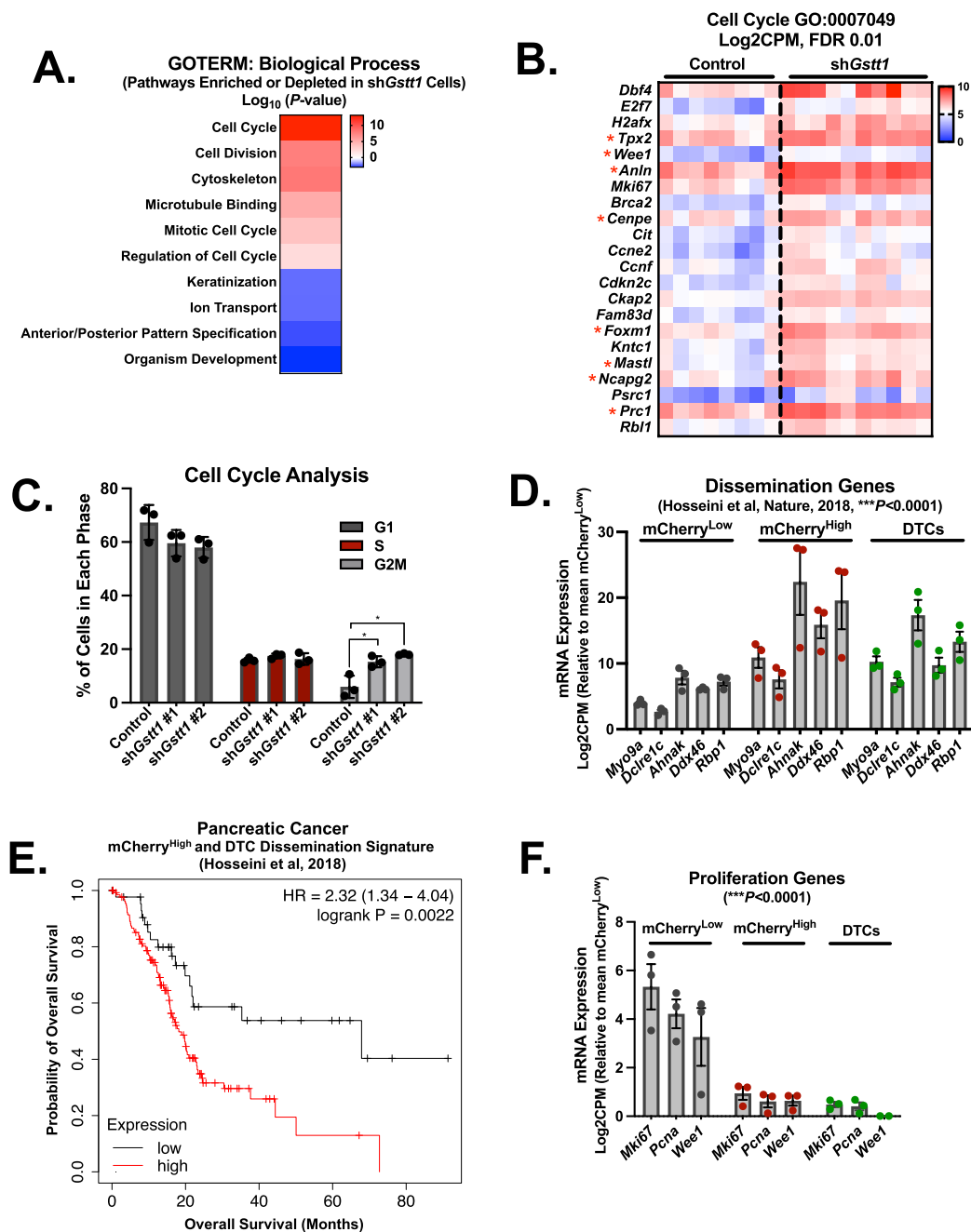
tumor cells (DTCs) from (A) were stained with CK19 and *Gstt1*. Arrows indicate double-positive DTCs. (D) Flow cytometry analysis of lung metastatic cell populations 0, 2, and 7-days post-incubation with membrane dye CM-Dil. Data represented as % of CM-Dil+ and CM-Dil- cells relative to the total live cell population. Quantification represents $n = 3$ independent sorting experiments in one cell line. Data are represented as mean s.e.m. A two-sided *t*-test was used to determine statistical significance between groups (*** $P = 0.009$, * $P = 0.0465$, * $P = 0.0433$).



Extended Data Fig. 6 | See next page for caption.

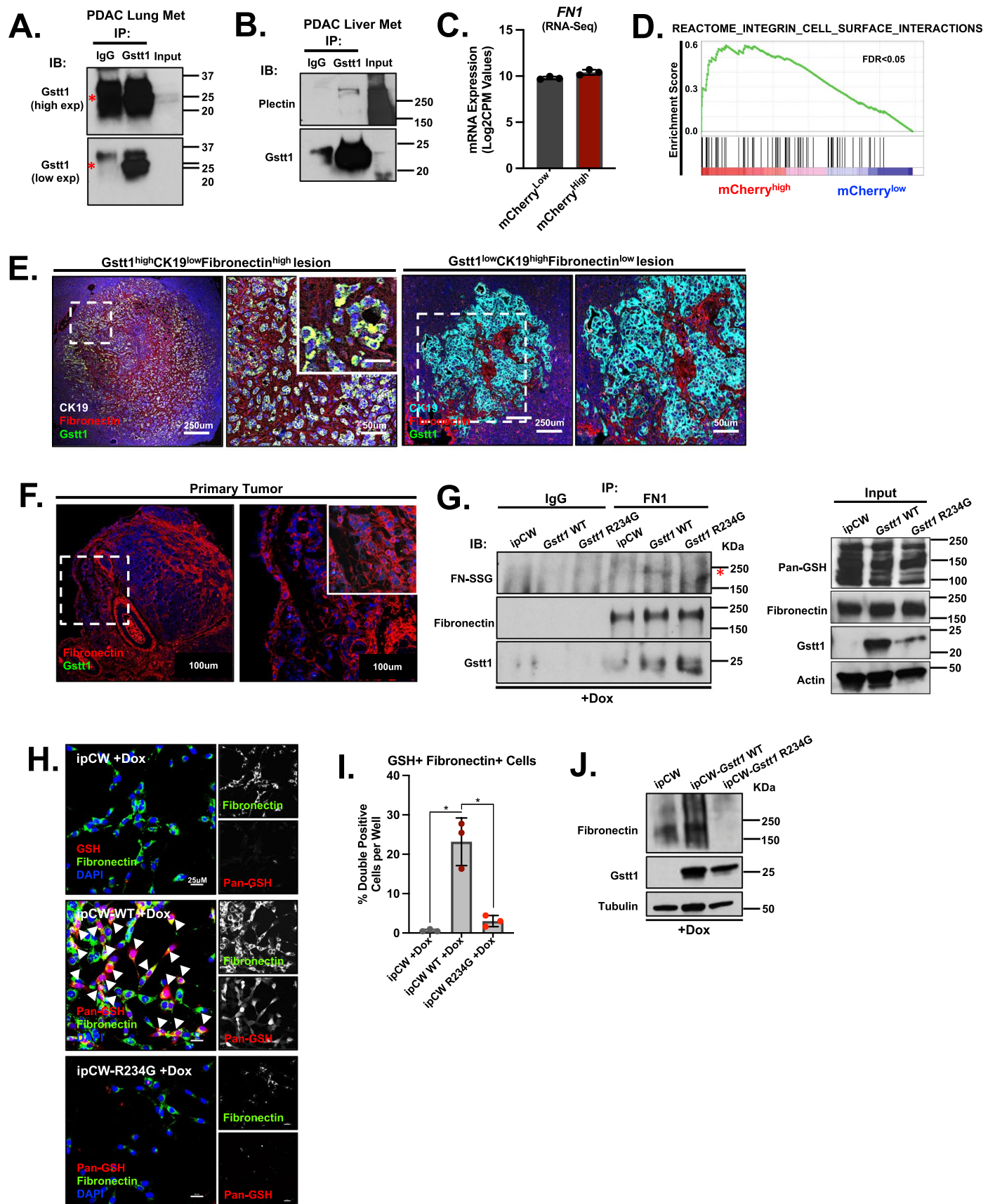
Extended Data Fig. 6 | *Gstt1* enhances EMT signaling and promotes anchorage-independent growth and metastasis in a subset of PDAC tumor cells. (A) Representative gating strategy of GFP+ metastatic mCherry populations isolated from lungs of SCID mice. Upper left part of image created with [Biorender.com](https://biorender.com). (B) Principal component analysis (PCA) of mCherry^{high} (n = 3) and mCherry^{low} (n = 3) cell populations based on identified differentially expressed genes (DEGs) (>2FC, FDR 0.05). Each paired sample set indicates sorted populations from n = 3 independent biological replicates and n = 3 independent sorting experiments. (C) Gene set enrichment analysis (GSEA) finds hallmark enrichment of 'Epithelial-to-Mesenchymal Transition', 'TGF-Beta Signaling' and 'Angiogenesis' pathways in the mCherry^{high} population. (D) mCherry^{low} sorted lung metastatic cell lines stably expressing ipCW, ipCW-*Gstt1* wild-type and ipCW-*Gstt1* R234G were treated with doxycycline for 5 days and subsequently subjected to soft agar growth assay. (E) ImageJ quantification of soft agar colony growth (averaged optical density per well) in all four conditions

expressed as relative to mCherry^{low}. Data represents n = 3 independent sorting experiments with n = 3 soft agar replicates each. Data are represented as mean s.e.m. A two-sided *t*-test was used to determine statistical significance between groups (**P* = 0.0335, **P* = 0.0496, *P* = 0.2465 (ns)). (F) Western blot depicting *Gstt1* levels in ipCW, ipCW-*Gstt1* wild-type and ipCW-*Gstt1*-R234G overexpressing mCherry^{low} cells used in experiment (E). (G) mCherry^{high} and mCherry^{low} populations were sorted and injected via tail vein into SCID mice (n = 10 cells, n = 10² cells, n = 10³ cells) to generate experimental metastases to the lung. Groups were sacrificed when the first mouse in each group displayed clinical evidence of metastasis. Quantification of metastatic burden in H&E-stained slides, n = 4 or n = 5 mice per group (as indicated). Data are represented as mean s.e.m. A two-sided *t*-test was used to determine statistical significance between groups (**P* = 0.0202, **P* = 0.0315). (H) Representative image of H&E stained mCherry lungs from mice injected with 10² cells per group.



Extended Data Fig. 7 | The $Gstt1^{\text{High}}$ macrometastatic subpopulation regulates cell cycle progression and shares dissemination gene signatures with latent DTCs. (A) A panel of metastatic cell lines (independently derived from PDAC liver and lung metastases) expressing either Control or shGstt1 were subjected to RNA-Seq. DAVID biological pathway analysis on Control vs shGstt1 differentially expressed gene signatures (95 UP, 217 DN) ($>2\text{FC}$, FDR 0.01) (GO_TERMs). Pathways were ranked by p-value (Log_{10}) using an unpaired, two-sided *t*-test with post-hoc Bonferroni correction. (B) Expression (Log_2CPM) of 'Cell Cycle' GO_TERM genes enriched in Control vs shGstt1 from (A) ($>2\text{FC}$, FDR 0.01). (C) Metastatic-derived PDAC cells stably expressing control, shGstt1 #1 or shGstt1 #2 were grown for 5 days, fixed, and analyzed for cell cycle stages using propidium iodide and flow cytometry. Cell cycle stages were analyzed using FlowJo. Data represents $n = 3$ independent experiments. Data are represented as mean s.d. ANOVA with Brown-Forsythe post-hoc test for multiple comparisons was performed to determine statistical significance between

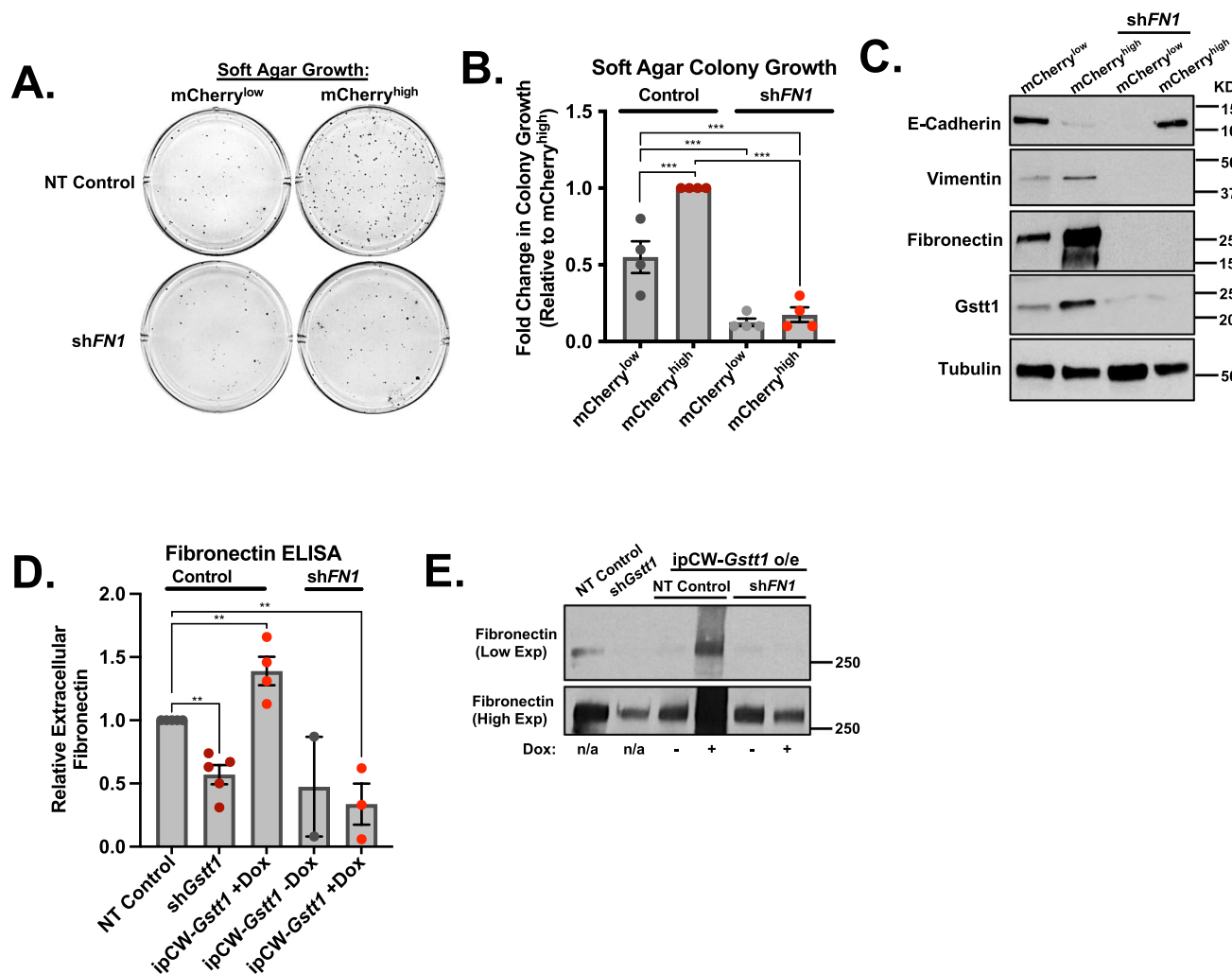
groups ($*P = 0.0247$). (D) Dissemination gene panel identified by Hosseini et al, 2018 was analyzed in $m\text{Cherry}^{\text{Low}}$ populations and DTCs. Data represented as genes commonly enriched in $m\text{Cherry}^{\text{High}}$ cells and DTC populations compared to $m\text{Cherry}^{\text{Low}}$. Data are represented as mean s.e.m. Two-way ANOVA with a post-hoc Tukey's multiple comparisons test was used to determine statistical significance between groups (Log_2CPM , **** $P < 0.0001$). (E) Dissemination gene panel ($n = 5$ genes) identified in Hosseini et al, 2018 from (D) were analyzed for impact on overall survival in pancreatic cancer (KMPlot). Data represents overall survival (OS) in $N = 177$ patient dataset based on mean expression of selected genes. A long-rank test was used to determine significance ($*P = 0.0022$). (F) Proliferation genes commonly downregulated in $m\text{Cherry}^{\text{High}}$ cells and DTC populations compared to $m\text{Cherry}^{\text{Low}}$. Data are represented as mean s.e.m. Two-way ANOVA with a post-hoc Tukey's multiple comparisons test was used to determine statistical significance between groups (Log_2CPM , **** $P < 0.0001$).



Extended Data Fig. 8 | See next page for caption.

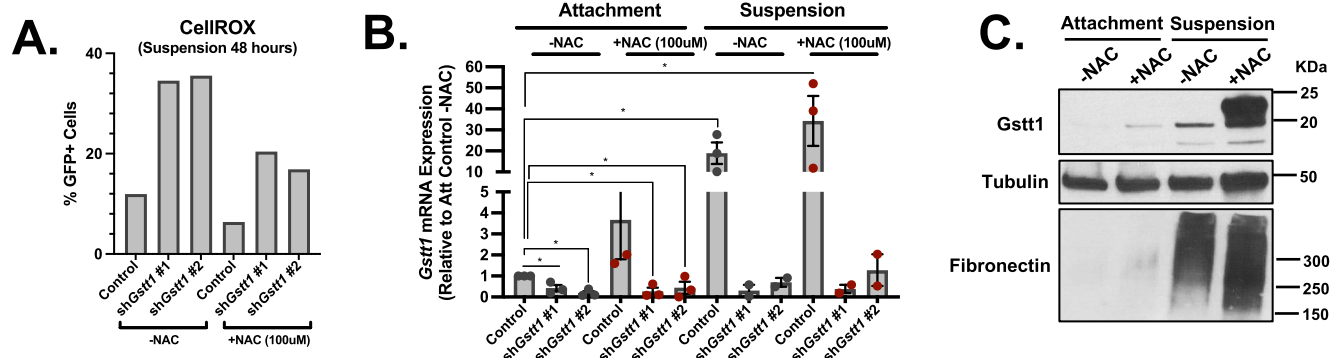
Extended Data Fig. 8 | Gstt1 interacts with and glutathione-modifies Fibronectin protein in a subset of metastatic cells. (A) Lung metastatic cell lines (PDAC) stably expressing wild-type ipCW-*Gstt1* were treated with doxycycline for 5 days, lysed and subjected to immunoprecipitation using a *Gstt1* antibody (whole cell lysate). Pull downs were analyzed for interactors and enriched peptides using unbiased mass spectrometry (M/S) for data in main Fig. 5A. Asterisks denote IgG band. (B) *Gstt1* pull downs in liver metastatic cells were blotted for validation of the interaction with Plectin. (C) Log2CPM expression values for *FNI* gene from mCherry^{high} vs mCherry^{low} RNA-Seq from Fig4. Data are represented as mean s.d. *FNI* was absent from the mCherry^{high} vs mCherry^{low} DEG list (using FDR 0.05 cutoff) and therefore considered not differentially expressed between populations. Data represent sorting from n = 3 independent experiments. (D) Gene set enrichment analysis (GSEA) for 'Integrin Cell Surface Interactions' pathways in the mCherry^{high} population. (E) Confocal imaging of immunofluorescence staining of *Gstt1*, Fibronectin and Cytokeratin 19 (pancreatic cell marker) in mouse CK19^{low}*Gstt1*^{high} and CK19^{high}*Gstt1*^{low} liver

metastatic lesions. A minimum of 5 metastatic lesions, across 3 independent mice were analyzed for co-staining. (F) Confocal imaging of immunofluorescence staining of *Gstt1*, Fibronectin and Cytokeratin 19 (pancreatic cell marker) in mouse pancreatic primary tumors. (G) Lung metastatic cell lines (PDAC) stably expressing ipCW, ipCW-*Gstt1* wild-type and ipCW-*Gstt1* R234G were treated with doxycycline for 5 days. Cells were lysed and subjected to immunoprecipitation using a Fibronectin antibody (whole cell lysate). Pull downs were blotted for FN-SSG (GSH antibody), Fibronectin and *Gstt1*. (Right panel) Input controls. (H) Lung metastatic cell lines (PDAC) stably expressing ipCW, ipCW-*Gstt1* wild-type and ipCW-*Gstt1* R234G were treated with doxycycline for 5 days. Cells were plated on glass chamber slides, fixed and stained with indicated antibodies. (I) Quantification of GSH and Fibronectin double positive cells. Quantification represents n = 3 biological replicates and an average of n = 5 fields of view per replicate (20X mag). Data are represented as mean s.d. ANOVA with Brown-Forsythe post-hoc test for multiple comparisons was performed to determine statistical significance (**P* = 0.0203). (J) Western blot from cells plated in (I).



Extended Data Fig. 9 | *Gstt1* mediates anchorage-independent growth, EMT, and Fibronectin ECM deposition through the regulation of intracellular Fibronectin in metastatic cells. (A) Sorted mCherry^{high} and mCherry^{low} populations were stably transduced with sh*FN1* and subjected to soft agar growth assay. Representative images of soft agar wells. (B) Quantification of soft agar colony growth in all four conditions expressed as relative to mCherry^{low}. Data represents n = 3 independent sorting experiments with n = 3 soft agar replicates each. Data are represented as mean s.e.m. ANOVA with Brown-Forsythe post-hoc test for multiple comparisons was performed to determine statistical significance ($***P = 0.0007$). (C) Western blot analysis of lysates from cells plated in (A) and (B). (D) Liver metastatic (PDAC) cell lines stably expressing

non-targeting Control, sh*Gstt1* or ipCW-*Gstt1* in the presence of control shRNA or shRNA targeting *FN1* were plated and conditioned media was collected 5 days after dH₂O or doxycycline treatment (where indicated). Conditioned media was subjected to an ELISA assay to measure extracellular Fibronectin deposition. Fibronectin levels were normalized to cellular protein content. Data is normalized to Control. ANOVA with Brown-Forsythe post-hoc test for multiple comparisons (compared to NT Control) was performed to determine statistical significance ($**P = 0.002$). Data represents a minimum of n = 3 independent experiments (except for ipCW · Dox sample, n = 2) with n = 2–4 technical replicates each. (E) Conditioned media from (D) was normalized to cellular protein content and subjected to western blotting for Fibronectin protein.



Extended Data Fig. 10 | *Gstt1* expression responds to glutathione availability to modulate cellular ROS in metastatic cells. (A) Metastatic cells were grown for 48 hours under suspension conditions +/- 100 uM NAC. Quantification of %GFP+ cells using CellIROXGreen analyzed by flow cytometry. Data are represented as mean s.d. Data represents n = 2 independent experiments. (B) Cells from CellIROX experiments in Fig. 6A, B and Supp Fig. 9A were subjected to RNA extraction and qRT-PCR for *Gstt1*. For attachment and suspension NT

Control results, data are represented as mean s.e.m. Two-way ANOVA was used statistical significance between groups (* $P = 0.0115$) and represent a minimum of 3 independent experiments. For suspension *Gstt1* KD conditions, data represent n = 2 independent experiments. (C) *Gstt1*^{Low} mouse PDAC-derived metastatic cells were treated with either dH₂O control or (100 uM) NAC under 2D attachment or low-attachment 'suspension' conditions for 48 hours. Cell lysates were subjected to western blotting for the indicated antibodies.

Reporting Summary

Nature Portfolio wishes to improve the reproducibility of the work that we publish. This form provides structure for consistency and transparency in reporting. For further information on Nature Portfolio policies, see our [Editorial Policies](#) and the [Editorial Policy Checklist](#).

Statistics

For all statistical analyses, confirm that the following items are present in the figure legend, table legend, main text, or Methods section.

n/a Confirmed

- The exact sample size (n) for each experimental group/condition, given as a discrete number and unit of measurement
- A statement on whether measurements were taken from distinct samples or whether the same sample was measured repeatedly
- The statistical test(s) used AND whether they are one- or two-sided
Only common tests should be described solely by name; describe more complex techniques in the Methods section.
- A description of all covariates tested
- A description of any assumptions or corrections, such as tests of normality and adjustment for multiple comparisons
- A full description of the statistical parameters including central tendency (e.g. means) or other basic estimates (e.g. regression coefficient) AND variation (e.g. standard deviation) or associated estimates of uncertainty (e.g. confidence intervals)
- For null hypothesis testing, the test statistic (e.g. F , t , r) with confidence intervals, effect sizes, degrees of freedom and P value noted
Give P values as exact values whenever suitable.
- For Bayesian analysis, information on the choice of priors and Markov chain Monte Carlo settings
- For hierarchical and complex designs, identification of the appropriate level for tests and full reporting of outcomes
- Estimates of effect sizes (e.g. Cohen's d , Pearson's r), indicating how they were calculated

Our web collection on [statistics for biologists](#) contains articles on many of the points above.

Software and code

Policy information about [availability of computer code](#)

Data collection

Differential gene expression in human metastatic pancreatic cancer was analyzed using the Human Metastatic Cancer Database (HCMDDB, hcmdb.i-sanger.com). KMplot was used to determine "Relapse-Free Survival" of differentially expressed genes. STAR aligner was used to map sequencing reads to the mouse reference transcriptome (mm9 assembly). Read counts over transcripts were calculated using HTSeq (v.0.6.0) based on a current Ensembl annotation file for NCBI37/mm9 assembly.

Data analysis

Differential expression analysis was performed using EdgeR. Analysis of enriched functional categories among detected genes was performed using DAVID.

Flow cytometry obtained data were analyzed using FlowJo (v10) ImageJ (1.53a), BD FACSDIVA

Image scanning was performed on the Vectra Polaris scanning microscope and analyzed using Halo AI by Indica Labs and Prism (v8.0/10)

For manuscripts utilizing custom algorithms or software that are central to the research but not yet described in published literature, software must be made available to editors and reviewers. We strongly encourage code deposition in a community repository (e.g. GitHub). See the Nature Portfolio [guidelines for submitting code & software](#) for further information.

Data

Policy information about [availability of data](#)

All manuscripts must include a [data availability statement](#). This statement should provide the following information, where applicable:

- Accession codes, unique identifiers, or web links for publicly available datasets
- A description of any restrictions on data availability
- For clinical datasets or third party data, please ensure that the statement adheres to our [policy](#)

All RNA-seq data that support the findings of this study have been deposited in the Gene Expression Omnibus (GEO) under accession codes GSE232199. There is no restriction of data availability. Previously published data that were re-analysed here can be accessed through the Human Metastatic Cancer Database (HMCD, <http://hcmdb.i-sanger.com/index>) and are also available under accession code GSE63124. Mass spectrometry data have been deposited in ProteomeXchange with the primary accession code PXD051110, link [10.6019/PXD051110](https://doi.org/10.6019/PXD051110).

Human PDA survival data were derived from KMPlot (<https://kmplot.com/analysis/>). The dataset derived from this resource that supports the findings of this study is available in <https://doi.org/10.1038/s41598-021-84787-5>.

In-house codes were previously used in the published works. Appropriate references to the original works are provided

Human research participants

Policy information about [studies involving human research participants and Sex and Gender in Research](#).

Reporting on sex and gender	Sex and gender were not considered during study design. Rapid autopsy samples have been de-identified to the researcher.
Population characteristics	Information on population characteristics was not collected.
Recruitment	Rapid autopsy samples have been de-identified to the researcher.
Ethics oversight	Tumor specimens derived from primary tumors and metastatic lesions from cadavers of rapid autopsy patients analyzed in this study were collected following institutional review board (IRB) approval. All subjects gave their informed consent for inclusion before they participated in the study. The collection and use of de-identified cadaver tissues was reviewed and approved by the Dana-Farber/Massachusetts General Hospital (DF/MGH) IRB (protocol no. 13-416).

Note that full information on the approval of the study protocol must also be provided in the manuscript.

Field-specific reporting

Please select the one below that is the best fit for your research. If you are not sure, read the appropriate sections before making your selection.

Life sciences Behavioural & social sciences Ecological, evolutionary & environmental sciences

For a reference copy of the document with all sections, see [nature.com/documents/nr-reporting-summary-flat.pdf](https://www.nature.com/documents/nr-reporting-summary-flat.pdf)

Life sciences study design

All studies must disclose on these points even when the disclosure is negative.

Sample size	We wished to obtain 80% power at a two-sided alpha level of 0.05 to detect an effect size of 1.3, using a two-sample t-test, requiring a minimum of at least 5 mice per group.
Data exclusions	Mice were excluded from data points when injections failed, or where mice reached euthanasia status or died prior to completion of the experiment, as indicated in the Figure legends.
Replication	Student's two-sided t-test was performed for two-group comparisons. Unequal variances were adjusted according to Welch's correction. Multiple comparisons were performed using an ANOVA with post-hoc Holm-Sidak's, Bonferroni or Geisser-Greenhouse adjusted P values. A log-rank test was used to determine significance for Kaplan-Meier analyses. All western blots represented have been repeated a minimum of two times. Representative IF images demonstrate a minimum of n = 5 areas from each section. All attempts at replication were successful.
Randomization	For animal experiments, mice injected with the same conditions were randomly assigned to treatment groups (ie, doxycycline, NAC).
Blinding	Group allocation to injection groups was not blind (shRNA, iCas9 injections), since we were aware of which cage received which injection as these treatments could not be done in a blind fashion. Assessment of metastatic area and quantification was performed by the pathologist in a blind manner. Assessment of metastatic burden via bioluminescence imaging was performed blindly by the center for systems biology imaging core at Massachusetts General Hospital – mice were assigned cage numbers blindly and the imaging technician was unaware of the nature of the study. Assessment of immunofluorescence staining and quantification in TMA slides was performed using automated software.

Reporting for specific materials, systems and methods

We require information from authors about some types of materials, experimental systems and methods used in many studies. Here, indicate whether each material, system or method listed is relevant to your study. If you are not sure if a list item applies to your research, read the appropriate section before selecting a response.

Materials & experimental systems

n/a	Involved in the study
<input type="checkbox"/>	<input checked="" type="checkbox"/> Antibodies
<input type="checkbox"/>	<input checked="" type="checkbox"/> Eukaryotic cell lines
<input checked="" type="checkbox"/>	<input type="checkbox"/> Palaeontology and archaeology
<input type="checkbox"/>	<input checked="" type="checkbox"/> Animals and other organisms
<input checked="" type="checkbox"/>	<input type="checkbox"/> Clinical data
<input checked="" type="checkbox"/>	<input type="checkbox"/> Dual use research of concern

Methods

n/a	Involved in the study
<input checked="" type="checkbox"/>	<input type="checkbox"/> ChIP-seq
<input type="checkbox"/>	<input checked="" type="checkbox"/> Flow cytometry
<input checked="" type="checkbox"/>	<input type="checkbox"/> MRI-based neuroimaging

Antibodies

Antibodies used

Proteins were analyzed by immunoblotting using the following primary antibodies: anti-Gstt1 (Abcam, ab175418), β -actin (Sigma-Aldrich, A5316), Tubulin (Sigma-Aldrich, T6199), E-Cadherin (BD, 610181), Vimentin (BD, 550513), PCNA (PC10) (Santa Cruz, sc-56), Fibronectin (Abcam, ab199056), GSH (D8) (Santa Cruz, 52399). All primary antibodies were used at a 1:1000 dilution. The following primary antibodies and their dilutions were used: anti-GSTT1 (Abcam, ab175418, 1:200 for mouse and human tissues), anti-Tromall1 (DSHB, 1:500, for mouse tissues), anti-Cytokeratin (Dako, M351529-2, 1:500, for human tissues), Cytokeratin19-555 (Abcam, 203444, 1:500, for human tissues), anti-PCNA (PC10) (Santa Cruz, sc-56, 1:200, for mouse tissues), anti-Ki67 (Abcam, 1:200, for human tissues), and anti-Fibronectin (Santa Cruz, 271098, 1:200, for mouse and human tissues). Slides were kept in dark containers. Samples were washed three times for 10 min each in PBST and incubated with secondary antibodies for 2h at RT. The following secondary antibodies and their dilutions were used: anti-rabbit, anti-mouse and anti-rat conjugated to Alexa Fluor 488 (Molecular Probe; 1:500), Alexa Fluor 555 (Molecular Probe; 1:500), Alexa Fluor 647 (Molecular Probe; 1:500).

Validation

All primary antibody validations were validated by the manufacturer, please see catalog numbers provided.

Eukaryotic cell lines

Policy information about [cell lines and Sex and Gender in Research](#)

Cell line source(s)

p48-Cre/p53F/+KrasL/+ (Sirt6 WT and KO) primary tumor-derived as well as lung and liver metastatic cell lines were established at Massachusetts General Hospital from genetically engineered mice on a mixed 129SV/C57BL/6 background as previously described (22,41,42). Metastasis-derived human pancreatic cancer cell lines, KP3, KP4 and CFPAC1 were obtained from the Center for Molecular Therapeutics at the Massachusetts General Cancer Center. CFPAC1 cell line is available from ATCC (CRL-1918). The 4T1 parental cell line was purchased from ATCC (CRL#2539). PDAC derived cell lines were generated from both male and female mice.

Authentication

Human pancreatic cancer cell lines, KP3, KP4 and CFPAC1 were authenticated at the Center for Molecular Therapeutics at the Massachusetts General Cancer Center. Mouse tumor cell lines have not been authenticated other than through injection into mice to generate tumors. Human pancreatic cancer cell lines were authenticated via cell morphology and via STR profiling

Mycoplasma contamination

Cell culture supernatants were tested for mycoplasma using Agilent Mycoplasma PCR Detection Kit at Massachusetts General Hospital. Cells found to be positive for Mycoplasma contamination were treated with Plasmocin Mycoplasma Elimination Reagent (Invivogen, ant-mpt1) for a minimum of 2 weeks and retested. Cell lines determined to be free of mycoplasma contamination were subsequently used for experiments.

Commonly misidentified lines (See [ICLAC](#) register)

No commonly misidentified lines were used in this study.

Animals and other research organisms

Policy information about [studies involving animals](#); [ARRIVE guidelines](#) recommended for reporting animal research, and [Sex and Gender in Research](#)

Laboratory animals

The PDAC genetically engineered models (p48-Cre/p53F/+KrasL/+ (Sirt6 WT and KO)) have been previously described (citation in the manuscript) and were maintained on a mixed 129SV/C57BL/6 background. The 4T1 breast cancer (BC) metastasis model can spontaneously metastasize from the primary tumor in the mammary gland to multiple distant sites preferentially the lung. To generate lung metastases, female BALB/c mice were injected with 1×10^5 4T1 breast cancer cells into the 4th inguinal mammary fat pad. For the analysis and prospective isolation of tumor cell populations from both primary tumors and spontaneous metastases, we

generated p48-Cre/p53F/+KrasL/+ROSA26-LSL-YFP (Sirt6 cKO) animals, as well as Sirt6 WT p48-Cre/p53F/+KrasL/+ROSA26-LSL-YFP animals to specifically isolate YFP+ epithelial cells by FACS. 4T1 breast cancer cells were stably transduced with retrovirus containing pMSCV-luc-PGK-Neo-IRES-eGFP to generate GFP expressing cells for sorting experiments. For cell injection experiments, NOD.CB17-Prkdcscid/J mice (Jackson Laboratory) were injected into either the venous sinus or tail vein to establish disseminated tumor cells and lung metastases and orthotopically into the pancreas to generate pancreatic tumors and disseminated tumor cells. The mice were housed in the vivarium maintained at 20+/-2oC with 12-h light/dark cycle with free access to food and water. All animals were maintained on a standard diet (Prolab Isopro RMH 3000, 0006972). Mice were housed maximum 5 to a cage, unless recovering from orthotopic surgery (1 to a cage), and then placed back into 5 per cage. Maximum tumor size allowed under this protocol was 1500mm³. No tumors in our experiments exceeded this size.

Wild animals	No wild animals were used in this study.
Reporting on sex	Sex and gender were not considered during study design.
Field-collected samples	No field collected samples were used in this study.
Ethics oversight	All experiments were performed under protocol 2019N000111 approved by Subcommittee on Research Animal Care at Massachusetts General Hospital. Mice were housed in pathogen-free animal facilities maintained at 20 ± 2°C, at 42% humidity, with 12-h light/dark cycle with free access to food and water. A maximum of 5 mice were housed per cage.

Note that full information on the approval of the study protocol must also be provided in the manuscript.

Flow Cytometry

Plots

Confirm that:

- The axis labels state the marker and fluorochrome used (e.g. CD4-FITC).
- The axis scales are clearly visible. Include numbers along axes only for bottom left plot of group (a 'group' is an analysis of identical markers).
- All plots are contour plots with outliers or pseudocolor plots.
- A numerical value for number of cells or percentage (with statistics) is provided.

Methodology

Sample preparation	<p>p48-Cre/p53F/+KrasL/+ROSA26-LSL-YFP (Sirt6 cKO), as well as Sirt6 WT p48-Cre/p53F/+KrasL/+ROSA26-LSL-YFP as well as 4T1-eGFP tumor bearing mice were euthanized and entire tissues (primary tumors, livers and lungs) were minced and incubated with 1.3mg/ml collagenase (Sigma-Aldrich, C6079) on a horizontal shaker at 37 °C for 30 min, vortexing every 5 min. Serially filtered and digested tissues using 70-µm and 40-µm strainers (BD Biosciences) were inactivated using 10% FBS in HBSS and centrifuged at 1,200 r.p.m. at 4 °C for 10 min. In order to obtain a single cell suspension, incubate digested tissues with 0.25% Trypsin-EDTA. Cell pellets were resuspended with PBS containing 4% chelated FBS and then transferred into FACS tubes with a 40µm filter.</p> <p>Flow Sorting of mCherry Populations. Lung metastatic derived cell line generated to express mCherry from the endogenous Gsst1 locus was cultured under 2D conditions, trypsinized and filtered through 40µm mesh filters. DAPI (4',6-diamido-2-phenylindole) (3 nm) was added to the cell suspension to negatively select live cells. mCherryhigh and mCherrylow populations were gated on live populations as well as GFP+. For in vitro and in vivo assays, top 15-20% and bottom 15-20% were chosen as mCherryhigh and mCherrylow populations, respectively. Proper single-color and negative controls were used in every experiment to optimize gating.</p>
Instrument	Cells were analyzed and sorted using a FACSAria II (BD Biosciences).
Software	Data were analyzed with FACS Diva (BD Biosciences) and FlowJo softwares.
Cell population abundance	Biological negative controls (matched non-transgenic tissue) or cells not expressing Gsst1-mCherry construct were used to set gates. Top 20% mCherry expressing cells were used to isolate and sort mCherryHigh populations, and Bottom 20% mCherry expressing cells were used to isolate and sort mCherryLow populations.
Gating strategy	Dead cells and debris were excluded by FCS, SSC and DAPI staining profiles. mCherry sorted cell populations and DTCs were further gated on GFP+ as a tumor cell marker.

- Tick this box to confirm that a figure exemplifying the gating strategy is provided in the Supplementary Information.